Master's thesis

NTNU
Norwegian University of Science and Technology
Faculty of Natural Sciences
Department of Chemistry

Maja Olava Lindmo Ryan

Particulate matter released from Austre Brøggerbreen; a study on the potential impact on chemical conditions in Bayelva and Kongsfjorden

Master's thesis in Environmental Chemistry and Toxicology
Supervisor: Øyvind Mikkelsen
July 2021

NTNU
Norwegian University of
Science and Technology

Maja Olava Lindmo Ryan

Particulate matter released from Austre Brøggerbreen; a study on the potential impact on chemical conditions in Bayelva and Kongsfjorden

Master's thesis in Environmental Chemistry and Toxicology
Supervisor: Øyvind Mikkelsen
July 2021

Norwegian University of Science and Technology
Faculty of Natural Sciences
Department of Chemistry

NTNU
Norwegian University of
Science and Technology

Abstract

The decreasing mass balance of Arctic glaciers is a direct consequence of increasing temperatures due to climate change. The glacier Austre Brøggerbreen, situated close to Ny-Ålesund on Svalbard, is one of the glaciers with the highest negative cumulative mass balance over the period of 1967 up until today. The melting of glaciers does not only release large amounts of water to the glacier-fed river Bayelva but also large amount of particulate matter such as supraglacial material. The release of particulate matter can affect physical and chemical conditions in the river Bayelva and the fjord Kongsfjorden.

This thesis studied the chemical composition of solid material in the Bayelva basin and Kongsfjorden. Supraglacial material from the glacier Austre Brøggerbreen, overbank sediment from the river Bayelva and marine sediment from the fjord Kongsfjorden were collected and analyzed for elemental composition with ICP-MS. In addition, TC, TN, TOC, TIC, ROC, and pH were determined in the supraglacial material. The chemical composition and levels of selected trace elements, Pb, Cd, As, Cr, Zn, Fe and Al, were compared between the matrices to determine potential impact on the release of fine particulate matter from the melting glacier to the glacier-fed river system. Elevated levels of trace elements in supraglacial material have been reported, and with increased melting of Austre Brøggerbreen, the release of supraglacial material to Bayelva and eventually to the fjord, Kongsfjorden, is expected to increase. Therefore, a comprehensive study of the chemical composition of supraglacial material from Austre Brøggerbreen has been carried out and the relative composition of elements in different colored material (red, red-brown, brown, and black) was compared.

Red and red-brown material had higher concentrations of Fe and Al, while black material was highly associated with Pb and As, which were found in levels higher than crustal background levels indicating possible external local sources and/or long-range transport. The concentrations of several trace elements were also higher in supraglacial material than in overbank and marine sediment. Marine sediment further out from the river outlet showed higher concentrations of Fe and Al which are associated with the particulate matter released from Austre Brøggerbreen. Concentrations of Pb and Zn were elevated in supraglacial material as well as correlating strongly with Fe and Al in the marine sediments, which suggests trans-

portation of these elements with particulate matter from Austre Brøggerbreen to Kongsfjorden. This could be the reason for the higher levels of Pb, Cr and Zn in marine sediment further out in the fjord from the river outlet. The obtained results in this thesis provide valuable knowledge on the chemical status and composition of the glacier-fed Bayelva river system and Kongsfjorden.

Sammendrag

En direkte konsekvens av stigene temperaturer i Arktisk grunnet globale klimaendringer, er smelting av isbreer. Isbreen Austre Brøggerbreen, nærliggende Ny-Ålesund på Svalbard, har hatt den største nedgangen i massebalanse siden 1967 og frem til i dag. Når en isbre smelter, slipper den ikke kun ut store mengder smeltevann, men også store mengder partikulært materiale som for eksempel supraglacial materiale. Partikulært materiale fra smeltevann kan påvirke både fysiske og kjemiske egenskaper i Bayelva og Kongsfjorden.

I denne oppgaven ble den kjemiske sammensetningen av fast material fra tre områder, isbre, elv og fjord, studert. Prøvertakning av supraglacial materiale fra Austre Brøggerbreen, elvesediment fra Bayelva og marint sediment fra Kongsfjorden ble utført og prøver ble analysert for elementær sammensetning med ICP-MS. I tillegg ble TC, TN, TOC, TIC, ROC og pH i supraglacial materiale bestemt. Den kjemiske sammensetningen og nivåer av utvalgte sporelementer, Pb, Cd, As, Cr, Zn, Fe og Al, ble sammenlignet mellom de ulike matriksene for å kartlegge den mulige påvirkningen av utslipp av partikulært materiale fra en smeltende isbre til et smeltevannselvesystem. Forhøyede nivåer av sporelementer i supraglacial materiale har tidligere blitt rapportert, og med økende smelting av Austre Brøggerbreen er det forventet at utslipp av supraglacial materiale fra breen til Bayelva og Kongsfjorden vil øke. Derfor er en omfattende studie av den kjemiske sammensetningen av supraglacial materiale fra Austre Brøggerbreen utført og den relative elementære sammensetning av forskjellige farger (rødt, rødbrunt, brunt og svart) av materiale ble sammenlignet.

Rød og rødbrunt materialet hadde høyere konsentrasjoner av Fe og Al, mens det svarte materialet var sterk assosiert med Pb og As, som ble funnet til ha konsentrasjoner høyere enn forventende bakgrunnsnivåer i området. Dette kan være en indikasjon på mulige eksterne lokale kilder og/eller lang transport av Pb og Zn. Konsentrasjonene av flere sporelementer var også høyere i supraglacial materiale enn i elvesediment og marint sediment. Marine sedimenter funnet lenger ut i fjorden fra elveutløpet hadde høyere konsentrasjoner av Fe og Al som er assosiert med partikulært materiale i smeltevann fra Austre Brøggerbreen. Forhøyede konsentrasjonene av Pb, Cr og Zn i supraglacial materiale, i tillegg til en sterk korrelasjon til Fe og Al, indikerer transport av disse elementene med partikulært materiale fra

Austre Brøggerbreen. Dette kan være årsaken til at det ble funnet høyere konsentrasjoner av Pb, Cr og Zn i marint sediment lenger ut i fjorden. Resultatene funnet i denne oppgaven bidrar med verdifull kunnskap om kjemisk status og sammensetning av smeltvannselva Bayelva og Kongsfjorden.

Acknowledgements

This thesis concludes my master's degree in Environmental Chemistry at NTNU. It has been a challenging but a truly interesting and educational process. I have learned the true patience of waiting and for situations I have no control over. I wish to express my gratitude to the people that made this thesis possible.

First and foremost, a huge thank you to my supervisor Øyvind Mikkelsen. Thank you for giving me the opportunity to work on this project and for believing in me. Thank you for your patience, feedback, knowledge and encouragement. Your genuine interest and passion for this field will always be an inspiration to me. I also want to thank Anica Simic for the help and knowledge on freeze drying, UltraCLAVE and ICP-MS, and for always being available for questions and discussions.

Thank you to Polarinstituttet and Kings Bay in Ny-Ålesund for making the field work feasible. I also wish to thank Forskningsrådet for the economic support through the Arctic Field Grant and for making this project possible. Thank you to Per Ole Gundersen at St.Olavs hospital, Marianne Kjos at SINTEF and Anica Simic at NTNU for analyzing my samples and for the helpful insight on ICP-MS.

Thank you to my fellow ENVITOX students for two fun years. A special thank you to Morten Heistad and Sigrid Bergseng Lakså for the cooperation, good discussions, helpful input, long hours in the lab, morning meetings, venting of frustration and motivation. Must the adventures of Ole, Dole and Doffen continue. Martin Andreas Wiken, thank you for the cooperation with SPSS. Simen Fossum Morken and Tor Strømsem Haugland needs to be thanked for the help with coding. Thank you, Tonje Gottenberg Skaalvik for proofreading and for your good eye for detail. Katrine Melvold, Kristin Salvesen and Solveig Haug, thank you for taking the time to read through even though this is not your field. Thank you so much, Tonje and Tor for the help with finalizing this thesis.

On a personal note, thank you to all my friends and family for showing genuine interest in my thesis and for always believing in me. In particular, thank you mom, dad and Benjamin for the endless encouragement and support. Thank you to Nora, Tonje and Sigrid for the support and fun through these six years. Without you, this thesis would never exist. Nina, there are not enough words. Camilla, Katrine, Katinka and Solveig, thank you for the long phone calls and for always being there for me, even though we are miles apart. At last but not least, thank you so much to the Among Us crew in Oslo for keeping me sane through these trying times. I love you all.

Contents

List of Figures

List of Tables

Abbreviations

CRM	Certified reference material
DOM	Dissolved organic matter
HP-LC	High Performance Liquid Chromatography
HR-ICP-MS	High resolution Inductively Coupled Plasma - Mass Spectrometry
IC	Ion Chromatography
IR	Infrared
ISO	The International Organisation of Standardization
LOD	Limit of detection
LOQ	Limit of quantification
MF	Mobile phase
PCA	Principal component analysis
PP	Polypropylene
RCC	Residue Carbon Content
ROC	Residue Oxidizable Carbon
RSD	Relative standard deviation
SF	Stationary phase
TC	Total Carbon
TIC	Total Inorganic Carbon
TOC	Total Organic Carbon
TN	Total Nitrogen
QA	Quality assurance
QC	Quality control

1. Introduction

Temperatures in the Arctic have increased simultaneous with increasing global temperatures due to global warming [1]. From 1971 to 2017 the annual average change in Arctic air temperature increased with 2.7°C, 3.1°C in the cold season (October-May) and 1.8°C in the warm season (June-September). A consequence of the increasing temperatures, is the melting of glaciers [1]. The Norwegian Polar Institute has since 1967 measured the mass balance of several glaciers on Svalbard, including Austre Brøggerbreen [2]. Austre Brøggerbreen situated close to Ny-Ålesund has shown among the most dramatic trend with a cumulative mass balance of -27.26 m over the monitoring period, and the study has shown that the negative mass balance gets larger every year [3].

The melting of the glacier does not only release large amounts of water but also large amounts of clay and soil material, which are flushed out at the snout of Austre Brøggerbreen in to the glacier-fed river Bayelva [4]. This material can be from eroded moraines, whirled up sediment from the river bank or material deposited on the surface of the glacier i.e. supraglacial material. Supraglacial material consist of fine grained and large sand-sized organic and inorganic particles. This material is often found in mounds or water-filled holes called cryoconite holes on the surface and varies in color and texture [5–8].

Supraglacial material accumulates on the surface of glacier from local sources, such as rock and debris avalanches from the local terrain, weathering of rocks and debris eroded from the glacier bedrock, and distance sources, such as wind deposition of dust and long-range transported particles [5–8]. Studies have reported elevated concentrations of trace elements including toxic metals such as lead and cadmium in supraglacial material on glaciers in Svalbard [9, 10] . Supraglacial material and cryoconite holes have received attention due to reported microbial communities in cryoconite holes on glaciers in both the Arctic and Antarctic. However, studies on the chemical composition of supraglacial material is scarce. Trace elements have a strong affinity to fine particles and supraglacial material is a potential source of heavy metals to overbank and marine sediemnts. With increased melting of Austre Brøggerbreen, the release of supraglacial material to Bayelva and eventually to the fjord, Kongsfjorden, is expected to increase [11].

The particulate matter transported with meltwater may both affect physical and chemical conditions of water and sediments. Fine particles impact physical conditions, among light, sight and barriers between water and euphotic zone, and chemical conditions like pollutant mobilization and transport, essential gasses, nutrients and their availability, redox potential etc. [12].The particle load varies with the river flow and a significant increase in turbidity has been measured during the melting season [13, 14].

Particulate matter originating from melting glaciers of typically very fine suspended particles are of critical importance for chemical conditions in rivers, coastal water and ocean [15]. The aim of this thesis is to study the chemical composition of the material released from Austre Brøggerbreen and through chemical analysis evaluate chemical properties and potential interactions with selected pollutants, heavy metals. This is to increase the knowledge on the chemical composition of the particulate supraglacial material released from Austre Brøggerbreen and to get a better understanding and interpret the potential impact of such particulate material. Austre Brøggerbreen represent glaciers with long-term mass balance monitoring valuable for this project. Additionally, results from this project may in general generate new knowledge on the chemical status and composition of the Bayelva water system valuable to itself and for the ongoing research connected to the Ny-Ålesund flagship "Kongsfjorden system".

2. Theoretical background

2.1. Svalbard

Svalbard is an archipelago situated in the Arctic Ocean between 74°and 81°N latitude, and 10°and 35°E longitude [16]. Spitsbergen is the largest island where both the settlements Longyearbyen and Ny-Ålesund are situated. Approximately 60% of the land is glacier covered, 30% is barren ground (rock, scree, moraines, fluvial sediments, etc.) and only 10% is covered by vegetation giving the archipelago a scarce vegetation [17]. The climate is arctic but milder and with a lower mean annual temperature than areas at the same latitude due to the warm North Atlantic Current, a current part of the Golf Stream, which reaches the west cost of Spitsbergen. Due to this the west side of Spitsbergen can be ice-free large parts of the year. The prevailing westerly or south-westerly winds between Iceland and Norway bring mild air to lower latitudes. The fluctuation in wind masses and land ice cover causes a great variations in weather, especially in the winter. The mean annual air temperature is between -4°and -6°and can vary between several degrees below zero to above 15°C in the summer [16]. Permafrost on Svalbard can reach down to 450 m and only the top layer melts in the summer. Precipitation is generally low and the majority of the precipitation comes with polar eastern winds from the Barents Sea [18]. The polar night in Ny-Ålesund lasts from 25th of October to 17th of February and midnight sun lasts from 18th of April to 24th of August [19]. The species diversity is low on Svalbard, including migratory birds, seals, reindeer, polar fox and polar bears, with few steps between the top and the bottom of the food chain [20].

2.2. Arctic glacier-fed river system

Glaciers are an important part of the water storage on Earth and in the Arctic. Most of the glaciers on Svalbard are polythermal, meaning that they have both "cold based" and "warm-based" ice. Warm-based or temperate ice is ice at temperatures close to or at the pressure melting point of water whereas cold-based is ice with temperatures under the pressure melting point. Polythermal glaciers thus

have temperate parts and parts that are frozen to the bed [16, 21].

Glaciers can be divided into two sections: accumulation area and ablation zone. The accumulation area is where ice and snow are added and accumulated primarily from precipitation. The ablation zone is where ice and snow are removed by melting, wind erosion, evaporation and calving (Figure 2.1) [22, 23]. During the winter, accumulation of snow and ice is dominant. During the summer months with increasing temperatures, melting of snow and ice on the surface is dominant. Temperatures are increasing in the Arctic due to climate change, causing multiple glacier to decrease in their mass balance, indicating that the removal of ice is larger than the accumulation in the winter [2, 3].

The melting season in the Arctic last from the end of May until early October [16, 24]. Meltwater, derived from melting snow and ice, flows in rill channels and canyons on the surface of the glacier. Meltwater can flow down in moulins which are large holes in the glacier reaching all the way down to glacier bedrock, or along the margins of the glacier. Meltwater reaching the bed of the glacier flows beneath the ice and emerges from the glacier in one stream at the snout (Figure 2.1 and 2.4). The meltwater brings suspended material and sediment both from eroded material beneath the glacier (subglacial) and from the surface of the glacier (supraglacial). Supraglacial material is brought with the meltwater through moluins and marginal channels often as suspended particles [4, 14]. Supraglacial material is further discussed in section 2.2.1.

Glacial erosion is the processes of a glacier transporting rock fragments and sediment to another location [23]. Glacier erosion occur through several processes. The focus in this thesis will be on meltwater erosion. Meltwater erosion happens through two processes: mechanical and chemical erosion. Mechanical erosion is the transport of suspended sediment and bedload with meltwater at the base of the glacier. Chemical erosion is the removal of rock debris and sediment in solution in the meltwater. Chemical erosion is prominent in subglacial meltwater channels due to high flushing rates, availability of large amounts of chemically reactive rock debris and increased solubility of CO_2 at low temperatures which is a reactant in chemical erosion. Chemical erosion is also especially prominent in carbonate bedrock [23].

Through large amounts of meltwater released from glaciers during the melting season, large amounts of suspended material and sediment consisting of clay, silt and soil material are flushed out at the snout often making glacier-fed rivers. Flushed out water and particulate matter run through moraines which are accumulated sediment and rocks due to the movement of the glacier. The path of the river is dependent on the terrain and vegetation, and can flow down to and out into the

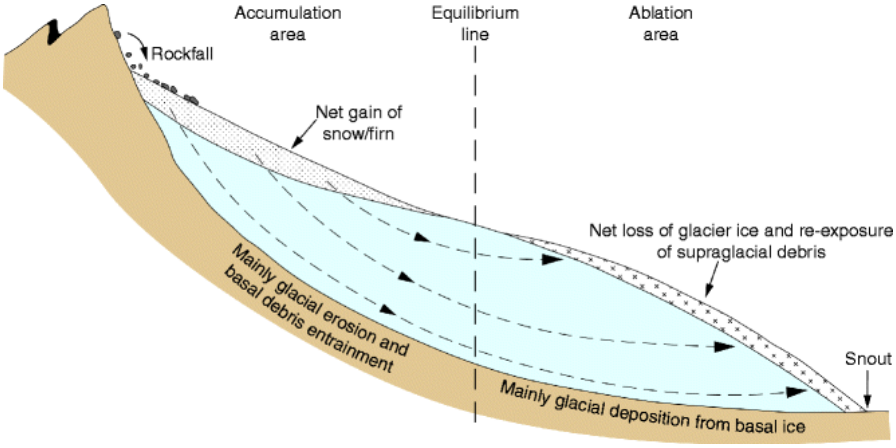

Figure 2.1.: Longitudinal profile of a glacier, illustrating the relationship between mass balance, particle paths and debris entrainment processes. Reprinted with permission from Hambrey and Glasser (2011) [23]. Copyright (2021) Springer Nature.

sea if located close to the coast [12, 14, 23]. Figure 2.4 illustrates a glacier-fed river system.

2.2.1. Supraglacial material and cryoconite holes

On the surface of glaciers (supraglacial), debris can occur in various amounts, colors, shapes and forms. The supraglacial debris can be from both local and distant sources [5–8]. The local sources are believed to be the major sources for the debris and are from within the catchment of the glacier. The dominant local sources are from mass wasting, washing and aeolian processes of e.g. dust from surrounding terrain, mountains and soil and local bird guano deposition. Gravitational processes like rockfalls, rock avalanches, debris flows and debris-laden ice and snow avalanches, and weathering of rocks are major contributes to the supraglacial debris [25]. The debris can also derive from eroded material underneath the glacier by transport from debris-rich basal ice layer deformation including folding and thrusting (Figure 2.2) [23]. Distant sources are atmospheric-transported dust from wind-transported minerals from widespread arid terrains, volcanic ash, marine and organic aerosols, sea spray, extra-terrestrial material and pollution sources like factories, mining or other anthropogenic activity [5–8].

Through the different processes described, the debris and particulate matter from different origin accumulate on the surface of the glacier forming a particulate matter consisting of silt, clay, and fine-grained and large sand-sized particles of

both inorganic and organic matter [5, 6, 25]. This material is often referred to as cryoconite ("cryo" meaning ice and "conite" meaning dust). The use of the term cryoconite is not consistent and is often used when the material is black or dark-brown due to the presence of humic substances, which are dark-colored biogenic organic matter [26, 27]. Supraglacial material can be found in various color and composition and is therefore further referred to as *supraglacial material*.

Supraglacial material can be transported by gravitation processes, meltwater, rain or wind to form mounds in various sizes or accumulate in cryoconite holes. Cryoconite holes are formed when heat from solar radiation is absorbed to the material on the surface, melting the ice beneath forming water-filled cylindrical or D-shaped holes with nearly vertical sides and a layer of the material at the bottom [5]. The water in the hole usually freeze in the winter. Cryoconite holes occur in the ablation zones of the glacier and the size of cryoconite holes varies from a few centimeters to tens of centimeters in diameter and tend to be no more than 50-60 cm deep [6, 7]. Cryoconite holes where discovered and named by A. E. Nordenskjold on his expedition over the Greenland Ice Cap in 1870 and has been reported from the Antarctic, the Arctic and in more temperate areas including Alpine glaciers and Asian glaciers [5].

The composition of supraglacial material varies from glacier to glacier due to differences in local and distant sources and is, as mentioned, a mixture of both inorganic and organic components. The supraglacial material and cryocronite holes have receive attention due to the reporting of microorganisms and microbial communities including algae, bacteria, fungi, virus-like particles and diatoms in cryocronite holes on glaciers in both the Arctic and Antarctic. Studies have mainly focused on the biological composition of the cryocronite water and material [5–7, 27–29]. Studies on the chemical composition of supraglacial material is scarce, though presence of metals and trace elements have been reported [7–10].

2.2.2. Transport of particulate matter in rivers

Particulate matter and sediment is transported in rivers by several processes of river erosion, depending on the size of the particles, amount of water in the river and the velocity of the river flow. Particles and sediment transport can be divided into the dissolved load, the suspended load and the bed load. Bed load consist of the heavy particles like gravel and sand that are moved by the water flow at the bed of the river. The heaviest gravel and particles may never leave the bottom and can be moved by traction which is rolling, sliding or dragging along the river bed or by abrasion. Abrasion is the erosion by grinding and friction of gravel and sand [30].

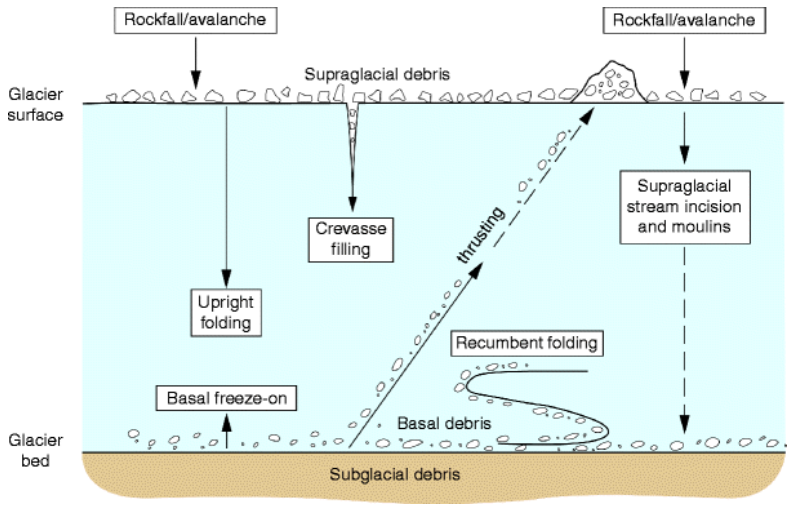

Figure 2.2.: Illustration of glacier debris processes. Reprinted with permission from Hambrey and Glasser (2011) [23]. Copyright (2021) Springer Nature.

Sand and smaller particles on the river bed can be lifted up by turbulent water and transported with the river flow. The particles are lifted and transported when the veocity of the flow is high, and settled when the velocity is low, causing transportation through several "hops" in a process called saltation [14, 31].

Even smaller particles are kept suspended in the water and can often be visually seen in rivers with high flows and water load. In contrast to the bed load, the suspended load remains lifted above the river bed and are transported in the water flow. The suspended load contributes to most of the transport of particulate matter in rivers. During heavy rain and floods, the suspended load is large due to upwhirling of light particles from the river bed. During low flows, some of the suspension can settle [14, 31].

The dissolved load consist of soluble ions and compounds that are chemically weathered. Chemical weathering is the change in the chemical composition of rocks and soil by chemical reactions with air or water. An example is the dissolution of rocks by carbonation. The dissolved load can be transported far but can also be precipitated out of solution [32]. Figure 2.3 illustrate the different transportation processes of particulate matter in a river.

Overbank sediment is formed by river erosion and sedimentation of particles. During high river flows, particles from overbank sediments can re-disperse and follow the suspension load [33].

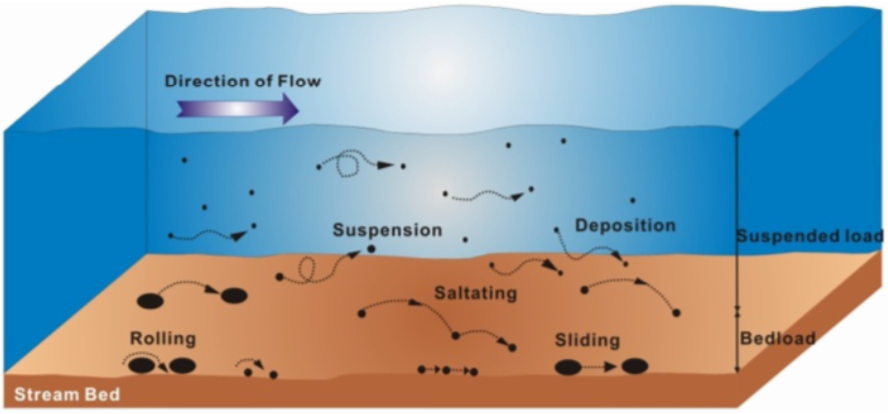

Figure 2.3.: Particulate matter and sediment-transport processes in rivers. Reprinted with permission from Tsai and Lai (2014) [30]. Copyright (2021) American Society of Civil Engineers.

2.2.3. Transport of particulate matter to the sea

An esturay is where rivers meet the sea and fresh water and seawater mix and are often found in fjords. Estuaries plays a large role in the transport of particulate matter and thus ions and nutrients to the ocean. The fast flowing river water that meet stagnant seawaer often cause particulate matter in the water to settle, forming a delta. Freshwater with suspended material flows into the slightly denser seawater making brackish water (Figure 2.4). A higher concentration of salts and ions in the seawater causes chemical reactions with ions and components in the river water which decides the fate and further transport of the particulate matter. Transport of suspended particulate matter from an esturay is also dependent on physical factors including currents, wind, tide waves and vertical mixing. Marine sediments can undergo the same processes of erosion and transportation as river beds [31, 33].

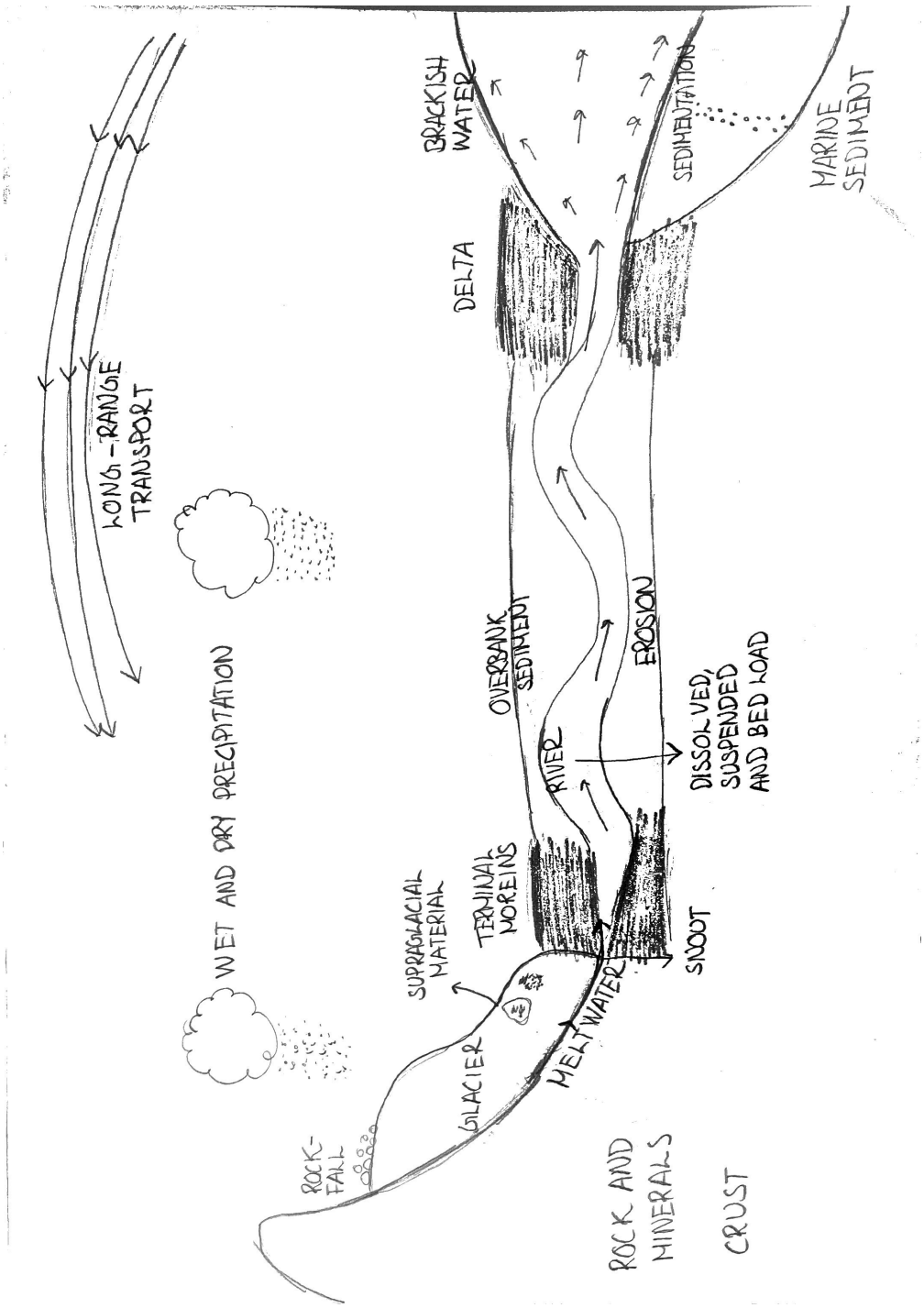

Figure 2.4.: Illustration of glacier-fed river system.

2.3. Trace elements in the Arctic

90 elements are naturally occurring on the earth and can be divided into *major* elements, *minor* elements and *trace* elements. The major elements are C, H, N and O, the minor elements are Ca, Cl, Mg, P, K and Na and the remaining is the elements found in trace amounts [34]. The trace elements are found in a wide variety of chemical forms depending on the chemical and physical properties of the natural compartment they occur in. The environment can be divided into four natural compartments or spheres: the atmosphere (air), the biosphere (living organisms), the hydrosphere (water) and the geosphere (rock, mineral matter and soil). In addition, there are the anthroposphere, which is the part of the environment that is man made [35]. Matter and elements are exchanged between these spheres as illustrated in Figure 2.5 [36].

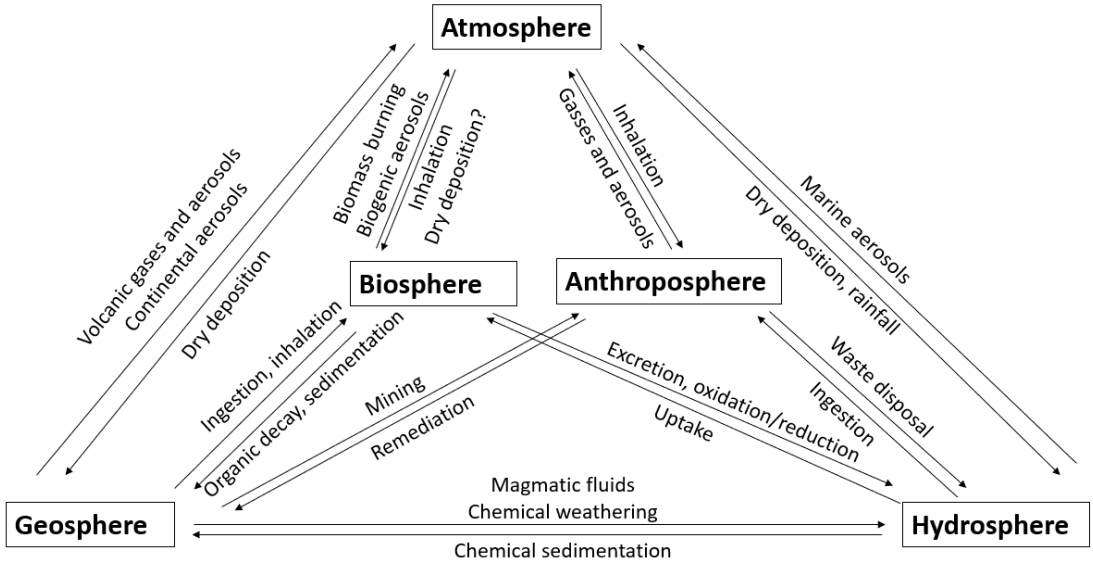

Figure 2.5.: Processes of exchange of elements between spheres in the environment. The figure is adapted from Larocque and Rassmussen (1998) [36].

The main sources for trace elements are natural including weathering of rocks, volcanoes, sea spray, thermal springs, lake and river sediments, vegetation and forest fires [37]. In the geosphere, trace elements are present in minerals, glasses and melts [36]. In the hydrosphere, trace elements are present as dissolved ions and complexes, colloids and suspended solids. Trace elements are present as particles and aerosols and may be present in gaseous form in the atmosphere. Trace elements enter the biosphere through inhalation of gaseous and particulate forms, and ingestion or absorption of solid or liquid forms. The geosphere is in addition

to being a major source, a sink for metals and trace elements. The hydrosphere is an important sink but also an important transport route for elements. The ocean is especially an important reservoir for trace elements where they can undergo diagenesis and return to the geosphere. The atmosphere can also be considered a sink but is mainly responsible for the transport of trace elements [36].

Trace elements are often categorized into essential and non-essential in the biosphere and anthroposhere. Essential trace elements are essential for biochemical processes like iron (Fe), zink (Zn), magnesium (Mg) and copper (Cu), while the non-essential, like lead (Pb), cadmium (Cd), arsenic (As) and mercury (Hg) are not and are toxic at relatively low concentrations. Essential elements are also toxic when exceeding high concentrations [38]. The non-essential elements are classified has hazardous not just because they are toxic to most organisms but also due to their ability to bioaccumulate. Some, like Hg, also has the ability to biomagnify. These toxic elements has received a lot of attention since the last century because they are produced and released to the environment as a result of anthropogenic activities [39]. These elements have also received attention because they have been found in the Arctic in levels exceeding the local sources and therefore have shown to be subjected to long-range transport [40, 41]. Arctic ecosystems are especially vulnerable to high concentrations of toxic elements due the extreme living conditions and the low species diversity thus small steps between low and high trophic levels. A small change in the organisms body conditions, can therefore lead to fatal consequences for the Arctic ecosystems [42].

Trace elements originate both from natural and anthropogenic sources. They are present in low concentrations in rocks and bedrocks and are due to weathering processes naturally present in soil and surface waters [43]. Erosion of rocks and soil account for the largest part of the natural sources (>20% of natural derived Pb and Zn). Volcanic activity (around 20% of As, Cd, Cr and Pb), sea spray and burning of biomass are among the natural sources of toxic trace elements. Anthropogenic sources include combustion of fossil fuels, wood and coal, emission from metallurgical industry, high temperature industrial processes and manufacturing, road traffic (erosion from means of transport) and waste treatment [43].

2.3.1. Trace elements in the geosphere

As mentioned, trace elements occur naturally in the Earth's crust. The crust mostly consist of light silicate-based minerals such as quartz, SiO_2, or orthoclase, $KAlSi_3O_8$. In total, 49.5% of the Earth's crust is oxygen and 25.7% is silicone. Other major components of the crust are aluminum (7.4%), iron (4.7%), calsium (3.6%), sodium (2.8%), potassium (2.6%) and magnesium (2.1%). Trace elements

are an even smaller part of the crust and are incorporated in minerals. Trace elements are transported to soil, water and air through physical and chemical weathering. The local composition of geosphere varies depending on the types of rocks and minerals in the area [44].

Soil is the part of the geosphere that are able to support life and consist of a unconsolidated mixture of minerals and organic matter. Soil can be divided into mineral soil and organic soil. Organic soil is the top layer and are the part that has the most organic matter. Soil also contains water due to small size of soil particles and the presence of capillaries and pores. Metals are bound strongly to organic matter in the top soil. Top soil contains humic substances and clays which have ion exchanging capacities due to their negatively charged ligands. The negatively charged ligands have strong ability to bind to cations especially polyvalent ions. Cations can thus be retained in the top soil from water passing through the soil [45].

Sediments consists of clay, silt, sand, organic material and minerals. Marine sediments are mainly fine grained alumino silicates. Cd, Co, Cr, Cu, Fe, Mn, Mo, Ni and Pb are found in significant amounts in sediments. They occur as organic complexes with low solubility or are sorbed on to clays and Mn(IV) or Fe(III) hydrous oxides. The chemical form of trace elements in sediments depends on the pH, the redox conditions and the nature of ligands [34].

2.3.2. Trace elements in the atmosphere

Long-range atmospheric transport

Since the observation of the Arctic haze in the 1950s, contaminants in the Arctic has gained much attention and concern [46]. The discolored haze was observed by planes flying over the High Arctic in the 1950s and later acknowledged as originating from anthropogenic sources outside the Arctic in the 1970s. High levels of contaminants like persistent organic pollutants (POPs), toxic trace elements and radionuclides have been observed for several decades despite the very few sources of pollution in the Arctic. This indicates long-range transport of pollutants and that the Arctic, due to its cold climate, is a sink for contaminants from all over the globe [46].

The pattern and processes for how a contaminant ends up in the Arctic depends on its physicochemical properties [47]. Long-range atmospheric transport can be divided into different processes, which are illustrated in Figure 2.6. Global distillation or fractionation is the process of contaminates being transported from mid-latitudes towards high-latitudes, and the separation of them in the atmosphere

based on their volatility (Figure 2.6) [48]. Contaminants related to particles or aerosols tend to be "one-hop" contaminants meaning they follow the northflowing wind from their source and end up in the Arctic without being deposited on the way. They tend to stay where they are deposited and can travel great distances depending on season, location related to the Arctic airmass, precipitation patterns and wind patterns. Examples of one-hop contaminants are non-volatile metals and radionuclides [46].

Volatile and semi-volatile contaminants tend to be multi-hop contaminants and follow the "grasshopper effect" (Figure 2.6) [46, 47]. Volatile and semi-volatile contaminants evaporate to the atmosphere and are transported by winds as gases. They can be deposited onto soil, ice or in the ocean by adhering to particles or organic films, or dissolve in water. They can then re-volatilize and enter the atmosphere once again, e.g. due to increasing temperature. The contaminant will again be transported by winds and can deposit at a new site. In the processes, contaminants can break down to less harmful compounds or deposit in sediments in the ocean or lakes. These processes can be repeated several times and can eventually end up in the Arctic. When reaching the Arctic, it is unlikely that contaminants will re-volatilize into the atmosphere due to the low temperatures and gases have higher solubility in colder water [46, 47].

Trace elements can be deposited from the atmosphere to terrains and water systems through wet or dry deposition processes [43]. Dry deposition is the direct deposition or sedimentation of trace gases and particles from the atmosphere. Dry deposition of gases are the uptake of gases by plants and water bodies. Wet deposition is the precipitation of gases, aerosols and particles as dissolved or particulate form in rain, snow or fog. Dry and wet deposition is dependent on particle size, concentration and the reactivity between the particles and the surface it is being deposited onto. Metals and trace elements are mostly transported in the air in fine particles, thus wet deposition is the dominating deposition process. Wet deposition includes scavenging in and below the cloud. Scavenging in the cloud happens when condensation form around one or more aerosols and is called nucleation because the aerosols serve as a core. Washout of particles that are in the air below clouds by incorporation into droplets is called scavenging below the cloud. These processes can happen separately or at the same time [43].

The transport patterns of airmasses to the Arctic is dependent on season and position of major weather systems [46]. The Arctic front is a weather front where cold Arctic air meets warmer more humid air often traveled over open and warmer ocean waters. The Arctic front affects both weather and the transport of air from lower latitudes to the Arctic. The expansion of the Arctic front is dependent on season. In the summer, transport of air to the Arctic from mid-latitudes decreases

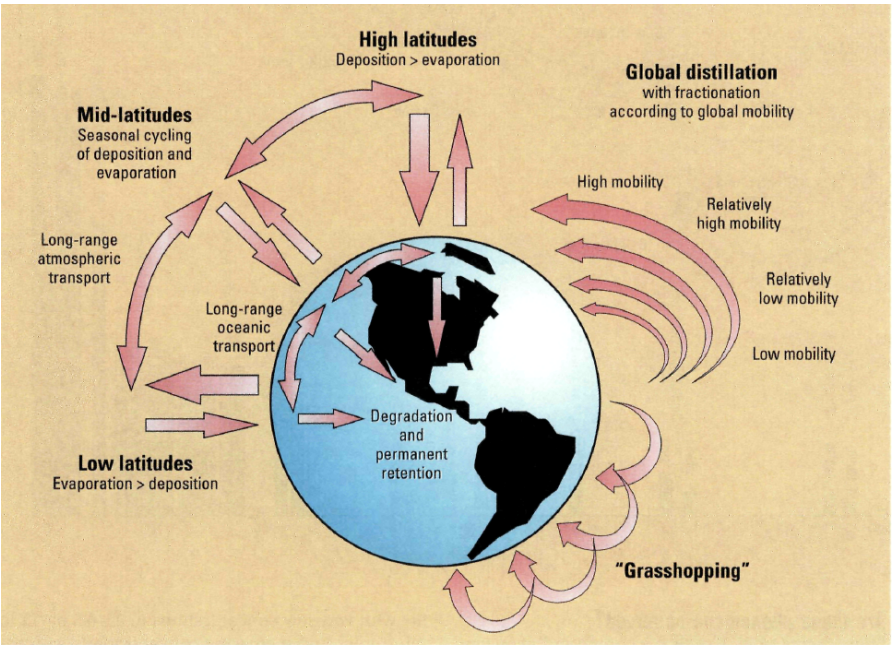

Figure 2.6.: Illustration of long-range atmospheric transport processes. Reprinted with permission from Wania *et al.* (1996) [48]. Copyright (2021) American Chemical Society.

due to the breaking of continental high-pressure systems and weaker low-pressure systems over the ocean. The removal of contaminates from the air increases due to more cloud formation and higher temperatures. This prevents the contaminants from being transported over long distances. In addition, photochemical degradation of some contaminants increases due to increased solar radiation. The transport of air and thus contaminates to the Arctic is highest in the winter and fall. High-pressure systems over Siberia expand the Arctic front to the south leading to heavy polluted areas in Eurasia to be within the Arctic front. The accumulation of contaminants in the atmosphere is higher in the winter due to lower temperatures. Precipitation and cloud formation over high-pressure areas is low in the winter, leading contaminants to stay in the atmosphere rather than being removed by clouds and rain. Lower wind speeds, temperature inversions and the lack of sunlight to degrade contaminates are all factors contributing to the higher accumulation of contaminants to the atmosphere and it following the large-scale atmospheric circulation patterns [46].

2.3.3. Trace elements in the hydrosphere

In natural water trace elements are present in a wide range of chemical forms, ranging from the particulate phase to the dissolved phase. The difference between dissolved and particulate phase, is operationally defined by filtration on a 45 µm pore size membrane. The fraction left after filtration, is referred to as the dissolved phase [49]. Speciation is the different physiochemical forms that an element can have [50]. Trace elements can be found as hydrated ions, inorganic or organic complexes, colloids or absorbed onto particles. The dissolved phase includes hydrated ions, inorganic and organic complexes, heterogeneous colloidal dispersion and organometallic compounds [51]. Specitation is dependent on many factors: pH, redox potential, valance state of the element, dissolved organic matter and the bonded functional groups of the species formed. In natural waters, most trace elements accumulate in sediments because they do not exist in soluble form for long [34].

In water trace elements exist as ions, either cations or anions [51]. The ions in water are not stable by themselves. Table 2.1 presents possible species of metals and trace elements in natural water in soluble, suspended, colloidal and solid form with lead as an example. In the soluble form trace elements can be found hydrated by water molecules, as ions pairs or as inorganic or organic complexes. Ions pairs are formed by two ions of opposite charge, e.g. NaCl. Inorganic or organic complexes are formed by a covalent bonds between the metal ion and ligands. Complexes where the metal ion is bound to a ligand in two or more places are called chelation and are more stable. Complexation and chelation plays a large role in the solubility, precipitation, adsorption, transport and bioavailability of metals and trace elements [51].

Dissolved organic matter (DOM) is a group of heterogeneous water-soluble organic compounds found in natural waters. DOM is derived from biological matter and organisms and consists of carbohydrates, carboxylic acids, amino acids, hydrocarbons and humic substances [52]. Most of the DOM consist of humic substances which are an important compound in humus and are the major component of soil, peat and coal. Because of their strong acid-base properties, humic substances easily form complexes with metals and trace elements. DOM is thus important for speciation, solubility, mobility and bioavailability of metals and trace elements in natural waters. Examples of complexes of metals and DOM are Cu bound to fulvic acid and Cu-$Fe(OH)_3$-humic acid [53].

Colloids are particles ranging from 1-1000 nm in size and remains evenly distributed in solution, also referred to as colloidal dispersion since they do not settle to sediments. Dispersed particles that are smaller than colloids are referred to as a

solution while dispersed particles larger than colloids (up to 1mm) are referred to as suspension [54]. Colloids consist of organic compounds, inorganic compounds and humic substances e.g clay. Ions are easily adsorbed to the surface of colloids due to their high specific surface areas and surface to charge ratio. Colloids are therefore important for the transport of metals and trace elements in natural water, especially in rivers where the flow velocity is dependent on season [49].

Trace elements bound to larger particles settle relatively quickly to sediments while metals and trace elements bound to smaller particles will have a higher residence time in water and may be transported over long distances in rivers [55]. When colloids are kept dispersed over a longer period of time, they are referred to as colloidal stable. Colloids can aggregate and form irregular unstable assemblages, flocs or agglomerates. Aggregation can lead to sedimentation of the agglomerates when becoming large in size. Agglomertes can re-disperse and again become colloids or suspension [55, 56].

The high concentrations of salts and ions in seawater causes aggregation of particles, especially where river water meet seawater. Ions and charged particles are more stable in fresh water. In saline water, ions become unstable causing more aggregation. This is a major processes forming river deltas [55].

pH is another important factor for speciation and transport of trace elements in water. The pH in natural water ranges from 6.5 to 8.5 [57]. pH effects speciation of trace elements by changing the oxidation state of and by the difference in the presence of H^+, OH^-, $CO_3{}^{2-}$, $HCO_3{}^-$. H^+ is a competing agent for binding sites to ligands. pH also effects the charge and speciation of the ligands that trace elements form complexes with [51]. Most metals are present as free ions at pH 6 without the presence of dissolved organic matter. For Pb, the formation of carbonate complexes increases at pH 8. At pH 8, Cd and Zn are mostly still present as free ions. At pH 6 with the presence of DOM, Cu and Pb were mostly present as organic complexes while Cd and Zn is still present as free ions [58]. The different processes effecting the speciation and transport of metals and trace elements in natural waters are summed up in Figure 2.7.

Table 2.1.: Speciation of lead (Pb) in natural waters [51].

Speciation	Lead	
Free metal	Pb^{2+} (not found in natural water but bound to water molecules $\rightarrow$ free hydrosized)	
Ion pair	$PbHCO_3$	SOLUTION
Complexes with organic pollutants	Pb^{2+}/EDTA	
Complexes with natural acids	Pb^{2+}/fulvic acid	SUSPENSION
Ion adsorbed onto colloids	$Pb/Fe(OH)_3$	COLLOIDAL
Metal within decomposing organic material	Pb in organic soils	SOLID
Ionic solids	Pb^{2+} held within the clay structure, $PbCO_3$	

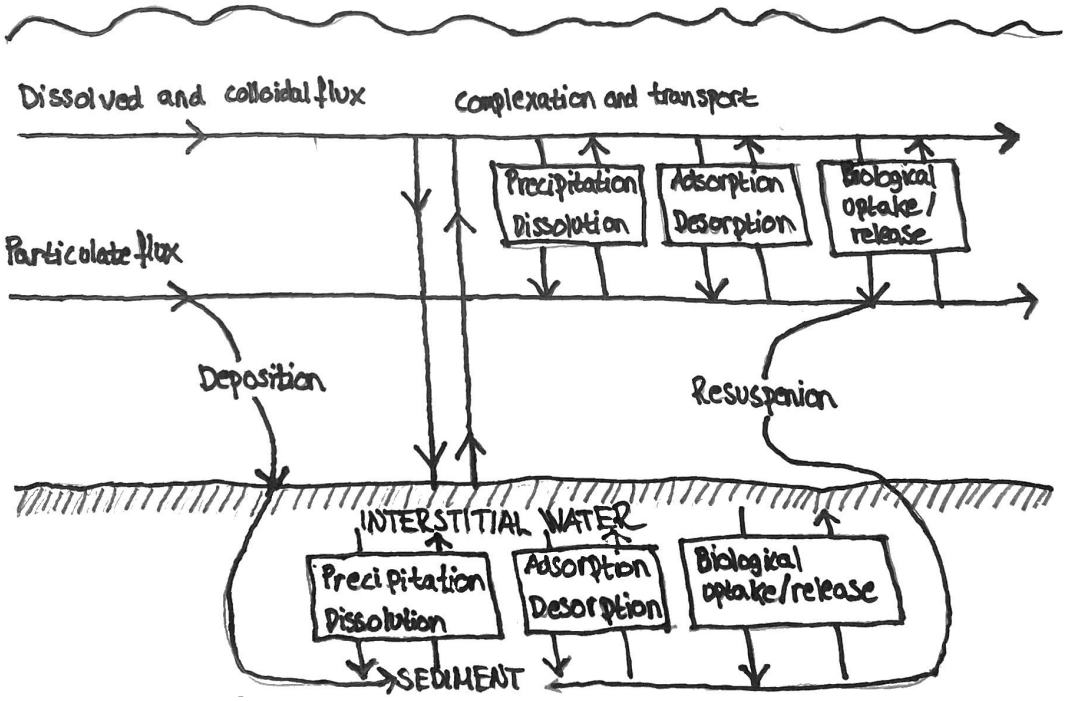

Figure 2.7.: Physiochemical processes of metals and trace elements in natural waters. Adapted from Morrison (1989) [59].

2.4. Sample preparation and analysis

In this chapter, a short introduction on the different sample preparation and analytical techniques will be presented. The focus will be on their main principles, strengths and weaknesses.

2.4.1. Freeze drying

Freeze drying is the removal of water and other solvents through sublimation and desorption [60]. The process consists of two steps of drying, primary drying and secondary drying. Under primary drying the samples are completely frozen and set under vacuum under the triple point of water (4.58 torr and 0.0098 °C) and water is sublimated. Under secondary drying the temperature is increased and the remaining water molecules bound to the sample are desorbed [60].

2.4.2. Microwave acid digestion

Microwave digestion is a preparative technique for elemental analysis of solid samples were the analyzing technique requires the samples to be in solution, e.g. ICP-MS [61]. Microwave digestion is used to wash out the elements that are adsorbed on particles. Elements adsorbed on particles can be a source of contamination when studying and analyzing trace elements/metals. Microwave acid digestion exploits electromagnetic radiation to generate heat, high pressure and concentrated acid to decompose and oxidize the components in the sample [62, 63]. The samples are digested to a solution consisting of organic material at various stages of decomposition and metal ions with uniform oxidation states with high solubility. Microwave acid digestion in a closed vessel is favorable due to problems with evaporation of components in the sample in open vessels and it allowing the acid to be heated above its boiling point which increases the acids oxidation potential [63].

Nitric acid is a much-used acid in microwave digestion due to its increasing oxidation potential at high temperatures and its ability to digest samples with high content of organics without addition of auxiliary regents, e.g. sulfuric acid or perchloric acid [64]. HNO_3 does not dissolve particulate matter completely but dissolves the outer layer of particles where ions are absorbed, leaving some of the particulate matter in precipitation. Another disadvantage with microwave digestion is residue carbon content (RCC). RCC is insoluble carbon that will appear as a precipitation after digestion and can cause interferences in further analytical instruments [61].

Closed microwave acid digestion with concentrated nitric acid (HNO_3) can be done

with Milestone UltraCLAVE. UltraCLAVE consist of a reaction chamber where the samples, in Teflon vials, are placed in a base load consisting of deionized water, hydrogen peroxide and sulfuric acid to ensure reproducible conditions. In the first step, the chamber is pressurized with inert nitrogen gas (N_2 to prevent boiling and avoid cross-contamination. The reaction chamber is then heated with a microwave power source and pressure is applied [63, 65]. After the digestion, the samples are diluted with deionized water to prevent instrument interferences due to high concentrations of acid and RCC. For example can high contents of nitric acid and RCC cause isobaric and transport interferences in ICP-MS [61, 66].

2.4.3. ICP-MS

Inductively Coupled Plasma - Mass Spectrometry (ICP-MS) is one of the most effective and powerful analyzing techniques for qualitative and quantitative multi-element determination, including trace elements and isotopes [67]. The principle of the technique is that a sample is atomized, further ionized, and thereby detected on their mass to charge (m/z) ratio. The ICP-MS instrument is divided into a ICP part and a MS detector. The sample is injected into a nebulizer with inert argon gas and the sample is transformed to an aerosol. At high temperature (6000-10 000 K) and pressure, an argon plasma is formed, and the analyte species are ionized. The sample is then focused by ion optics, through a chamber were the pressure is set to vacuum, into the mass analyzer. Four quadrupoles with alternately AC and DC current will separate the species according to their m/z ratio and the ion species will be measured at the detector [67].

The main limitations for ICP-MS are spectroscopic interferences and matrix effects. Spectroscopic interferences are interferences that occur when non-analyte species have the same m/z ratio as an analyte species. Spectroscopic interferences can be divided into four categories: polyatomic ions, double charged ions, isobaric elements and tailing interference [67, 68]. Polyatomic interferences occur due to formation of polyatomic ions in the plasma from incomplete atomization or recombination reactions during extractions of ions into the mass spectrometer. This can come from the sample matrix, reagents used for sample preparation, argon plasma gas or entrained atmospheric gases. An example is the formation of ArO^+ which has the same m/z ratio as $^{56}Fe^+$ at 58 amu and will therefore be analyzed as the same ion species [69]. Another example are for samples containing chloride, e.g. seawater, where $^{35}Cl^{16}O$ and $^{40}Ar^{35}Cl$ are formed and have the same m/z ratio as ^{51}V and ^{75}As [68]. Double charged interferences occur for elements that can form a double positive charge and have a fraction of double charged ions that will generate isotopic peaks at half its mass. Isobaric interferences occur when isotopes of different species has the same m/z ratio, for example Fe and Ni both have isotopes

occurring at m/z 58 [70]. Tailing interferences are spectral overlap occurring from an adjacent ion species when the mass spectrometer has an abundant sensitivity [68].

Matrix effects are interferences that occur due to the properties of the components in the sample and leads to suppression or enhancement of the analyte signals. This can occur in all parts of the instrument and can be sample introduction effects, plasma effects and space-charge effects.Samples with high concentrations of organic solvents, can lead to cross-contamination and clogging of the instrument due to a tendency for carbon deposits to build up on quarts tubes in the ICP source [67].

2.4.4. Determination of Total Carbon and Total Nitrogen content

Total Carbon and Total Nitrogen content in solid material and sediment samples can be determined through combustion with oxygen at 1200°C [71]. The samples are weighted out and analysed in ceramic crucibles. Through combustion the carbon content is converted to CO_2 gas and the nitrogen content is converted to nitrogen oxides. After combustion, the gas mixture is led by nitrogen free helium carrier gas through a splitter where a part of the mixture gas is collected. The gas mixture remaining after the splitter is led to an IR detector where CO_2 is detected and the total carbon content is measured. The collected gas after the splitter is led through a copper reduction oven, where nitrogen oxides are reduced to nitrogen gas (N_2), and further through scrubbers where CO_2 and water is eliminated. The nitrogen gas is then detected with a Thermal conductivity detector (TCD) and the total nitrogen content is measured [71, 72].

Determination of Total Organic Carbon (TOC), Total Inorganic Carbon (TIC) and Residue Oxidizable Carbon (ROC) content can be carried out through combustion with oxygen at 400°C, 900°C and 600°C respectively with the same instrument as described. The carbon is combusted to CO_2 gas and detected with an IR detector at the different temperatures [72, 73].

The concentration is determined by making a calibration curve with different weights thus known concentrations of a suitable calibration standard. The calibration curve is made by plotting the signal from the detector as a function of the concentration of the standard [71, 73].

Sources of error for both these analysis are contaminated crucibles, errors in the weight of the sample and errors related to or in the calibration curve. Contamination on or in the crucibles, can cause a higher determined concentration of the analyte than actual present in the sample. This is why it is important to not

touch the crucibles because this can leave grease and other contaminants on the crucibles. Factors causing the weight of the sample to be different than believed, affects the determined analyte concentration to be higher or lower than the actual concentration in the sample. Wrongly determined concentrations can also be caused by an error in the calibration curve, making the linear relationship between concentration and signal inaccurate. Results outside of the calibration curve can be inaccurate due to the uncertainty of a linear relationship between concentration and signal [72, 74].

2.4.5. UV/VIS-spectrometry

Light is absorbed, reflected and transmitted when colliding with an object or a liquid [75]. In UV/VIS-spectrometry, light with a wavelength in the visible and ultraviolet spectra is sent through the sample which will cause the analyte to transit from the ground state to a higher energy state or excited state. Light is thus absorbed in the sample and the intensity of the light decreases. The light that is not absorbed is detected by a detector and are measured as the transmittance, T. The transmittance is expressed as

$$T = \frac{P}{P_0} \tag{2.1}$$

where P_0 is the intensity of the light beam sent through the sample and P is the decreased intensity after light is absorbed. The transmittance is then related to absorbance (A) by

$$A = -logT. \tag{2.2}$$

This is then connected to Beer-Lambert's law which states that measured absorbance is directly proportional to the concentration of the absorbed species, c (mol/L), and the path length, b (cm), of the absorbing medium:

$$A = \varepsilon bc \tag{2.3}$$

ε is a proportionality constant called molar absorbitivity and has the unit of L $mol^{-1}cm^{-1}$. Absorbance is measured by sending light through the sample with the wavelength the analyte absorbs at, in a kyvett placed in a closed and dark vessel with constant path length [75].

To find the concentration of the analyte through the measured absorbance, a calibration curve must be made where the absorbance is plotted as a function of known concentrations of a calibration standard [75].

Beer-Lambert's law is only applicable within a interval of concentrations. If the concentration of the analyte in the sample is too high, the calibration curve will flatten. This happens due to the absorbing particles colliding, changing the charge distributions and the energy states, thus also the absorbance. When using UV-spectrometry for quantification, it is important to use the linear area of the calibration curve. Interferences can occur by other species in the sample that absorbs the light at the same wavelength as the analyte, chemical reactions in the sample altering the analyte, and particles or dirt on the glass of the kyvett that will absorb the light. If the analyte is not fully dissolved and there is a equilibrium between dissolved and precipitated analyte, the right concentration will not be measured [75].

2.4.6. Ion chromatography

Ion chromatography (IC) or ion-exchange chromatography is a technique for the separation of charged species and analysis of their concentrations. Separation of ions is done with the principle of varying affinity to a liquid mobile phase (MF) and a solid stationary phase (SF) [76]. In anionic IC, weak anionic exchangeable functional groups or counterions are linked to the surface of silica or polymer particles, which are positively charged [77]. The anions (B^-) in the sample undergo electrostatic interactions with the positive SF (R-X^+) and the counterions (A^-) in the SF are exchanged with analyte anions. The reaction can be expressed as:

$$R{-}X^+\,A^- + M^+\,B^- \Longleftrightarrow R{-}X^+\,B^- + M^+ + A^- \tag{2.4}$$

The analytes are then eluted or retained based on their charge. The ions that do not bind or bind weakest to the SF, will elute first. To further elute the stronger bound ions, a pH gradient at constant ion strength or a ion gradient at a constant pH is applied. pH changes the charge of the ions and will gradually elute the stronger bound ions. For the ionic strength gradient, a gradual increase of the counterions are applied and will compete with the analyte ions for the places on the positive SF [76, 77].

The instrument set-up is similar to a high-performance liquid chromatography (HPLC) instrument, consisting of a pump which pumps the liquid through the instrument, injector, pre-column, the analytical column, detector and software which processes the detector signals. The sample is injected after the pump and

before the column and are mixed with the MF. Often a pre-column is used for removal of potential inferences and particulate matter that can clog and break the analytical column. When eluted out of the column, the analytes are detected by a conductivity detector. The signals are then plotted as a function of retention time [76].

2.5. Quantification and quality control

Quality assurance (QA) and quality control (QC) is important in environmental and analytical chemistry to asses that the quality standards are met and to ensure accuracy and precision in the analytical results [78]. QA is the guarantee that the quality of the analytical results is what is claimed in the basis of the quality control applied in all stages from sampling to analysis. QA is not synonymous with quality control. QA is meant to protect the failures of the quality control and QC is therefore a essential component in QA. QA and QC are thus usually jointly recognised and often refereed to as QA/QC. QC is the maintenance and statement of the quality of the analytical results, specifically that it meets or exceeds some minimum standard based on known testable criteria [78]. The direct involvement of QA in this thesis is limited thus the focus of discussion will be on quality control.

QC is included in all steps from sampling to analysis and includes storage, transportation, preservation, preparation and analyses of the samples [79]. QC measures are important for the control of possible contamination when handling samples and from instruments, inferences, cross-contamination between samples, loss of the sample in preparation steps, inaccuracy in quantification etc. These effects can be accounted for through the usage of blanks, standards and replicates as well as validation of instruments [79]. Often due to limitations in time and resources, not all QC measures are possible to include but it is important to audit the effects the different steps have on the sample. Standardization of methods is important for securing the quality of the work, and for reproducibility and comparability of analytical data. The International Organisation of Standardization (ISO) provides guidance and standards for all the steps in management of environmental samples [80].

2.5.1. Sampling

Due to limitations in time and resources, especially for the field work, it is not always possible to follow all of the guidance in the ISO standards. However, basing

the field work on the standards will increase the quality, help prevent contamination and make the samples homogeneous and representative for the purpose [81].

The ISO 5667 series describes all the steps involved in water and sediment sampling. The series comprises of standards for designing and planning of the field work (ISO 5667:1) [81], sampling of river water (ISO 5667:6) [82], river sediment (ISO 5667:12) [83], seawater (ISO 5667:9) [84] and marine sediment (ISO 5667:19) [85] and the handling and preservation of water samples (ISO 5667:3) [86] and sediment samples (ISO 5667:15) [87]. ISO 5667:14 provides guidance on quality control and assurance [88].

Before sampling, it is important to plan the sampling so that the samples will be representative for the area and the objective wished investigated. When sampling for metal analysis, metal free equipment is important to use for sampling and handling to avoid contamination. Replicates for each sample location will increase the reliability of the analytical result [81]. For water sampling, the equipment should be rinsed with the sampling matrix at least three times to avoid cross-contamination. Preservation of water samples with acid, often nitric acid, and storage in low temperature in either refrigerator or freezer are important to prevent biological activity and chemical reactions in the sample [82, 84]. Labeling of samples and notes on exact sample location (e.g. GPS-coordinates and depth) are recommended to avoid mix-ups and for reporting and further monitoring of the site [81].

2.5.2. Blanks

Blanks account for interference by other species in the sample and for trace of analyte found in reagents used for sample preservation, preparation and analysis. Frequent measurement of blanks also detects whether analyte from previous samples are carried into subsequent analysis by adhering to vessels or instruments [89]. There are three types of blanks; field blank, method blank and reagent blank. Field blanks are brought out in the field and exposed to the environment that the samples are collected in to trace possible contamination from the sampling process. Method blanks are taken through all the steps in sample preparation and analysis to trace possible contamination from the preperation steps. A reagent blank is similar to a method blank but has not been subjected to all sample preparation procedures and monitors purity of reagents in analysis [90].

2.5.3. Standards

Standards are used for instrument calibration and instrument verification/accuracy. A standard is a material or solution containing a known amount of a specific substance(s) [74]. Certified reference material (CRM) is a standard with certified levels of analyte in realistic material similar to the matrix of the sample and is used for testing the efficiency of the sample preparation steps [91]. An external standard or a calibration standard is used for calibration of a analytical technique/instrument. The standard is an analyte or a group of analytes similar to the analyte of interest in the sample and is run separately from the sample in different concentrations. Concentration is then plotted as a function of peak area in a calibration curve. The unknown concentration in the sample is then determined by using the measured peak area and the calibration curve. An internal standard is an analyte or a group of analytes chemically similar to the analytes of interest and are added to the sample at a constant concentration. The internal standard must be an analyte chemically similar but different from the analytes of interest in the sample. A calibration curve is then made by plotting the internal standard peak area to analyte peak area ratio as a function of the known constant concentration [74].

2.5.4. LOD and LOQ

Limit of detection (LOD) is the smallest concentration of analyte in the sample which can be reliably distinguished from zero [92]. LOD is often set to being the concentration which induces signals that is three times higher than the background noise levels. Noise is the change in detector response caused by drift, chemicals, electrical components and other variations in the system without the sample being present. Concentrations over the LOD is not necessarily quantifiable. Limit of quantification (LOQ) is the smallest concentration of analyte in the sample which can be reliably quantified. LOQ is often set to the concentration which induces signals that are ten times higher than the background noise level [92].

2.6. Statistical analysis and data treatment

Statistical analysis and data treatment is essential to evaluate the reliability of analytical data [93].

2.6.1. Mean

When a data set is symmetrical distributed, the mean is the best statistical representation of the central tendency in the data set [93]. The mean of a data set is the arithmetic average ($\overline{x}$) and is defined by

$$\overline{x} = \frac{\sum_i x_i}{n} \tag{2.5}$$

where x_i is the individual result and n is the number of results [93].

2.6.2. Median

When no assumptions on the distribution of a data set can be made or if the distribution is distinctly asymmetrical, the median is the best statistical representation of the central tendency in the data set [93]. The median is the value in the middle of a data set put in ascending order of magnitude. The place of the median of a data set can be found with

$$\frac{n+1}{2} \tag{2.6}$$

where n is the number of data. If the number of data is even, the formula 2.6 will give a place in between two values. The median of the data set is then the mean between these two values [93].

2.6.3. Standard deviation

The standard deviation is a measure of spread in a data set and how close the values in the data set is distributed around the mean [93]. The standard deviation (STD) of a data set is defined by

$$STD = \sqrt{\frac{\sum_{i=1}^{n}(x_i - \overline{x})^2}{n-1}} \tag{2.7}$$

where x_i is an individual measurement, $\overline{x}$ is the mean and n is the number of results. A low standard deviation means that the data is closely clustered around the mean, while a high standard deviation means the data is dispersed over a wider range of values. The relative standard deviation (RSD) is also commonly used and is the standard deviation relative to the mean. RSD is expressed by

$$RSD = \frac{STD}{\overline{x}} \tag{2.8}$$

RSD in percentage is also used, RSD x 100 and is called the coefficient of variation [93].

2.6.4. Normal distribution

A data set is normally distributed when the results are distributed symmetrical around the mean in a bell-shaped curve [94]. The curve can be divided into three areas: 68.2%, 95.4% and 99.7% or $\pm 1\sigma$, $\pm 2\sigma$ and $\pm 3\sigma$. In the area around the mean, where the curve is highest and has the biggest area, 68% of the data lies within $\pm$ one standard deviation, or 1σ, of the mean. 95.4% of the data will lie within $\pm$ two standard deviations (2σ) of the mean and 99.7% of the data will lie within $\pm$ three standard deviations (3σ) of the mean. This means that most of the data will be distributed around the mean within $\pm$ one standard deviating [94]. A Shapiro-Wilk test can be applied to confirm if a data set is normally distributed [95].

2.6.5. Statistical tests

To test if the variances in data sets are caused by random variation or errors, statistical test can be applied. The statement being tested is called the null hypothesis (H_0), often assuming that there are no differences between the results

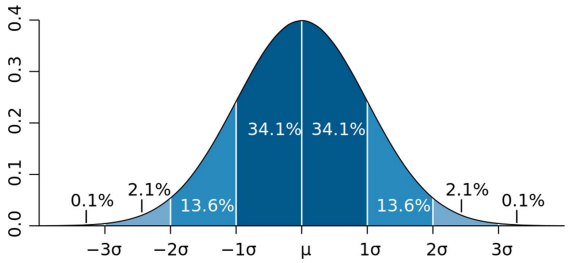

Figure 2.8.: Normal distribution curve. Source: Wattels *et al.*, 2014 [94].

in the data set [96]. Statements that are contradictory to the null hypothesis is called the alternative hypothesis (H_1). The null hypothesis is tested for statistical significance by calculating a p-value. The p-value is given a threshold, often 0.05. If the p-value is below 0.05, the null hypothesis is rejected and the result is statistically significant meaning that the variance in the data set are significantly different. If the p-value is over 0.05, the null hypothesis is approved and the result is not statistically significant meaning that the variance in the data set are not significantly different. The threshold of 0.05 means that in 5% of the cases due to random variations, the null hypothesis will be falsely rejected [96].

Parametric tests assume a normal distribution of the data, while non-parametric tests do not. A student t-test is a parametric test and is used when comparing means of two normally distributed data sets. When comparing means of several data sets a one-way ANOVA test can be applied [97, 98]. When comparing non-normally distributed data sets, the non-parametric Mann Whitney U-test and the Kruskal-Wallis test can be applied when comparing two or several data sets respectively [99, 100].

2.6.6. Correlations

Linear correlation

To test the linear correlation between two variables, linear regression can be applied [96]. This will give a formula for the linear correlation with a coefficient of correlation, R, and a coefficient of determination, R^2. R is a value between -1 and 1, indicating if there is a negative or postive correlation. -1 is a perfect negatice correlation and 1 is a perfect positive correlation. R^2 is a value between 0 and 1, and will give an estimate on how strong the correlation is. $R^2 = 1$ is considered a perfect correlation and $R^2 = 0$ indicates no correlation. A R^2-value of 0.98 means that 98% of the variance is accounted for by the regression of the data [96].

Spearman correlation test

A Spearman correlation test is a non-parametric test and measures the strength and direction of a monotonic association between two ranked variables [101]. The test will give a correlation coefficient (r_s) which is a value between -1 and 1, - indicating a negative relationship between the variables and + a positive relationship. $r_s = -1$ is a perfect negative correlation, $r_s = 1$ is a perfect positive correlation and $r_s = 0$ means no correlation. The test will also give a p-value which will accept or reject the null hypothesis and confirm or deny if the correlation is significant. Five assumptions are made for the Spearman correlation test [101]:

- The data must be a truly random sample representative of the population of interest
- The data must exhibit a monotonic correlation
- Both variables should be measured on a continuous (interval or ratio) or ordinal scale
- The data contains paired variables (there must be data for each ranking of the data)
- The variables should be independent of each other

Principal component analysis

When having a large set of data, it can be difficult to recognize patterns and relationships between the variables. Principal component analysis (PCA) is a multivariate mathematical technique that simplifies the complexity of high-dimensional data while retaining trends and patterns [102, 103]. PCA reduces the data by projecting it to lower dimensions called principal components (PCs) while most of the variables are retained. PCs are linear combinations of the variables in the data and convert the correlations to a two-dimensional (2D) plot [103].

The axes in the 2D-plot, PC1 (horizontal axes) and PC2 (vertical axes), are ranked in the order of importance. PC1 accounts for most of the variance in the data, while PC2 accounts for the second most of the variance, meaning that differences in the variables in PC1 are more important than the differences along PC2. The variables that are closely related will appear as clusters spread along the two axes. Due to PC1 accounting for more of the variance, clusters that are close to each other along the PC1 axes are more correlated, than those who are close along the PC2 axes. The further apart the clusters are from each other, the less they are correlated, depending on if they are separated in the PC1 or PC2 direction [102, 103].

3. Field work

3.1. Study area and sampling sites

Field work and sampling were carried out from 17th-24th of August 2020 in Brøgger Peninsula (Brøggerhalvøya) in Kongsfjorden, Spitsbergen (79°N, 12°E). This study's focus is on the glacier Austre Brøggerbreen and the river Bayelva placed in Brøggerdalen and the fjord Kongsfjorden, all situated close to Ny-Ålesund International Research Facility. The study area covers an area of about 33 km^2 [24]. Maps of the study area are presented in Figure 3.1 and photos of the area is presented in 3.2a-3.2d.

The Bayelva basin contains two glaciers, Austre (eastern) and Vestre (western) Brøggerbreen which are bounded by steep mountains and they cover about 50% of the catchment area [104]. Meltwater and runoff from the glaciers form streams that cut through moraine deposits and form braided drainage systems. The streams flow through a sandur, consisting of mostly boulders and gravel with patches of sand and silt (Figure 3.2a), and form large lateral channels from both glaciers which converge after approximately 1 km from the glacier mouths (Figure 3.2b). Bayelva river is then formed by the joining of these channels at the end of the basin and flows as a single or braided channels through resent terminal moraines and a rock channel (Figure 3.2c) 2 km down to and out into the fjord Kongsfjorden at a large delta (Figure 3.2d) [24, 105, 106].

Austre and Vestre Brøggerbreen extends from 650 to 50 m above sea level and each covers about 50% of the glacier covered area in the basin. Austre Brøggerbreen covers an area of 5 km^2 (2017) and has a thickness of less than 100 m. Austre Brøggerbreen is a polythermal glacier. Runoff from the glacier to Bayelva is from surface melting during the melting season [104, 107, 108]. The melting season lasts from the end of May until early October and creates the most intense flows in June, July and August. During the winter, Bayelva freezes to the stream bed [24]. Most of the runoff from Austre Brøggerbreen reaches the catchment and Bayelva through small lateral channels on the surface of the glacier and through moulins [104, 106]. The moulins are believed to reach the bed of the glacier [109]. The water reaching the bed of the glacier flows in a subglacial channel and reaches

the snout of the glacier [110].

Bayelva is approximately 4 km long and it is indicated that >50% of the discharge originates from Austre Brøggerbreen [108]. In addition to runoff from the glaciers and snowmelt during the melting season, two streams contribute with runoff to Bayelva: Tvillingsbekken and Mørebekken. Tvillingsbekken (east of the Bayelva basin) runs from Tvillingsvatne, a lake close to Bayelva which serves as water supply for Ny-Ålesund, to Bayelva approximately 2 km downstream from the glacier mouth (Figure 3.1). Mørebekken is a meltwater stream from the glacier Mørebreen (west of the Bayelva basin) and meets Bayelva at the delta close to the outlet to Kongsfjorden.

Kongsfjorden, located to the north of the basin, is about 20 km long and varies from 4 km to 10 km in width [111]. The depth is relatively shallow, less than 100 m along the islands of Lovenøyane and Blomstrandøya. There is a submarine hallow in the center of the fjord with a depth of more than 400 m [111].

The Bayelva basin is located approximately 2 km west from Ny-Ålesund. Ny-Ålesund was originally established as a mining settlement in 1916 but was closed down after a major mining accident in 1962 [112]. Between 1917 and 1962, an estimate of approximately 1.43 million tons of coal was exported from Ny-Ålesund [2]. Since 1964, Ny-Ålesund has been a research facility with 30-150 inhabitants depending on the season [112]. A small airstrip is located close to the basin. Ny-Ålesund has been a destination for tourism since the last century which has increased largely the last ten years. Approximately ten thousand tourists visit Ny-Ålesund every year which has led to an increase in cruise ship traffic to the area [112].

3.1.1. Geology

The basin consist of many different types of rocks due to thrusting 145-2.6 million years ago (Cretaceous/Tertiary) [105]. The rock types in the basin mainly consist of silicates and carbonates. Silicates are composed by SiO_2 in various structures. Carbonates are composed by ions bound to $CO_3{}^{2-}$, e.g., calcium carbonate ($CaCO_3$). Carbonates are easily weathered while silicates often are resistant to weathering [114]. The mountains in the southern part of the basin, consist mostly of Proterozoic basement rock, including quartzites and phyllites which are silicate based metamorphic rocks. Patches closest to Austre Brøggerbreen, also consist of conglomerate, reddish sandstone and shale [105, 115, 116]. Shale is silicate or aluminosilicate based. Reddish sandstone is mainly composed of quartz (SiO_2) and feldspar (aluminosilicates). Reddish sandstone is enriched with iron oxide, coloring it red [114]. The reddish sandstone is what colors the runoff from Austre

Figure 3.1.: Map of study area, including Austre and Vestre Brøggerbreen, Brøggerdalen, Bayelva, Kongfjorden og Ny-Ålesund. Source: Norwegian Polar Institute n.d. [113].

Brøggerbreen and makes Bayelva reddish [105, 115, 116]. This is shown in Figure 3.2b where runoff from Austre and Vestre Brøggerbreen meet. The reddish runoff can be seen in contrast to the gray runoff from Vestre Brøggerbreen.

The south-eastern part is dominated by garnet-mica schist and quartz carbonate schist, while the eastern part is dominated by carbonate rocks, phyllite and quartzite. In the northern and western part, chert, sandstone, limestone, dolomite, anhydrite, siliceous shale and coal are mostly present [105, 115, 116]. Limestone and dolomite are calcium carbonate based. Dolomite can also consist of magnesium carbonate while chert is composed of quartz [114]. The bedrock of the river is sedimentary and consists mostly of limestone, shale and sandstone [24]. The vegetation is otherwise sparse with a uniform cover of lichen with patches of mountain avens (*Dyras octopetala*) and rock sedge (*Carex rupestris*) [104]. There are no trees or shrubs.

Trace elements can be incorporated in rocks and minerals. Shale can contain Cu, Pb, and Zn. Coal often includes metals considered especially toxic, like Hg, Pb, As, Cd and Cr. Limestone can also be enriched with toxic trace elements [117, 118]. A more detailed overview of the geochemistry in the Bayelva basin is presented in Table 3.1.

Table 3.1.: Composition of different types of minerals and rocks found in Brøggerdalen. The table continues on the next page.

Name	Rock type/mineral	Composition
Apatite	Mineral	$Ca_5(PO_4)_3(FCIOH)$ [114]
Amphibole	Mineral	$(Mg, Fe, Ca, Na)_{2-3}(Mg, Fe, Al)_5(Si, Al)_8O_{22}OH_2$ [114]
Anhydrite	Mineral	Calcium calcite ($CaSO_4$) [119]
Calcite	Mineral	Calcium carbonate $CaCO_3$ [114]
Chlorite	Mineral	Group of silicate minerals with a negative charge $[(R^{2+}, R^{3+})_3(Si_{4-x}R^{3+}_x)O_{10}(OH)_2]^-$ that is balanced by a positivly charged interlayer octahedral sheet $[(R^{2+}, R^{3+})(OH)_6]^+$ [120]
Coal	Mineral	C, O and H, N, S (Anthracite and bituminous coal) [114]
Feldspar	Mineral	$NaAlSi_3O_8$, $KAlSi_3O_8$ and $CaAlSi_2O_8$ [114]
Garnet	Mineral	$Ca_3Al_2(SiO_4)_3$ [114]
Illite	Mineral	$K_{0.65}Si_{3.35}Al_{0.65}Al_2O_{10}(OH)_2$ [121]
Kaolin	Mineral	$Al_4Si_4O_{10}(OH)_8$ [114]
Kyanite	Mineral	Al_2SiO_5 [122]
Mica	Mineral	Aluminosilicate of K/Na, Fe/Na and rarely Li or Cr [114]
Montmorillonite	Mineral	Phyllosilicate: Mg, Al, K, Na, Ca silicates (Si_2O_5) hydrated with either water or hydroxyl groups [123]
Muscovite	Mineral	$KAl_2(AlSi_3O_{10})(OH)_2$ [124]
Paragonite	Mineral	$NaAl_2[(OH)_2AlSi_3O_{10}]]$
Quartz	Mineral	Silicone dioxide (SiO_2) [114]
Sericite	Mineral	Mica made of muscovite, illite or paragonite [114]
Smectite	Mineral	$(Ca^{2+}, Mg^{2+})_{0.33}Al_2(Si_{3.67}Al_{0.33})O_{10}(OH)_2$ [123, 125]
Staurolite	Mineral	$Fe_2Al_9O_7(OH)(SiO_4)_4$ [114]
Talc	Mineral	$3MgO, 4\,SiO_2H_2O$ [114]

Name	Rock type/mineral	Composition
Argillite	Sedimentary rock	Lithified mud and oozes [114]
Chert	Sedimentary rock	Microcrystalline or cryptocrystalline quartz [114, 126]
Conglomerate	Sedimentary rock	Clasts of preexisting rocks and minerals within fine-grained matrix [114]
Dolomite	Sedimentary rock	$Ca/MgCO_3$ and/or silica [114]
Flint	Sedimentary rock	Cryptocrystalline quartz [127]
Limestone	Sedimentary rock	Mainly calcite (calcium carbonate ($CaCO_3$) mineral), aragonite (crystalline $CaCO_3$, skeletal fragments of marine organisms and silica (chert and flint) [114]
Sandstone	Sedimentary rock	Mainly quartz and/or feldspar and other durable minerals in between [114]
Shale	Sedimentary rock	Argillaceous sediments of aluminosilicates and clay mineral (kaolin, montmorillonite, illite and chlorite [114]
Phyllite	Metamorphic rock	Quartz, sericite, mica and chlorite [114]
Quartzite	Metamorphic rock	Monomineralic and dominantly of quartz [114]
Schist	Metamorphic rock	Micas, chlorite, talc, quartz, feldspar, garnet, kyanite, staurolite [114]

(a) Meltwater channel at the snout of Austre Brøggerbreen.

(b) Meltwater (red) from Austre Brøggerbreen meets meltwater (gray) from Vestre Brøggerbreen.

(c) Bayelva flowing trough moraines in braided channels.

(d) The delta where Bayelva flows into Kongsfjorden.

Figure 3.2.: Photos of Bayelva.

3.2. Sampling

Samples were collected from three sampling sites: the glacier Austre Brøggerbreen, from the river Bayelva and the fjord Kongsfjorden. Field work and sampling was planned and carried out based on *ISO 5667-1:2020(E) Water quality — Sampling — Part 1: Guidance on the design of sampling programmes and sampling techniques* [81]. Metal free equipment and gloves were used when sampling and handling samples to avoid contamination. Sample data on sample ID, sample type, sampling site, sampling point, sampling container and sampling depth are given in Table B.1.

3.2.1. Austre Brøggerbreen

Supraglacial material and glacier water samples from Austre Brøggerbreen were collected from seven points. A map of sampling points is shown in Figure 3.3 and their respective coordinates are presented in Table A.1. A total of 14 supraglacial material samples, two at each point, were collected from cryocoonite holes (water-filled holes) or small mounds on the surface of the glacier. The supraglacial material was fine grained with varying color, texture and density. The samples are descried in more detail in Table 3.2 and example photos are shown in Figure 3.4a-3.4d.

Supraglacial material was collected in 50 mL metal free polypropylene (PP) tubes. For the samples collected from cryoconite holes, water was included in the sampling tubes. Sample ID and sampling points are presented in Table 3.2. Supraglacal material samples were later transferred to metal free cc-cups and stored in the freezer at -20°C. Excess water from samples collected in water was avoided transferred to cc-cups. The remaining water was kept in the PP tube and frozen at −20 °C. These water samples are denoted with a "W" after its respective supraglacial material sample number (Table 3.2). Supraglacial material and glacier water sampling and handling was carried out based on *ISO 5667-3:2018(E) Water quality — Sampling — Part 3: Preservation and handling of water samples*, *ISO 5667-6:2014(E) Water quality Sampling Part 6: Guidance on sampling of rivers and streams* [82], *ISO 5667-14:2014(E) Water quality — Sampling — Part 14: Guidance on quality assurance and quality control of environmental water sampling and handling* [88], [86], *ISO 5667-12:2017(E) Water quality — Sampling — Part 12: Guidance on sampling of bottom sediments from rivers, lakes and estuarine areas* [83] and *ISO 5667-15:2009(E) Water quality — Sampling — Part 15: Guidance on the preservation and handling of sludge and sediment samples* [87].

Table 3.2.: Sampling ID and description of color, the sampling point, texture and density of supraglacial material samples collected from the glacier Austre Brøggerbreen. Example photos of the supraglacal material are shown in Figure 3.4a-3.4d. Respective coordinates for the sampling points are presented in Table A.1.

Sample	Point	Color	Found in	Description
1 + 1W 2 + 2W	P1	Red	Cryoconite hole	Light
3 + 3W 4	P2	Red-brown	Cryoconite hole	
5 6	P3	Black	Mound	Dense
7 + 7W 8	P4	Brown	Cryoconite hole	
9 + 9W 10 + 10W	P5	Red	Cryoconite hole	Light
11 12	P6	Brown	Cryoconite hole	Dense
13 + 13W 14 + 14W	P7	Brown	Cryoconite hole	

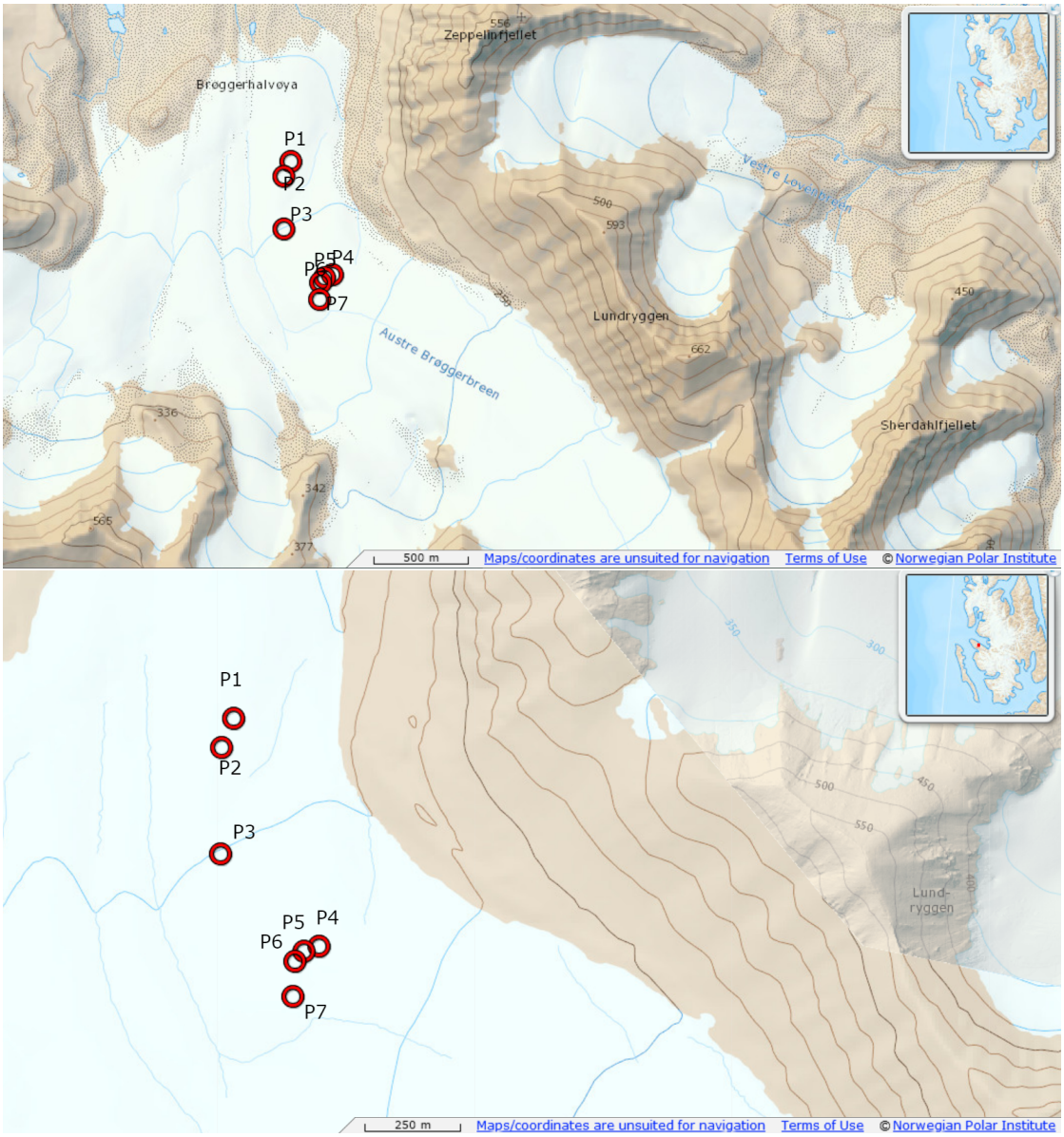

Figure 3.3.: Map of sampling site and points on the glacier Austre Brøggerbreen. Respective coordinates for the sampling points are presented in Table A.1. Source: Norwegian Polar Institute n.d.

(a) Photo of mound with black, dense supraglacial material.

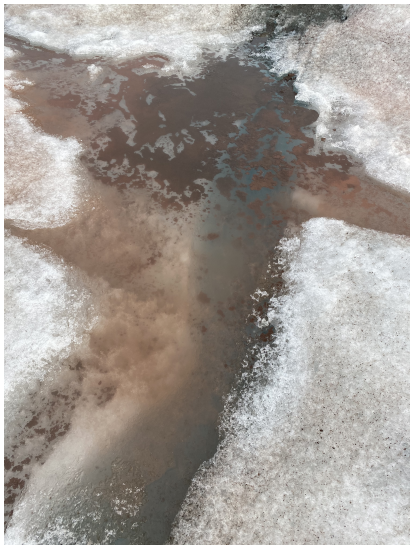

(b) Photo of cryoconite hole with red, light supraglacial material.

(c) Photo of cryoconite hole with brown supraglacial material.

(d) Photo of cryoconite hole with red-brown supraglacial material.

Figure 3.4.: Photos of supraglacial material collected from Austre Brøggerbreen.

3.2.2. Bayelva

River water and overbank sediment samples were collected from eight different points along the river Bayelva. A map of sampling points is shown in Figure 3.5 and their respective coordinates are presented in Table A.1. A total of 16 water samples, two at each point, were collected in 50 mL metal free PP tubes. A total of 12 overbank sediment samples were collected in metal free cc-cups. Two samples were collected at each point except for at point P12, P13 and P15. Only one sample of overbank sediment was collected at point P12 and P13 and none at point P15 due to limited sampling equipment. Sample ID and sampling points are presented in Table 3.3.

River water samples were filtered with a 0.5 µm filter and 10 mL filtered water was transferred to 15 mL metal free PP tubes. Samples were conserved with three drops of ultra-pure concentrated (65%) nitric acid (HNO_3) before stored in the refrigerator at 4 °C. Overbank sediment samples were stored in the freezer at −20 °C. River water sampling and handling was carried out based on *ISO 5667-3:2018(E) Water quality — Sampling — Part 3: Preservation and handling of water samples*, *ISO 5667-6:2014(E) Water quality Sampling Part 6: Guidance on sampling of rivers and streams* [82] and *ISO 5667-14:2014(E) Water quality — Sampling — Part 14: Guidance on quality assurance and quality control of environmental water sampling and handling* [88]. Overbank sediment sampling and handling was carried out based on [86], *ISO 5667-12:2017(E) Water quality — Sampling — Part 12: Guidance on sampling of bottom sediments from rivers, lakes and estuarine areas* [83] and *ISO 5667-15:2009(E) Water quality — Sampling — Part 15: Guidance on the preservation and handling of sludge and sediment samples* [87].

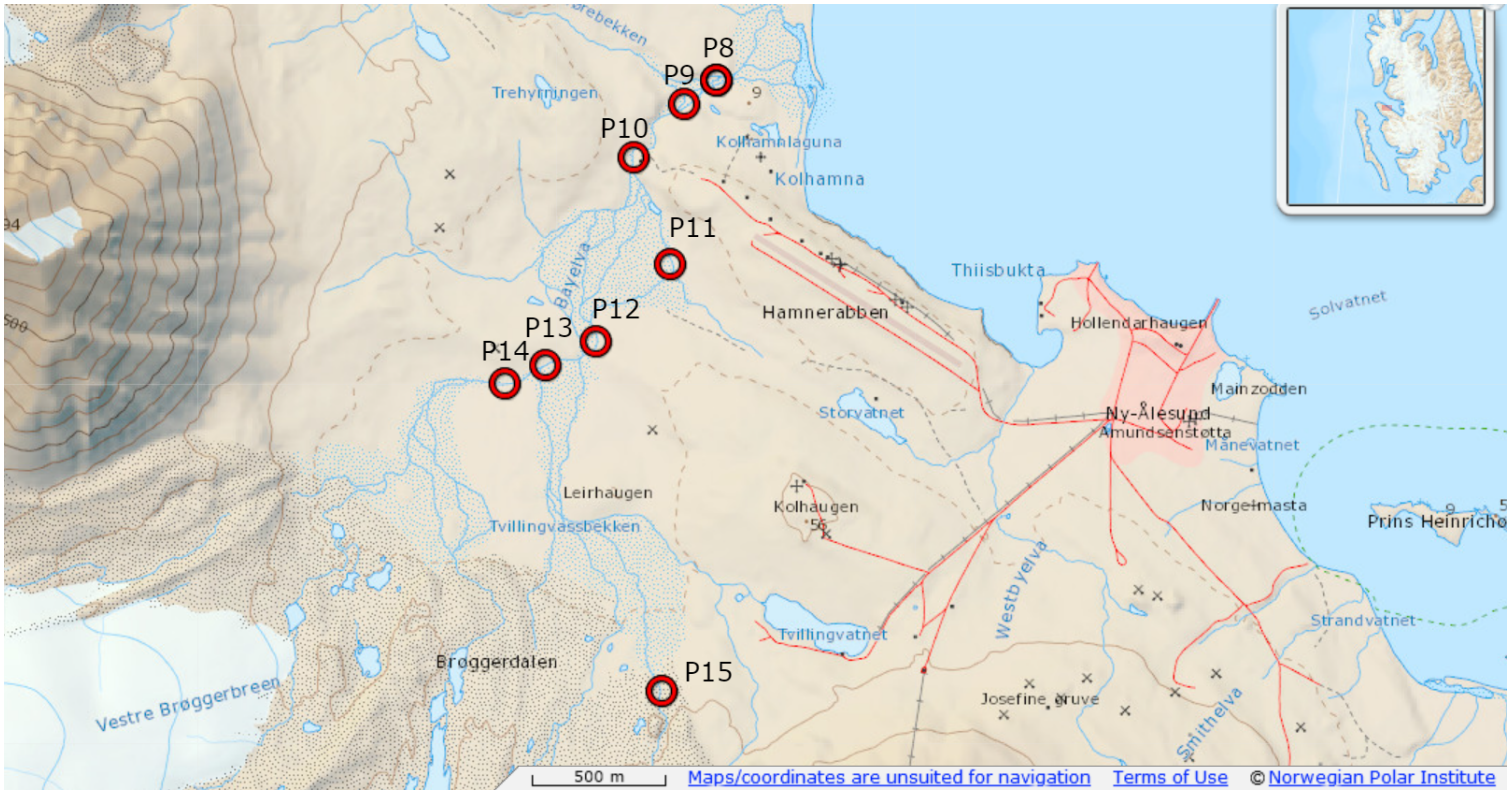

Figure 3.5.: Map of the sampling area and sampling points along the river Bayelva. Respective coordinates for sampling points are presented in Table A.1. Source: Norwegian Polar Institute n.d.

Table 3.3.: Sample ID for river water and overbank sediment samples collected from the river Bayelva and their respective sampling points. Respective coordinates for the sampling points are presented in Table A.1.

Sample		Point
Water	**Overbank sediment**	
15	31	P8
16	32	
17	33	P9
18	34	
19	35	P10
20	36	
21	37	P14
22	38	
23	39	P13
24		
25	40	P12
26		
27	41	P11
28	42	
29	-	P15
30		

3.2.3. Kongsfjorden

Sample collection in the fjord Kongsfjorden was carried out by boat (Teisten [128]) at eight different points. A map of sampling points is shown in Figure 3.6 and their respective coordinates are shown in Table A.1. Seawater was collected at different depths, 1 m, 2 m, 5 m, 10 m and close to the bottom, if possible. Seawater samples at 1 m was sampled with a hose. For depths below 1 m, water samples were collected with metal free Teflon 10 L Niskin bottles. A total of 34 seawater samples were collected in 15 mL metal free (PP) tubes. For sampling point P16-P19, a total of 16 seawater samples were also collected in 50 mL metal free PP tubes for filtering. Seawater samples at each sampling point at the different depths are shown in Table 3.4.

Seawater samples collected in 50 mL metal free PP tubes (sample 77-92) were filtered with a 0.5 µm filter. 10 mL of filtered seawater was transferred to 15 mL metal free PP tubes and conserved with three drops of ultra-pure concentrated (65%) HNO_3. Unfiltered seawater samples (sample 43-76) were conserved with five drops of ultra-pure concentrated (65%) HNO_3. Seawater sampling and handling was carried out based on *IS0 5667-9: 1992(E) Water quality - Sampling - Part 9: Guidance on sampling from marine waters* [84] and *ISO 5667-14:2014(E) Water quality — Sampling — Part 14: Guidance on quality assurance and quality control of environmental water sampling and handling* [88].

Marine sediment samples were collected with a Van Veen Grab 500 cm^2. 12 samples, two samples at each point, of the top 2 cm was collected in metal free cc-cups. Sediment was not sampled at site P16 and P17 due to seaweeds and gravel at the bottom. Sampling points and sampling depths are presented in Table 3.5. Sediment samples were stored in the freezer at −20 °C. Marine sediment sampling and handling was carried out based on *ISO 5667-19:2004(E) Water quality — Sampling — Part 19: Guidance on sampling of marine sediments* [85] and *ISO 5667-15:2009(E) Water quality — Sampling — Part 15: Guidance on the preservation and handling of sludge and sediment samples* [87].

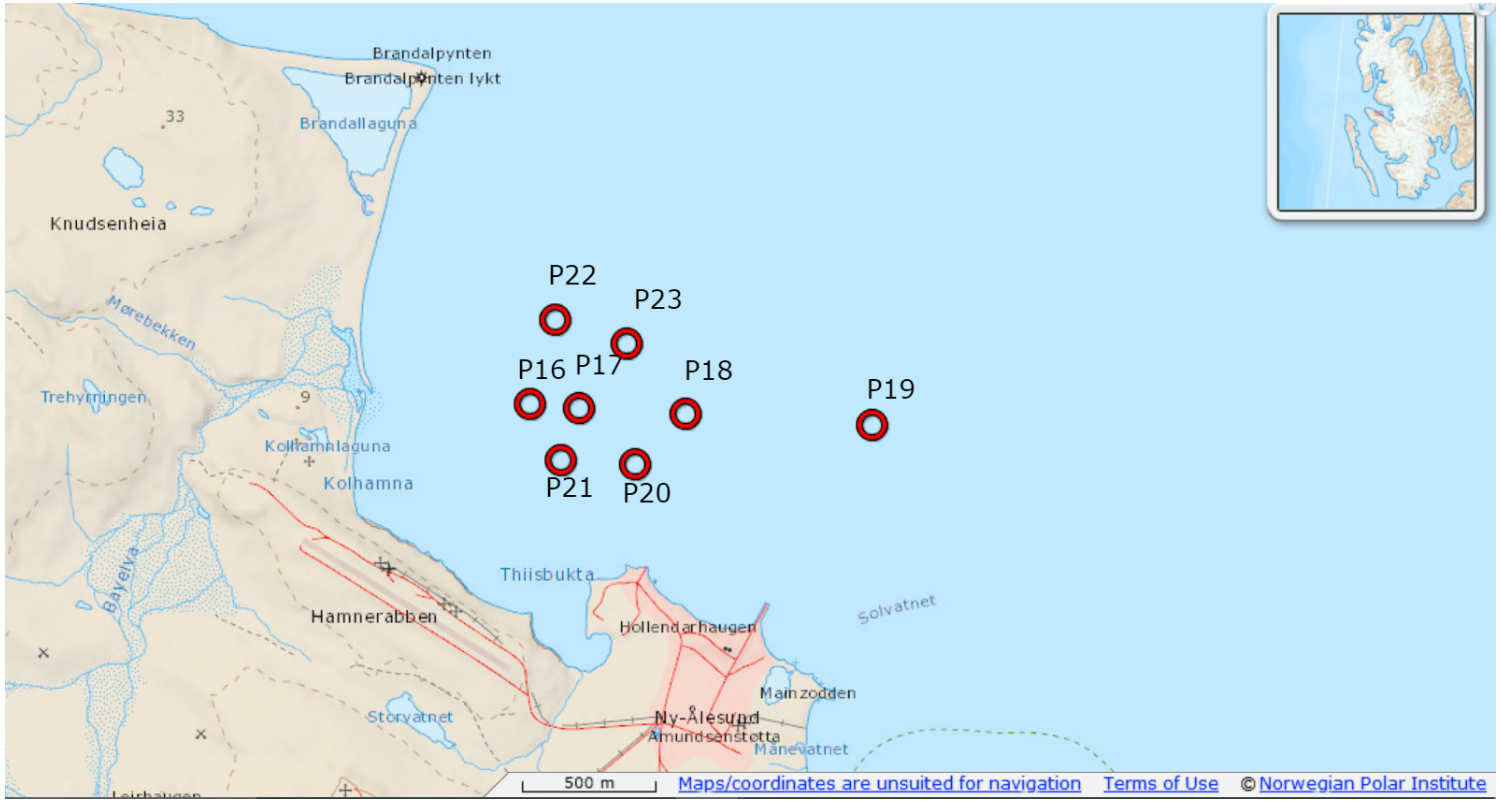

Figure 3.6.: Map of the sampling area and sampling points in the fjord Kongfjorden. Respective coordinates for sampling points are presented in Table A.1. Sorce: Norwegian Polar Institute.

Table 3.4.: Sample ID for unfiltered and filtered seawater samples collected from the fjord Kongsfjorden. Respective coordinates for sampling points are presented in Table A.1.

Sample		**Point**	**Depth [m]**
Unfiltered	**Filtered**		
43	77		1
44	78	P16	2
45	79		5
46	80		1
47	81	P17	2
48	82		5
49	83		1
50	84		2
51	85	P18	5
52	86		10
53	87		48
54	88		1
55	89		2
56	90	P19	5
57	91		10
58	92		140
59			1
60			2
61	-	P20	5
62			10
63			25
64			1
65	-	P21	2
66			5
67			1
68			2
69	-	P22	5
70			10
71			18
72			1
73			2
74	-	P23	5
75			10
76			43

Table 3.5.: Sampling ID, sampling point and sampling depth (m) for marine sediment samples collected from the fjord Kongsfjorden. Respective coordinates for sampling points are presented in Table A.1.

Sample	Point	Depth [m]
-	P16	5
-	P17	5
93 94	P18	50
95 96	P19	142
97 98	P20	27.6
99 100	P21	5.7
101 102	P22	18.6
103 104	P23	47.6

4. Materials and methods

4.1. Sample preparation

4.1.1. Freeze drying

Supraglacial material samples (sample 1-14), overbank sediment (sample 31-42) and marine sediment (sample 93-104) samples in metal free cc-cups were covered with parafilm, to avoid cross contamination. A hole was made in the parafilm with metal free plastic pipettes to let vapor out during drying. Samples were then freeze dried with Christ Alpha 1-4 LD plus under vacuum at $-21\,^{\circ}\mathrm{C}$ (0.94 mbar) for 48 hours followed by a final drying under vacuum at $-43\,^{\circ}\mathrm{C}$ (0.090 mbar) for 20 minutes. Samples were weighted before and after freeze drying to determine water content (Table C.1). Samples were stored in cc-cups in room temperature after drying.

4.1.2. Digestion with UltraCLAVE

Milestone UltraCLAVE was used for microwave digestion of freeze-dried supraglacial material, overbank sediment and marine sediment samples. The temperature, pressure and power gradient program over time is presented in Figure C.1. Basic load contained 300 mL of ultra-pure type I water provided by an ELGA Purelab Chorus water purification system, 30 mL 30% hydrogen peroxide and 2 mL 96% sulfuric acid. 250-350 mg of sample was weighted out in Teflon vials for digestion (Table C.1) and added 9 mL of ultra-pure 50% nitric acid. Microwave digestion of the samples was done in two rounds. One vial with GBW07408 Soil certified reference material (CMR) and three blanks were included in both rounds for quality control. Samples were diluted with ultra-pure type I water to about 108-124 g after digestion (Table C.1). 15 mL digested and diluted samples were transferred and stored in metal free HDPP tubes in room temperature for ICP-MS analysis.

4.2. Analysis

4.2.1. Elemental analysis with ICP-MS

Due to instrument malfunctions, a 25 times dilution with ultra-pure type I water provided by an ELGA Purelab Flex 3 water purification system and 65% nitric acid (HNO_3) to make a 0.6 M solution, was carried out for digested and already diluted supraglacial material (sample 1-14), overbank sediment (sample 31-42) and marine sediment samples (sample 93-104) and a 30 times dilution with ultra-pure type I water and 65% HNO_3 to make a 0.1 M solution was carried out for seawater samples (sample 43-92). All samples (sample 1-104) were analyzed with high resolution Inductively Coupled Plasma - Mass Spectrometry (HR-ICP-MS) for elemental analysis at three institutions: St. Olavs Hospital, NTNU and SINTEF.

Supraglacial material and sediment samples

Element analysis of supraglacial material (sample 1-14), overbank sediment (sample 31-42) and marine sediment (sample 93-104) where performed at St. Olavs. Element levels were measured using HR-ICP-MS on a Thermo Finnigan Element 2 instrument (Thermo Finnigan, Bremen, Germany) of 64 elements. Tuning parameters applied are presented in Table 4.1.

Table 4.1.: Tuning parameters for analysis with Thermo Finnigan Element 2 HP-ICP-MS instrument.

Parameter	Value
Power	1250 W
Cool gas flow	16 L/min
Auxiliary gas flow	0.99 L/min
Sample gas flow	ca 1.0 L/min (optimized before every analysis)

The resolution mode used for the individual elements is indicated by LR (low), MR (medium) and HR (high) next to the element and atomic mass in the result sheet. The following internal standards at a concentration of 2 µg/L in solution were applied:

- Re for the elements Tb, Dy, Ho, Er, Tm, Yb, Lu, Hf, Ta, W, Eu og Gd
- Ir for the elements Pb, Pt, Au, Hg, Tl, Bi, Th, U
- Rh for the rest

Concentration of Cd in all samples is corrected according to the Mo content and formation of MoO which interfere with Cd. The same is for Hg from WO and Pt from HfO. Concentrations of all samples were also corrected for dilution factor of 1.020408 for the manually internal standard addition. Concentration of all elements were given in µg/L and were calculated to µg/g sample and corrected for the 25 times dilution done upon analysis.

River water samples

River water samples (sample 31-42) were analyzed with HP-ICP-MS on an Agilent 8800 ICP-QQQ instrument for 64 elements at NTNU. Tuning parameters for each sample are presented in Table D.1 and Figure D.1-D.3.

Seawater samples

Element analysis of seawater samples (sample 43-92) were performed with HP-ICP-MS for 64 elements at SINTEF. Samples were measured by an Agilent 8800 Triple Quadrupole ICP-MS (Agilent Technologies, USA) with ISIS (Integrated Sample Introduction System), SPS4 autosampler (Agilent Technologies, USA) and a standard sample introduction system (Micro Mist glass concentric nebulizer, quartz double pass spray chamber, quartz torch with 2.5 mm id and standard nickel cones). No gas and oxygen modes were used in this method. Tuning conditions are shown in Table 4.2.

Listed are corrections done for the following elements:

- 114Cd = M(114Cd) * 1 – M(118Sn) * 0.0270
- 115In = M(115In) * 1 – M(118Sn) * 0.0140 (In: Internal Standard)
- 208Pb = M(206Pb) * 1 + M(207Pb) * 1 + M(208Pb) * 1 (i.e. isotopes are summed up)

All results and LOQ's are corrected for the 30x dilution done upon analysis.

4.2.2. Determination of Total Carbon and Total Nitrogen content

Freeze dried supraglacial material samples (sample 1-14) were analyzed for Total Carbon and Total Nitrogen (TC/TN) content with the procedure based on *ISO 10694:1995(E) Soil quality - Determination of organic and total carbon after dry combustion (elementary analysis)* [71]. 75-125 mg samples (Table E.2) in ceramic

Table 4.2.: Tuning parameters for analysis with Agilent 8800 Triple Quadrupole ICP-MS instrument.

Parameter	Value
RF Power	1550 W
RF Matching	1.80 V
Sample depth	8.0 mm
Nebulizer Gas Flow	1.05 L/min
Option Gas Flow	0.0 L/min
Make Up Gas Flow	0.0 L/min
Nebulizer Pump	0.1 rps
S/C Temp	2°C
Cell tuning modes	NoGas and O_2
O2 Flow Rate	30%
Scan Type	MS/MS
Replicate/peak pattern/sweeps	4/3/30

Skalar crucibles (2SN100370) were analyzed for TC/TN through combustion with ultra-pure oxygen (99.9995% purity) at 1200°C with Skalar PrimacsSNC100. Nitrogen free helium (99.995% purity) was used as carrier gas. Total Carbon was detected with an IR detector and Total Nitrogen with a Thermal conductivity detector (TCD) after reduction from nitrogen oxides to nitrogen through a copper reduction oven. A calibration curve was made with 6.3, 11.1, 20.0, 40.0, 80.5, 122.0 and 160.3 mg of dry glycine with carbon content of 32.00% and nitrogen content of 18.66% in the range of 2-52 mg C abs./ 1-30 mg N abs. (Table D.2). The calibration curves are shown in Figure D.4a and D.4b. Linear regression line for Total Carbon is y = 54754x + 15998 with R^2 = 0.9999 and linear regression line for Total Nitrogen is y = 300000x + 1910.1 with R^2 = 1.0000. Two blanks of empty crucibles in the beginning and four blanks at the end of the analysis were included (E.2).

4.2.3. Determination of Total Organic, Inorganic and Residue Oxidizable Carbon content

Freeze dried supraglacial material samples (sample 1-14) were analyzed for Total Organic Carbon (TOC), Total Inorganic Carbon (TIC) and Residue Oxidizable Carbon (ROC) according to *DIN 19539:2016-12 Investigation of solids - Temperature-dependent differentiation of total carbon (TOC_{400}, ROC_{600}, TIC_{900})* with Skalar PrimacsSN100 [73]. Determination of TOC, ROC and TIC was done

by combustion with ultra-pure oxygen (99.9996% purity) of 75-125 mg samples (Table E.3) in ceramic Skalar crucibles (2SN100370) at 400°C, 600°C and 900°C respectively to CO_2 gas. CO_2 at the different temperatures was detected with an IR detector and TOC, TIC and ROC content were measured. A calibration curve was made with 10.5, 25.5, 50.6, 78.7, 100.3, 124.8 and 150.6 mg calibration standard containing 2% for each form of carbon according to Skalar (Table D.4). The calibration standard consists of ammonium oxalate monohydrate (carbon content 16.90%), carbon black (carbon content to be determined before use), calcium carbonate (carbon content 12.00%) and aluminum oxide (carbon free). Blanks of empty crucibles were included (Table E.3).

4.2.4. Analysis of Total Organic Carbon with UV-Spectrometry

Glacier water samples (sample 1W-3W, 7W, 9W-11W, 13W and 14W) were analyzed for Total Organic Carbon (TOC) content based on EPA 600/R-09/122 [129] using UV-Spectrometry (Shimadzu UV mini 1240 UV-VIS spectrophotometer). The samples were analyzed in a quartz cuvette with wavelength 2450 nm. Standard calibration solutions were made from a TOC standard containing 1000mg/L pottasium hydrogen phthalate in distilled water with trace phosphoric acid (0.05%). Concentrations of 0.1, 0.5, 1.0, 2.0, 5.0 and 10 mg/L were prepared by dilution of the KHP standard (1000 mg/L). The calibration curve is presented in D.6 and showed linearity with R^2=0.9989. Regression line y = 0.0165x + 0.0012. The instrument was calibrated with ultra-pure Type I water provided by an ELGA Purelab Flex 3 water purification system before use and after every third sample measurement.

4.2.5. Anion analysis with Ion Chromatography

Glacier water samples (sample 1W-3W, 7W, 9W-11W, 13W and 14W) and river water samples (samples 15-30) were analyzed with Ion Chromatography (IC) for fluoride (F^-), chloride (Cl^-), nitrite ($NO_2{}^-$), bromide (Br^-), nitrate ($NO_3{}^-$), phosphate ($PO_4{}^{3-}$) and sulfate ($SO_2{}^{4-}$) with Metrohm IC instrument with software MagIC Net 3.2 connected to 940 Professional IC Vario 1 Conductivity detector. A Metrosep A Supp 7 250/4.0 column was used for separation with 3.6 mM Na_2CO_3 anion eluent. Eluent flow rate was 0.700 mL/min with a temperature of 45.0 °C and pressure over 10.00 mPa. Calibration curves with standard concentrations 0.2, 1.0, 2.0, 5.0 and 10.0 mol/L of all analysts are presented in Figure D.7 - D.13. Blanks of ultra-pure Type I water provided by an ELGA Purelab Flex 3 water purification system were included (Table E.5 and Figure E.3a and E.3b).

4.2.6. Determination of pH

pH measurements of supraglacial material samples (sample 1-14) were carried out based on *ISO 10390:2005(E) Soil quality - Determination of pH* [130]. Due to limited sample volume, samples collected at the same sample point were combined (Table E.6). 1 mL of sample for samples from P1 and P5 and 2 mL of samples from P2, P3, P4, P6 and P7 was used, also due to limited sample volume (Table E.6). A solution of 0.01 M potassium chloride (KCl) was prepared from 1.0 M KCl solution by dilution. 0.01 M KCl was added to a volume of 10 times the sample volume (Table E.6). The suspension was stirred with an automatic mixer for one hour and then let sink for one hour. The pH meter was calibrated with buffer solutions of pH 4, 7 and 10 before use. The pH meter was washed with Ultra-pure Type I water provided by an ELGA Purelab Flex 3 water purification system three times and placed in a solution of 0.1 KCl between each measurement.

4.3. Data analysis and statistical treatment

Data analysis and statistical treatment was done in Office Excel and IBM SPSS Statistics 27. Figures illustrating results are made in Office Excel and IBM SPSS Statistics 27. All data sets were tested for normal distribution with a Shapiro-Wilk Normal Distribution test. Results from the test is presented in Table F.2 and F.1. A Spearman Correlation test was applied to determined possible correlations between lead (Pb), cadmium (Cd), arsenic (As), chromium (Cr), zinc (Zn), iron (Fe) and aluminum (Al) in supraglacial material. The results are presented and discussed in section 5.1.4. A principal component analysis (PCA) was applied for determining possible correlations between elements and the different colors and samples of supraglacial material from Austre Brøggerbreen. Plots and results are presented and discussed in section 5.1.5. For marine sediment samples from Kongsfjorden, PCA was applied for correlations between elements and sampling points. Plots and results are presented in section 5.3. Software used for the PCA was Unscrambler 11 from Camo Analytics. The data was pre-processed with centering (mean center data) and weighting 1/std. Algorithm used was NIPALS with validation with cross-validation.

5. Results and discussion

Due to a large amount of data in several different matrices, the focus in this thesis was decided to be on the supraglacial material collected: supraglacial material from the glacier Austre Brøggerbreen, overbank sediment from the river Bayelva and marine sediment from the fjord Kongsfjorden. Results from river water samples will be used to strengthen observations in the supraglacial material and sediment results and suggested explanations. First, the chemical composition and origin of supraglacial material will be presented and discussed. Further, the compositing of overbank sediment and marine sediment will be presented and discussed. By comparing the three matrices, a discussion on the transport of elements with particulate matter from glacier to fjord will be presented.

The focus will also be on seven selected elements: lead (Pb), cadmium (Cd), arsenic (As), chromium (Cr), zinc (Zn), iron (Fe), aluminum (Al) and calcium (Ca). Pb, Cd, As and Cr was chosen due to begin categorized as hazardous trace elements for biota. These elements, in addition to Zn are also associated with anthropogenic release and pollution and subjected to long-range transport. Mercury (Hg) was under the limit of quantification (LOQ) in all samples in all matrices and was therefore not possible to include. Fe, Al and Ca was chosen due to having known sources from parent material in the area, and are therefore used as indicators for local or distant sources of the elements.

5.1. Supraglacial material

5.1.1. Total Carbon and Nitrogen content

Total Carbon (TC), Total Nitrogen (TN), Total Organic Carbon (TOC), Total Inorganic Carbon (TIC) and Residue Oxidizable Carbon (ROC) content was determined with combustion. The average percentage per weight of TC, TN, TOC, TIC and ROC content for supraglacial material samples with the relative standard deviation in percentage (RSD%) as well the minimum and maximum value are presented in Table 5.1. N denotes the number of samples over the limit of detection (LOD). TN was <LOD in two samples, sample 2 and 4. Results for all

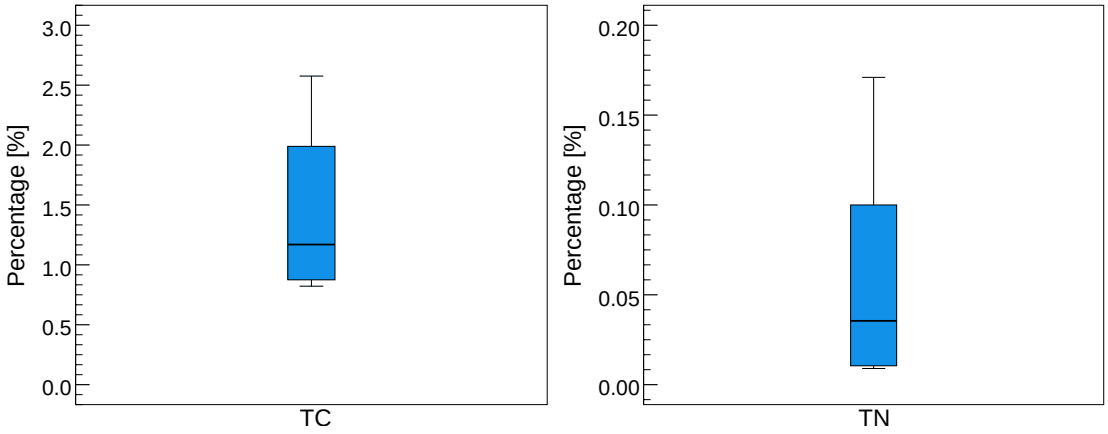

Figure 5.1.: Total Carbon (TC) and Total Nitrogen (TN) content in percentage by weight in supraglacial material samples presented as box and whisker plots. Only concentrations above detection limit (LOD) are presented. TN was <LOD in two samples (sample 2 and 4).

samples are presented in Table E.2 and E.3. Total Carbon and Total Nitrogen content in percentage per weight are presented as box and whisker plots in Figure 5.1. Only concentrations above the detection limit are presented. Results for TC and TN for all samples are presented in Table E.2 in Appendix E.2. TOC, TIC and ROC content in percentage per weight (%) are presented as box and whisker plots in Figure 5.2. Results for TOC, TIC and ROC in all samples are presented in Table E.3 in Appendix E.3.

Table 5.1.: Percentage per weight of Total Carbon (TC), Total Nitrogen (TN), Total Organic Carbon (TOC), Total Inorganic Carbon (TIC) and Residue Oxidizable Carbon (ROC) in supraglacial material samples. N denotes the number of samples over the limit of detection (LOD).

	N	**Mean**	**Minimum**	**Maximum**
TC [%]	14	1.40 ± 46.5	0.82	2.58
TN [%]	12	0.06 ± 97.0	0.01	0.17
TOC [%]	14	1.22 ± 37.5	0.64	2.04
TIC [%]	14	0.26 ± 58.0	0.11	0.57
ROC [%]	14	0.06 ± 14.5	0.05	0.08

The Total Carbon content in supraglacial material samples showed an average of 1.40% ± 46.5% and Total Nitrogen content showed an average of 0.06% ± 97.0%.

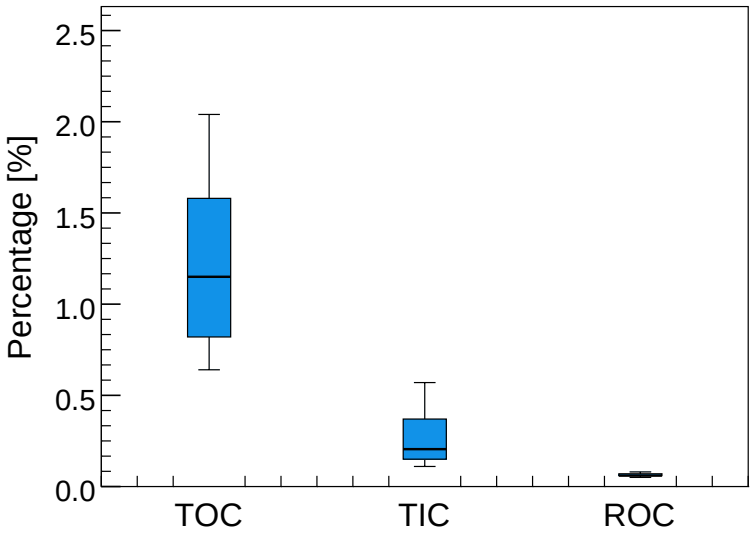

Figure 5.2.: Total Organic Carbon (TOC), Total Inorganic Carbon (TIC) and Residue Oxidizable Carbon (ROC) content in percentage by weight in supraglacial material samples presented as box and whisker plots.

This is recognized as a low TC/TN content compared to soil in the Brøggerdalen area. Heistad (2021) reported in their master's thesis, an average of 20.2% TC content ranging from 2.17% to 34.3% and an average TN content of 1.01% ranging from 0.07% to 1.45%. For both TC and TN the minimum being in mineral soil and the maximum in organic soil [131]. This indicates that the supraglacial material sampled at Austre Brøggerbreen is mostly composed of deposited eroded rock and minerals from the area around and under the glacier as described in the theory section 2.2.1.

Though, the TOC, TIC and ROC analysis showed that the Total Carbon content is mostly organic carbon with a mean percentage per weight of 1.22% $\pm$ 37.5%. Inorganic carbon mostly comes from carbonate while ROC is graphitic carbon [132]. The parent material around the glacier consists of, among other, limestone and dolomite which are calcium carbonate based rocks. Studies have reported the presence of microorganism and microbial communities in cryoconite holes on Austre Brøggerbreen [29, 133, 134]. This can be the reason for the carbon content being dominated by organic carbon.

A study by Takeughi (2002) reported a mean Total Carbon content in percentage by weight of 4.37% and a Total Nitrogen content of 0.40% of cryoconite collected

from Austre Brøggerbreen [27]. This shows a somewhat higher carbon and nitrogen content than found in this study, but not drastically different. Takeughi also studied cryoconite from two other glaciers in the Arctic: the Greenshield Glacier, Penny Ice Cap and Sverdrup Glacier, Devon Ice Cap. This showed a carbon content of 2.22% and 2.06 % respectively for the Greenshield Glacier and Sverdrup Glacier, which is in the span of the results found in this study. The nitrogen content is reported to be 0.22% and 0.23%, respectively for the Greenshield Glacier and Sverdrup Glacier. In addition, Takeughi studied three glaciers in the Himalaya and three glacier in Tibet, reporting carbon content between 0.54% and 3.71% and nitrogen content between 0.06% and 0.42% [26]. This indicates that supraglacial debris found in cryoconite holes are low in carbon and nitrogen content and are dominated by inorganic debris from eroded rocks and minerals in the local area.

5.1.2. General elemental characteristics

As described in section 3.2.1, the supraglacial material on Austre Brøggerbreen was found in different colors and textures. The color is a visual indication on different chemical compositions. In addition, there was also observed a visual difference in the color of the suspended particulate matter in Bayelva as described in section 3.1.1. Therefore, the differences in the element concentrations of *black*, *brown*, *red-brown* and *red* supraglacial material will be presented and discussed. All concentrations are presented in µg/g.

Results for elemental concentrations in supraglacial material was conducted with ICP-MS and calculated from µg/L to µg/g. Concentrations and calculations for the 64 elements analyzed can be found in a supplementary Excel sheet. The percentage of elements in black, brown, red-brown and red supraglacial material is presented as pie charts in Figure 5.3. The mean concentrations in µg/g ± the relative standard deviation in percentage (RSD%) of lead (Pb), cadmium (Cd), arsenic (As), chromium (Cr), zinc (Zn), iron (Fe) and aluminum (Al) are presented in Table 5.2. Concentrations of the selected elements in all of the supraglacial material is presented in Figure E.1 in Appendix E.1. Concentrations are presented as box and bar plots for Pb, Cd and As in Figure 5.4, for Cr and Zn in Figure 5.5 and for Fe and Al in Figure 5.6. The box plots are sorted by the color of the supraglacial material and the bar plots are sorted by sampling point.

In general, the supraglacial material is dominated by aluminum with 34.1-38%, iron with 32.8-36.1% and magnesium (Mg) with 10.8-11.7%. This is expected, due to the presence of, among others, reddish sandstone, and shale in the mountains around Austre Brøggerbreen. Silicone (Si) is only present in 2.4-2.9% and would be expected to be much higher due to the rocks in the area being mostly dominated by

silicates. This can be explained by mechanical loss of the sample after microwave digestion with nitric acid (HNO_3). As previously mentioned in the theoretically background, section 2.4.2, HNO_3 does not dissolve particulate matter completely but dissolves the outer layer of particles where ions are absorbed. This leaves some of the particulate matter in precipitation after the digestion. HNO_3 dissolves organic matter with high efficiency but does not dissolve silicates (SiO_2 in different crystal structures) [61]. All supraglacial material samples had precipitation at the bottom of the vial after digestion (Table C.1). It is therefore believed that this was residue of silicates. The precipitation was not transferred to the tubes for ICP-MS analysis due to the big risk of clogging and interferences in the instrument. Unfortunately, the precipitation was not weighted out and the exact amount of sample lost in this process is not known.

Even though some silicates are lost in the digestion process, it is evident that the supraglacial material mainly are composed of inorganic material. Edwards *et al.* (2011) sampled supraglacial material in cryoconite holes on Midtre Lovénbreen (a glacier close to Austre Brøggerbreen on the east side, see Figure 3.1), Austre and Vestre Brøggerbreen and found that the material in dry weight had an inorganic content of 84-99% dominated by inorganic minerals [134]. By polarized light microscopy, it was found that the material from Austre Brøggerbreen contained quartz, white and biotite mica, feldspar and appeared consistent with metamorphic origins. These minerals are associated with potassium (K), sodium (Na), calcium (Ca), iron (Fe), aluminum (Al) and rarely lithium (Li) and chromium (Cr) [114], which is compatible with the results presented here. It is though important to point out that this was showed in one representative sample and that the material was described as "dark-colored". They also suggested that the material had local origin and was recent deposited due to the shape and size of the particles [134].

5.1.3. Differences in black, brown, red-brown and red supraglacial material

In general, the different colors of supraglacial material is dominated by the same elements in the same order of magnitude, with Fe and Al being the most dominant (Figure 5.3). After Fe and Al, in decreasing percentage, the abundance of elements appearing over 0.1% are: Mg > K > Ca, Si, Cl $\geq$ Ti, Na > S, P, Mn, all associated with the crustal composition in the area. Interestingly, the black material stands out with the appearance of lead (Pb) in the pie chart at 0.1%. For the other colors, Pb are only present in 0.03% in red and red-brown material and 0.04% in brown material. This can also be seen in Figure 5.4, where the mean Pb concentration is visibly higher for black material and at point P3 which is the sampling point for

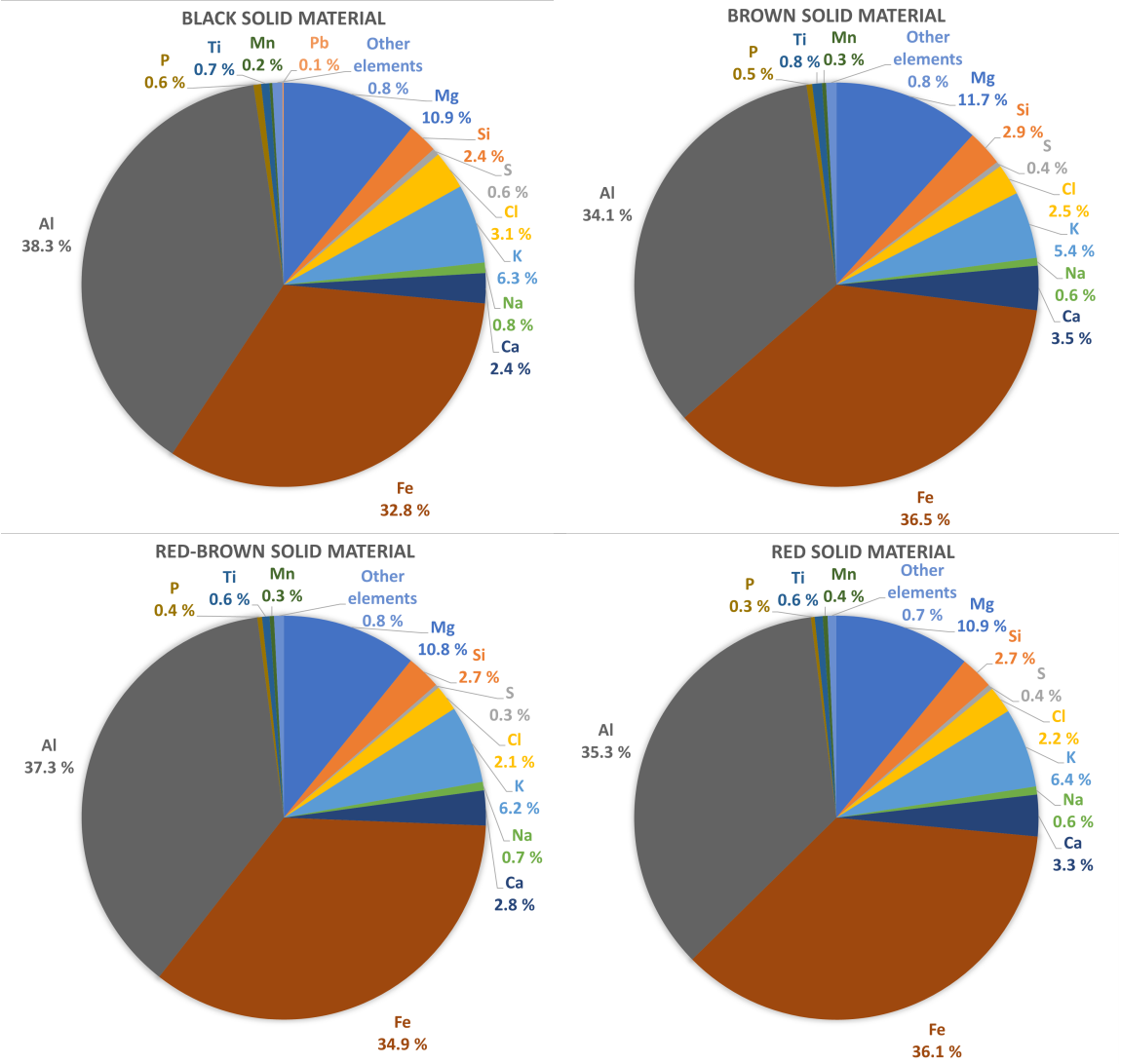

Figure 5.3.: Percentage of elements in black, brown, red-brown and red supraglacial material presented as pie charts.

the black material.

The mean Pb concentration in black supraglacial material is 119 µg/g ± 3.8% with the highest concentration of 122 µg/g compared to the mean concentration for the other colors of 52.4 µg/g ± 32.5%, 35.2 µg/g ± 2.5% and 39.9 µg/g ± 6.5%. The black material also has higher concentrations of arsenic with a mean value of 12.8 µg/g ± 1.7% (Table 5.2 and Figure 5.4). Furthermore, the black material also stands out with the lowest concentration of iron, as seen in Figure 5.6.

The brown material has the lowest concentrations of Cd, Cr and Al. But have higher concentrations of Pb an As than red-brown and red material. The brown material also has a low concentration of Fe, compared to red-brown and red material. Red-brown and red material have the highest concentrations of Fe and Al. Seemingly, there is a difference in the elemental composition of the different colors of supraglacial material.

The sample size is unfortunately too small to test if the differences in concentrations of the elements between the different colors are statistically significant. An indication for differences in the Pb and As concentrations is the criteria set by the Norwegian Public Pollution Control (now called Norwegian Environmental Agency) for polluted ground. The criteria is a five step scale from "very good" to "very bad" with limits for the concentration in each step. "Very good" is classified as background levels whilst "very bad" is classified as hazardous waste [135]. For Pb the concentrations for brown, red-brown and red material fall under the category "very good" (<60 µg/g) whilst for the black material, the Pb concentrations fall under "moderately polluted" (100-300 µg/g) with the category "good" (60-100 µg/g) in between. This is also the case for As, where the As concentration for the black material falls under the category "good" (8-20 µg/g) while the As concentrations for the other colors falls under "very good" (<8 µg/g). For Cd and Zn, all of the concentrations fall under "very good", and for Cr all of the concentrations fall under "good".

Table 5.2.: Mean concentration in µg/g ± RSD% of lead (Pb), cadmium (Cd), arsenic (As), chromium (Cr), zinc (Zn), iron (Fe) and aluminum (Al) for black, brown, red-brown and red supraglacial material.

	Black	**Brown**	**Red-brown**	**Red**
Pb	119±3.8	52.4±32.5	35.2±2.3	39.9±6.5
Cd	0.0976±10.0	0.0682±17.1	0.0930±8.1	0.120±21.6
As	12.8±1.7	6.61±30.5	4.58±10.8	5.12±21.5
Cr	67.6±2.8	58.5±2.2	68.0±1.5	67.9±13.2
Zn	111±2.8	99.3±7.7	101±4.1	112±8.3
Fe	40300±11.0	43100±6.1	48300±0.1	50400±3.3
Al	47100±3.4	40200±1.8	51500±0.3	49300±14.5

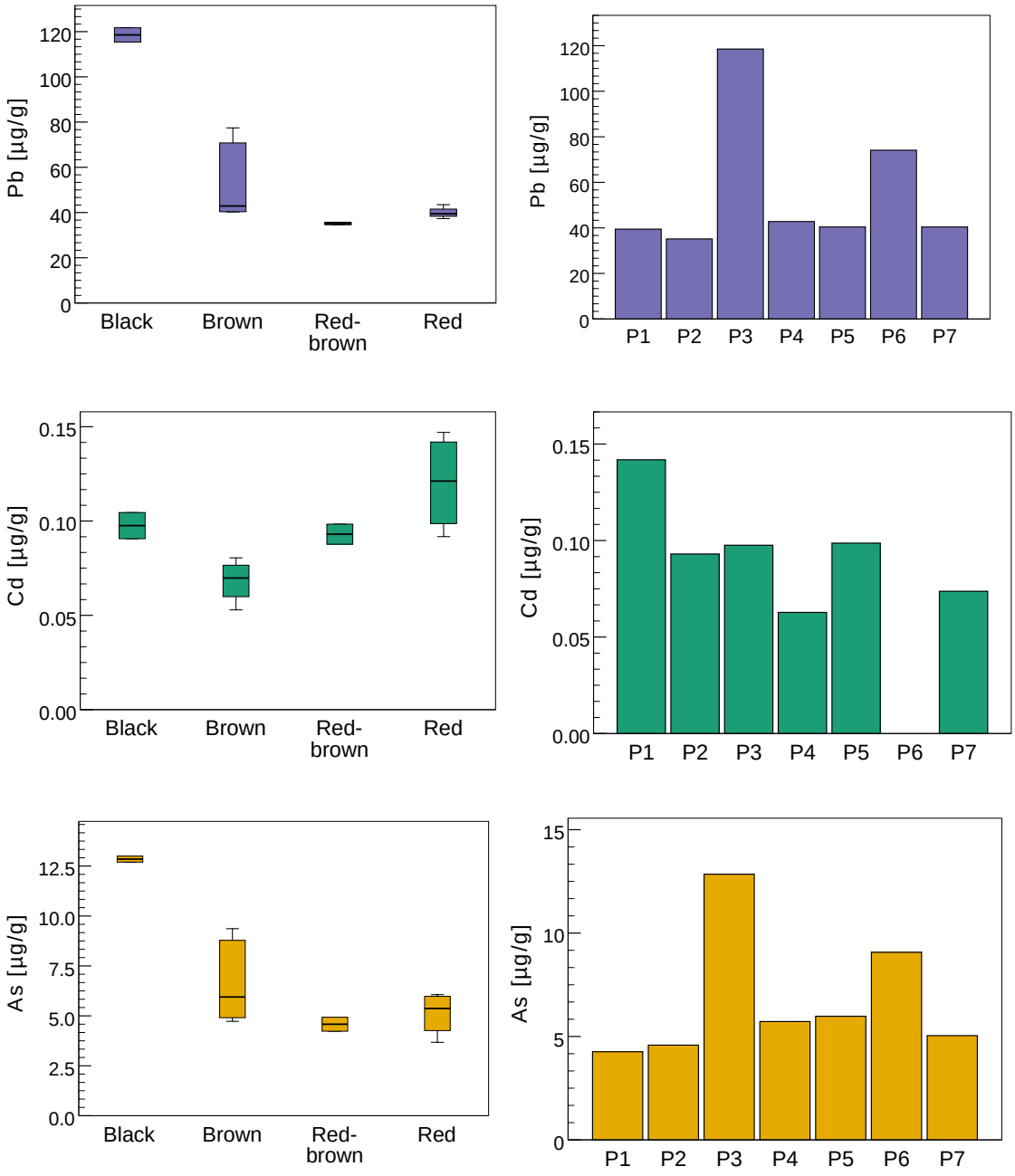

Figure 5.4.: Concentrations (µg/g) of lead (Pb), cadmium (Cd) and arsenic (As) in supraglacial material presented as box and bar plots. The box plots are sorted by the color of the supraglacial material and the bar plots are sorted by sampling point.

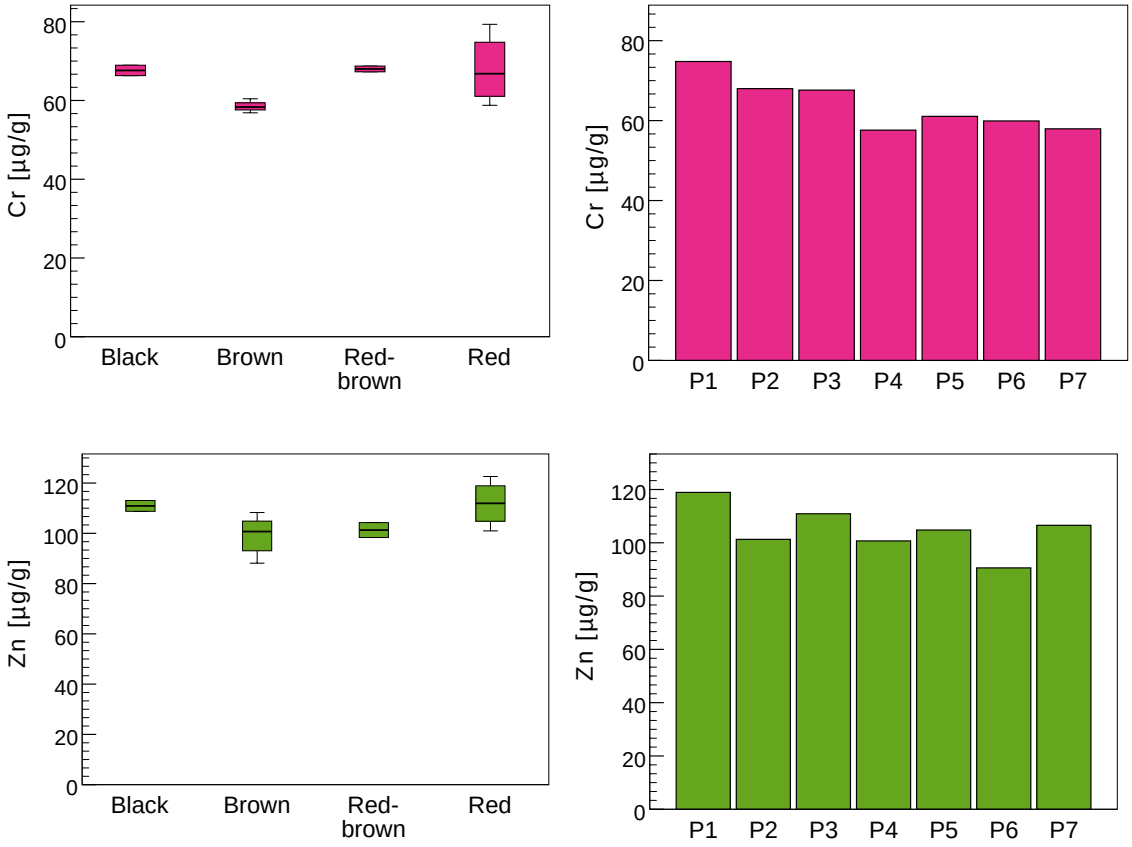

Figure 5.5.: Concentrations (µg/g) of chromium and zinc in supraglacial material presented as box and bar plots. The box plots are sorted by the color of the supraglacial material and the bar plots are sorted by sampling point.

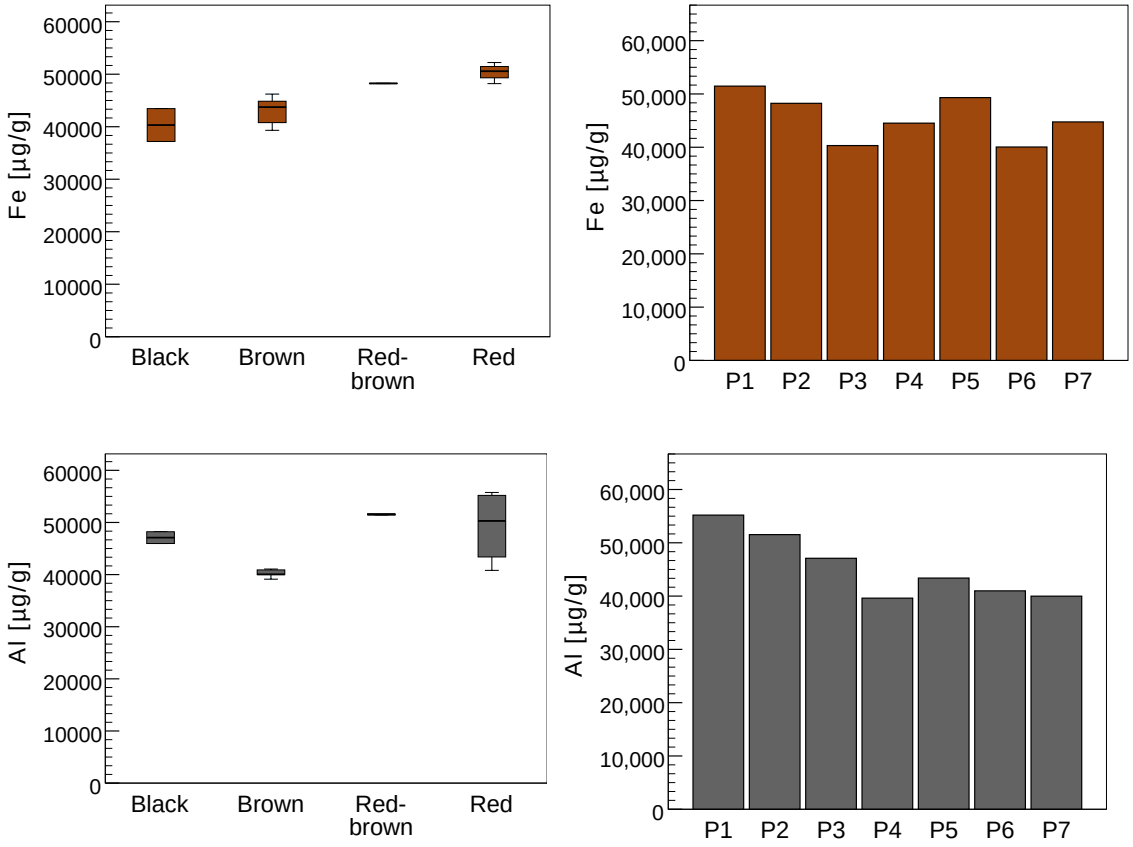

Figure 5.6.: Concentrations (µg/g) of iron and aluminum in supraglacial material presented as box and bar plots. The box plots are sorted by the color of the supraglcial material and the bar plots are sorted by sampling point.

5.1.4. Significant correlations between trace elements in supraglacial material

Since the distribution of Pb, As, Fe and Al is non-normal, a non-parametric Spearman correlation test was applied for determining possible significant correlations between Pb, Cd, As, Cr, Zn, Fe and Al. The correlation coefficient (R^2) explains the strength of the correlation while the p-value will declare if the correlation is statistically significant. A significant correlation is marked in bold. Correlations that are significant at the 0.05 level are labeled * and correlations that significant at the 0.01* level are labeled **.

Pb and As have a strong significant correlation. This can imply that they are originating from the same source. Pb and As have a significant negative correlation with Fe, which can imply that Pb and As have an external source that is not from crustal contribution. This agrees with the results of higher concentrations of Pb and As in the black material and and that the concentrations fall under the category of "moderatly polluted" from the limits set by the Norwegian Environmental Agency. Al and Cr have a strong significant positive correlation. This agrees with detection of mica in the samples collected by Edwards (2010) *et al.* [134]. Mica is a mineral composed of aluminosilicates and can have Cr incorporated in the crystal structure [114]. Cd has a significant strong correlation with Al. Cr and Cd have significant strong positive correlation. Cr also has a significant moderately strong correlation with Zn and Fe which can imply common source. This can also indicate sourcing from the rocks and minerals in the area.

Table 5.3.: Non parametric Spearman correlations between measured element concentrations in supraglacial material. R^2 denotes the correlation coefficient. Correlations that are significant at the 0.05 level are labeled * and correlations that are significant at the 0.01 level are labeled **.

		Pb	**Cd**	**As**	**Cr**	**Zn**	**Fe**	**Al**
	R^2							
Pb	p-value							
	N							
	R^2	-0.133						
Cd	p-value	0.681						
	N	12						
	R^2	**0.807****	-0.168					
As	p-value	0.000	0.602					
	N	14	12					
	R^2	-0.134	**0.846****	-0.073				
Cr	p-value	0.648	0.001	0.805				
	N	14	12	14				
	R^2	-0.033	**0.622***	-0.218	0.**538***			
Zn	p-value	0.911	0.031	0.455	0.047			
	N	14	12	14	14			
	R^2	**-0.754****	**0.643***	**-0.776****	0.420	0.464		
Fe	p-value	0.002	0.024	0.001	0.135	0.095		
	N	14	12	14	14	14		
	R^2	-0.253	**0.832****	-0.182	**0.978****	0.473	0.477	
Al	p-value	0.383	0.001	0.533	0.000	0.088	0.085	
	N	14	12	14	14	14	14	

5.1.5. Principal component analysis for supraglacial material

Principal component analysis (PCA) score- and loading-plot for PC1 and PC2 for correlations between the different colors of supraglacial material and elements are presented in Figure 5.7 and 5.8, respectively. In the score-plot, there is an evident difference between the colors. There is a gradient in the concentrations of elements from dark-colored to red-colored material along PC1, which explains 46% of the variance. The samples placed to the right in the score-plot gave higher concentrations of the elements to the right in the loading-plot. The same is for the samples and elements placed to the left in the score- and loading-plot. The elements in the opposite direction is negatively correlated with each other. PC2 explains 32% of the variance and seems to be explained by the different sampling points.

The black material is highly correlated with and has high concentrations of As and Pb, as already seen from the elevated concentrations (Table 5.2 and Figure 5.4) and the strong correlation from the Spearman correlation test (5.3). The black material is also associated with Bi, P and Cl. The brown material at point P6 has higher concentrations of Mo, S and Sn, while the brown material from point P4 and P7 are higher in Ti and Ca. The material categorized as red and red-brown are, among other, highly associated with Fe, Al, Co, Mg, Mn and Ni, especially from P1. This agrees with the observed increasing concentrations of Fe and Al from dark-colored to red-colored material (Table 5.2 and Figure 5.6). The red-colored are also highly associated with Cd, Zn and Cr, which also agrees with the results from the Spearman correlation test. In the test, Al where positively correlated to Cr and Cd, as seen in the loading-plot where they are placed close to each other. Cr and Cd are also significantly correlated. In addition, Zn and Cd also had a significant positive correlation, the same as for Zn and Cr. From the Spearman test Pb and Fe had a negative correlation, also observed in the PCA-plot with them being placed in the opposite direction of each other. These differences in the element concentrations and associations with the different colors of the supraglacial material, shows that there are clear differences in the composition of supraglacial material even though they are sampled in relatively close proximity to each other.

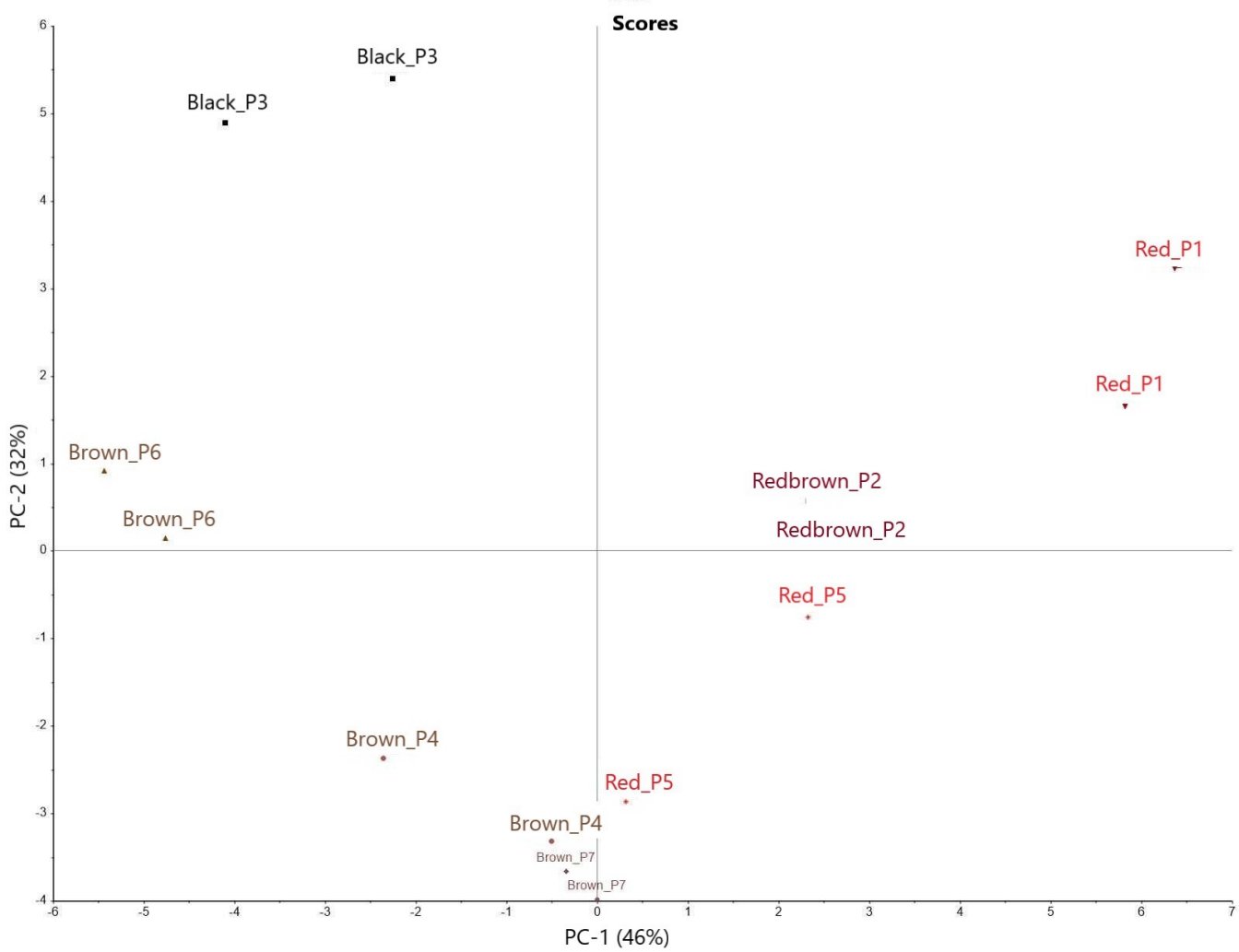

Figure 5.7.: Principal component analysis (PCA) score-plot for supraglacial material for PC1 and PC2 as color and sample point as displayed property.

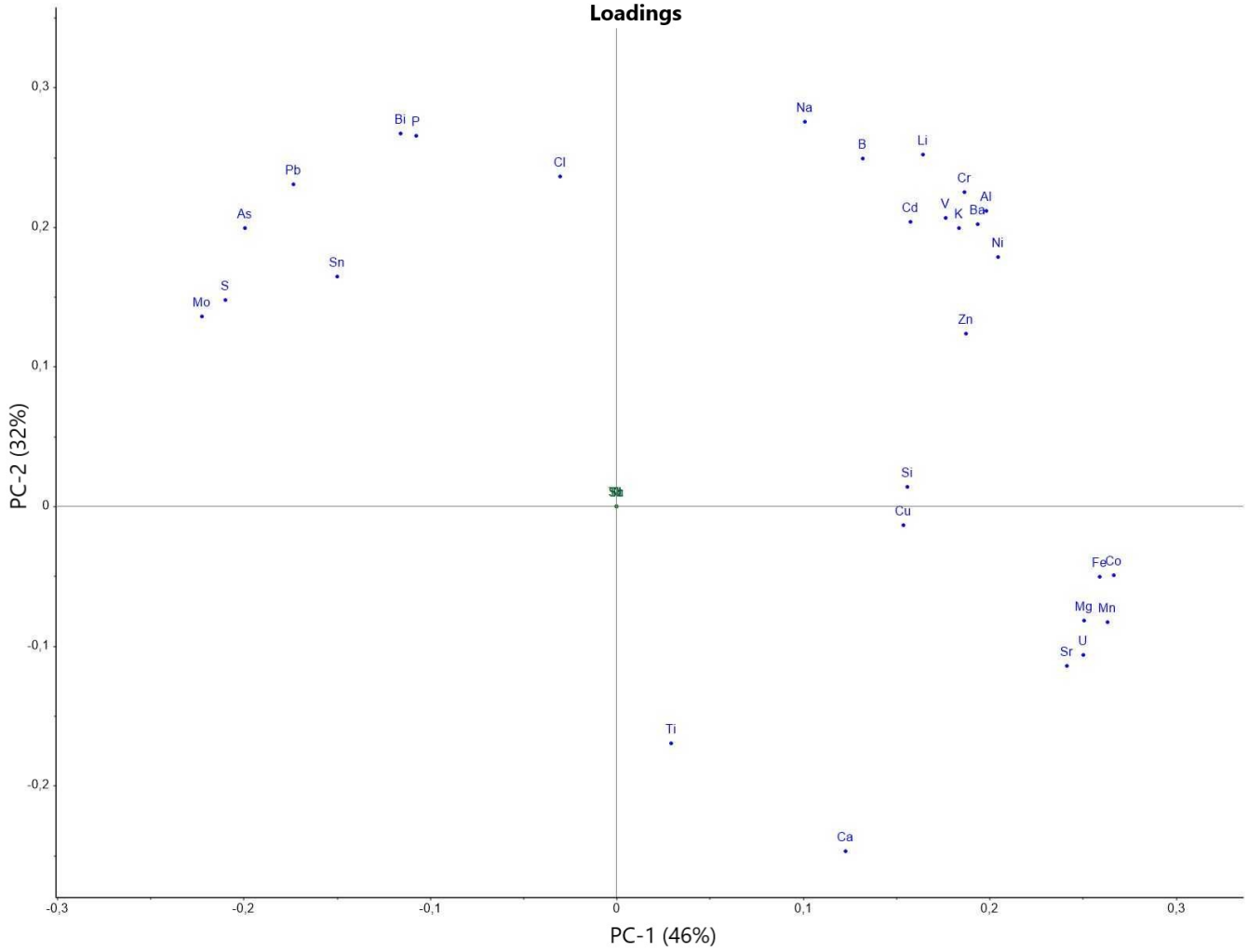

Figure 5.8.: Principal component analysis (PCA) loading-plot for PC1 and PC2 for selected elements in supraglacial material.

5.1.6. Probable sources of trace elements

The erosion rates on the surface of glaciers are high due to snow accumulating in the winter, high melting rates of snow and ice in the summer, strong wind and heavy rain floods that can appear. The diversity in rock types and minerals are also high in the catchment especially around Austre Brøggerbreen. The supraglacial material is therefore believed to be a mixture of different inputs both from the parent material and atmospheric precipitation processes.

A study by Singh *et al.* (2013) analyzed cryoconite, described as "brownish-black material" for trace elements on Midre Lovèvenbreen (Figure 3.1) [9]. The levels of the selected trace elements found in cryoconite in their study are presented in Table 5.7. In general, the levels found are in the span of the levels found in this thesis. The supraglacial material on Austre Brøggerbreen are higher in Fe and Al, probably due to the input of reddish sandstone. The Zn levels, ranging from a mean of 132 to 150 µg/g, found on Midre Lovènbreen was higher than on Austre Brøggerbreen, with the mean concentrations ranging from 99.3 to 112 µg/g. The concentrations for Pb (49.87-73.88 µg/g) and As (11.01-14.22 µg/g) is higher in the cryoconite from Midre Lovènbreen than for brown, red-brown and red supraglacial material from Austre Brøggerbreen. This corresponds to the higher concentrations of Pb and As found for black material and both the strong positive correlations both from the Spearman test and the PCA plot. This may indicate that dark-colored supraglacial material is associated with higher levels of Pb and As.

Sing *et al.* also compared the levels of trace elements of crustal composition of refraction seismic profile of Western Europe and Canada, derived from Shaw *et al.* (1967, 1976) and Wedepohl (1995) [136–138], to evaluate the possible crustal contribution to supraglacial material. These levels are also presented in Table 5.7. Comparison shows that the concentrations for Al and Cr in all the colors are below the levels found in the continental crust. With them begin strongly positively correlated from the Spearman test and in the PCA plot, shows that they most probably are from the local geology. Fe does exceed the crustal composition levels in red-brown and red material but are believed to be higher due to high input of reddish sandstone. Reddish sandstone consists of iron oxide, coloring it red, quartz (SiO_2) and feldspar consisting of alumina silicate. This also explains the higher concentration of Al in the red-brown and red material. The levels of Cd in black, brown, and red-brown material are within the crustal composition level. However, in all samples categorized as red material the Cd concentration is slightly higher than the crustal contribution level of 0.1 µg/g. Cd does on the other hand positively correlate with Al (R^2=0.832) and positively with Fe (R^2=0.643). In addition, Cd positively correlates with Cr (R^2=0.846). This may imply that the

concentrations of Cd are from crustal contribution from the rocks and minerals in the area. Pb, As and Zn concentrations for all four colors shows elevated values compared to the crustal levels [136–138]. This indicates that the elevated levels can have other sources of input in addition to the crustal contribution. This can also correspond to the positive correlation between Pb and As (R^2=0.807) and the significant negative correlation both Pb (R^2=-0.754) and As (R^2=-0.776) have with Fe, It is though important to point out that the differences between the values in supraglacial material form Austre Brøggerbreen can be due to differences in the crustal composition in the area compared to in Western Europe and Canada.

The Geological Survey of Norway (NGU) in cooperation with the Norwegian Water- and Energy Agency (NVE) published a geochemical atlas in 2010 with levels of elements in different areas in Spitsbergen, Kongsfjorden included, as a mapping of natural background levels. The levels reported in Brøggerdalen are presented in Table 5.7. The same conclusion is made for Pb and Zn in all four colors as above; the concentrations exceed the range found in the geochemical atlas indicating outer input than from the crustal contribution. The range for Cr is 10-70 µg/g, therefore the concentrations for Cr in all four colors can be considered as background levels, as already suggested above. For As the concentration in brown, red-brown and red is in the range of 0-9 µg/g. The concentration of As in black material exceeds this range with a concentration of 12.8 µg/g.

On the contrary, Zn does have a significant positive correlation with both Cd (R^2=0.622) and Cr (R^2=0.538) but not as strong as Cr and Cd have with Al (R^2=0.978 and R^2=0.832 respectively) and each other (R^2=0.978). This might indicate some input from crustal contribution. On Midre Lovenbreen, Zn did not correlate with any of the other trace elements and was suggested to probably be sourced from anthropogenic activity [9]. Even though these levels where higher than reported in this thesis, this suggests other sources of Zn in the Ny-Ålesund area.

The Pb concentration in all supraglacial material samples exceeds the range of 0.5-8.8 µg/g from the geochemical atlas [139] and the level of 14.8 µg/g from the crustal contribution value [136–138]. Pb is therefore considered to be from other sources in addition to the local geology. This is also strengthened by the significant negative correlation with Fe. Since As has a strong positive correlation and a significant negative correlation with Fe, this can suggest that As also has other inputs than the local geology.

Other contributions than that from the local geology, can be from local and/or long-range atmospheric transport of both natural and anthropogenic sources. Austre Brøggerbreen is highly exposed to wind-transported elemental dust to the shel-

tered high-altitude valley [9]. The lower air layers become more stable in the Austre Brøggerbreen valley and are more prone to pollution. High velocity winds blow from the sea to land and collapse in the valley which can lead to dust containing trace elements to deposit on the glacier. Trace elements can also stay in cryoconite holes over longer periods due to freeze-thaw cycles in the summer months over several years [9]. Sea spray has shown to be a dominant source of aerosols in the Ny-Ålesund area which can contain trace elements [140]. An important factor that likely has an influence on the accumulation of trace element on Austre Brøggerbreen is the previous coal-mining activity in the area. Coal is especially associated with Pb, As, Cd and Cr [117, 118]. Other local sources are the use of vehicles, airplane activity and larger cruise ships in the Ny-Ålesund area. This is especially associated with pollution of Pb [141]. High background levels of As have been reported in the Longyearbyen area [142].

A study by Łokas *et al.* looked at the levels of, among others, Pb, Cd, Cr, Zn and Fe in supraglacial material or cryoconite (dark-colored material) on Hansbreen, Hornsund [10]. The mean concentrations found in their study is presented in Table 5.7. The mean concentration of lead was found to be 54.38, closest to the concentration in brown material. The level of Cd was somewhat higher in the supraglacial material on Hansbreen with a mean concentration of 0.420 µg/g which exceeds the levels of geological input reported in the Hornsund area. The mean concentration of Fe was 54,280 µg/g exceeding the levels found in this thesis. The Fe levels on Hansbreen was considered to be from the local geology.

Łokas *et al.* also studied the levels of contamination by anthropogenic radionuclides which are bound to and transported with airborne particles to determine long-range transport and anthropogenic input of trace elements. These results showed a high accumulation of radionuclides in supraglacial material and cryoconite holes and concluded that long-range transport of trace elements was a contribution source. Especially Pb was found to have a large contribution from anthropogenic activity [10]. This contributes to the indications suggested above.

The black/dark color in supraglacial material is from the formation of humic substances by biological life [26, 27]. Takeuchi *et al.* (2001) found that the dark color was from highly polymerized compounds from bacterial decomposition of algal products and/or other organic particles in the supraglacial material [26]. Algae and bacteria have been found in supraglacial material on Austre Brøggerbreen [134] The process is similar to the dark coloration of soil organic matter. The dark colorization is due to the large amounts of conjugated molecular bonds which forms a part of the compounds which absorbs a wide range of wavelengths of visible light. As mentioned in the theory, humic substances bind strongly to metals and trace elements and be the reason for the elevated concentrations of Pb and

As in the black material. The Total Carbon, Total Nitrogen and Total Organic Carbon content in the supraglacial material studied in Takeuchi *et al.* (2001) was similar to that measured in the black supraglacial material. The black material in this thesis did not have higher TOC content than for the other colors but did have the highest TC content [26]. Another reason for the higher concentrations of Pb and As in black material can be due to the fact that the black material was not collected in a cryoconite hole and was not found in water. Other samples were found in water and some of the trace elements can therefore be dissolved out from the material.

5.1.7. pH measurement of supraglacial material

pH measurements of soils and sediments can give indications on the chemical and biological environment and are important to determine nutrient and trace element speciation and availability [143]. To the authors knowledge, pH is not yet reported on in supraglacial material from Austre Brøggerbreen. It is therefore of interest to include these results even though they were not put in relation to the elemental results and the previous discussion.

Results for pH measurement of supraglacial material samples are presented in Table 5.4. Samples from the same sample point was combined and are denoted with + sign between. The pH in the supraglacial material was measured to be between 4.10 and 4.57 with a mean of 4.37, except for at point P1 that was measured to 6.13. This is a markedly higher pH, emphasizing that pH is a logarithmic scale. The supraglacial material from this sampling point was from a cryoconite hole and was red in color. Factors increasing the pH in soils are the presence and weathering of silicates, aluminosilicate and carbonate rocks [143]. The two samples from this sampling point had the highest concentrations of Al, Ca and Mg which can be the explaination for the higher pH. The presence of organic matter and humic substances is another factor affecting pH, but the Total Carbon and Nitrogen content did not stand out or where markedly different from the other samples.

Stibal *et al.* (2006) measured the pH of supraglacial material on four glacier on Svalbard, Hansbreen, Werenskioldbreen, Nannbreen, and Austre Torellbreen [144]. They found that the pH in the supraglacial material varied greatly, ranging from 4.8 to 7.5. They also found that the pH in material sampled from cryoconite holes where lower compared to material sampled from mounds, pH 6.1 – 8.6. This was not the case for the samples collected from a mound (point P3) in this thesis. The pH in the black material collected from the mound was 4.50.

Table 5.4.: Results for pH measurement of supraglacial material samples. Samples from the same sample point was combined and are denoted with + sign between.

Sample point	Sample	pH
P1	1+2	6.13
P2	3+4	4.51
P3	5+6	4.50
P4	7+8	4.10
P5	9+10	4.57
P6	11+12	4.30
P7	13+14	4.25

5.2. Comparison of chemical composition between sites

5.2.1. General elemental composition of overbank and marine sediment

The elemental concentrations determined by ICP-MS for overbank sediment from Bayelva and marine sediment from Kongsfjorden was calculated from µg/L to µg/g. Concentrations and calculations for the 64 elements analyzed are found in a supplementary Excel sheet. The percentage of elements in supraglacial material (not separated by color), overbank sediment and marine sediment is presented as pie charts in Figure 5.9.

The average percentage composition of the overbank sediment is markedly different from the average percentage composition of supraglacial material. The dominant element in the overbank sediment is calcium (Ca) at 38.6%, an increase of 35.5% from the 3.2% in supraglacial material. The fraction of magnesium is also 9.5% higher in the overbank sediment than in the supraglacaial material. Iron is present at 14.3% and aluminum at 16.0% compared to 35.4% and 35.3% respectively in supraglacial material. The content of elements in overbank sediment is: Ca > Mg > Al > Fe > K > Cl > P, S > Na, Ti, Mn compared to Fe > Al > Mg > K > Ca > Cl > Na, Ti > P, S > Mn in supraglacial material. Si is omitted from the comparison due the probable mechanical loss from microwave digestion, as previously discussed in section 5.1.2.

This notable difference in composition between the supraglacial material and the overbank sediment shows that runoff to Bayelva is not influenced by sediment from

supraglacial runoff from Austre Brøggerbreen alone. The supply of sediment and elements to the glacier-fed river is complex and dependent on many factors but particulate matter and erosion from meltwater runoff are the dominant factors. Bayelva is fed by runoff from two glaciers, Austre og Vestre Brøggerbreen. As observed in the field and showed in Figure 3.2b in section 3.1, the two glaciers supply the river with different composed runoff. As seen, the runoff from Austre is reddish in color and the runoff from Vestre is light grey. This is already an indication on different elemental supply to the river. This is due to the differences in the bedrock on the western and eastern side of the basin where the eastern (Austre) side is dominated by reddish sandstone and silicate based rocks while the western (Vestre) side is dominated by carbonate rocks [115]. Higher input of carbonate rocks in the overbank sediment explains the large difference in percentage. Carbonate rocks are also easily weathered compared to silicate based rocks. The weathering of calcium carbonate ($CaCO_3$) has been found to be the dominant process of input of Ca to Bayelva [115].

Sediment and particulate matter supply to Bayelva from Austre Brøggerbreen is also dependent on different erosion processes, as described in the theory section 2.2. The sediment transported to the river can be eroded material from beneath the glacier bed, eroded moraines or from supraglacial material. Hodson *et al.* (1997) and Hodson and Ferguson (1999) reported that the suspended load in the meltwater stream from Austre Brøggerbreen was dominated by erosion of marginal and lateral moraines situated along the sides and in the ablation zone of the glacier, and that due to the cold based ice at the bed of the glacier, erosion of the glacier bed was minimal [11, 145]. This means that the sediment supply to Bayelva is more affect by sediments that are exposed to atmospheric processes compared to the isolated sediments beneath the glacier.

The mean percentage elemental composition of the marine sediments is similar to the overbank sediment with Ca as the dominating element at 26.9% followed by Al at 20.1%, Fe at 15.5% and Mg at 14.3%. The elemental content of marine sediment is Ca > Al > Fe > Mg > Cl > Na > K > A > P > Ti > Mn. As expected, Na and Cl has a higher fraction in marine sediment due to the input of seawater. The elemental input to the marine sediments in Kongsfjorden are dependent on more factors than for the overbank sediment in Bayelva. Kongsfjorden is a part of a more complicated system with sediment and elemental input from large ocean currents, several tidewater glaciers in the area, sea ice, erosion of coastal sediment and soils, atmospheric input and anthropogenic activity in the area. The sediment samples collected in this thesis are sampled closely to the river outlet and it is likely that the input from the river has a big impact on the sediment chemistry, which can be implied from the similarly composition to overbank sediment.

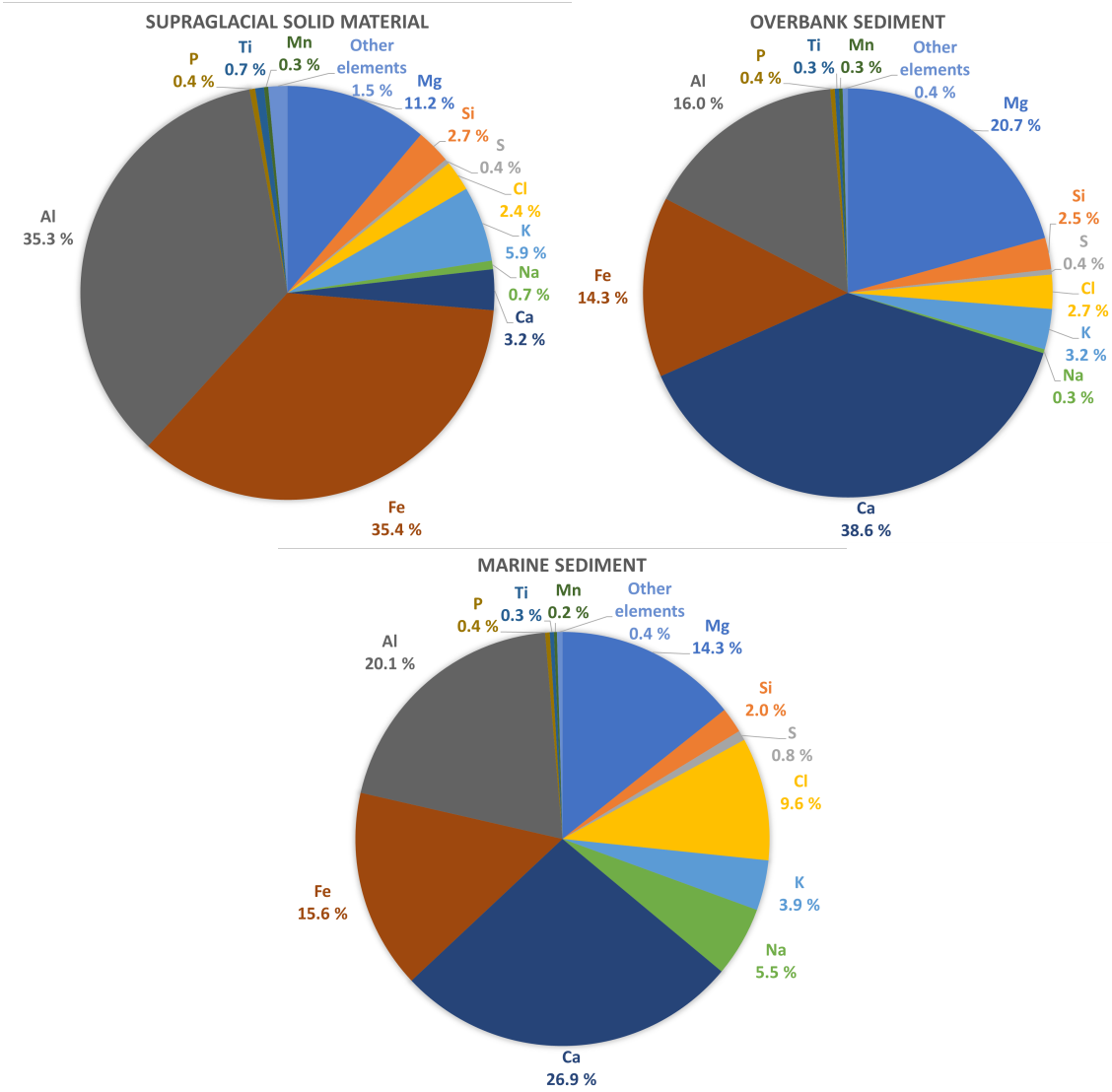

Figure 5.9.: Percentage of elements in supraglacial material from Austre Brøggerbreen, overbank sediment from Bayelva and marine sediment from Kongsfjorden presented as pie charts.

5.2.2. Levels of selected trace elements

The mean, relative standard deviation in percentage (RSD%), the median, the minimum and the maximum concentration (µg/g) of Pb, Cd, As, Cr, Zn, Fe, Al and Ca in supraglacial material from Austre Brøggerbreen, overbank sediment from Bayelva and marine sediment from Kongsfjorden is presented in Table 5.5. Table 5.7 presents the mean concentrations ± RSD% of Pb, Cd, As, Cr, Zn, Fe and Al in supraglacial material, overbank sediment and marine sediment in addition to, for comparison, values reported in other studies in supraglacial material, overbank sediment and marine sediment. Concentrations of Pb, Cd, As, Cr and Zn is presented as box and whisker plots in Figure 5.10 while box and whisker plots for the concentrations of Fe, Al and Ca are presented in Figure 5.11. Concentrations for the selected elements in all samples of overbank and marine sediment is presented in Table E.1 in Appendix E.1. All concentrations are presented in µg/g.

The differences in the elemental concentrations between matrices was tested for statistical significance with the non-parametric Mann Whitney U test or the parametric Student-t test depending on if the data is normally distributed or not. The p-values from the tests are presented in Table F.3 in Appendix F.2. The results from a Shapiro-Wilk Normal Distribution test is presented in Table F.2 in Appendix F.1.

The mean concentrations of the selected elements are in general lower in the overbank sediment in Bayelva than in the supraglacial material and the marine sediment. The concentrations of As, Cr, Zn, Fe and Al are significantly lower in the overbank sediment than in both the supraglacial material and the marine sediment. The Pb concentration in overbank sediment is significantly lower than in upraglacial material but not significantly different for marine sediment. On the other hand, Cd is significantly higher in the overbank sediment than in supraglacial material and marine sediment. For the Ca concentrations, the mean value in overbank sediment is significantly higher than in both supraglacial material and marine sediment. By studying the box and whisker plot for Ca in Figure 5.11, it can look like the concentrations of Ca in overbank sediment and marine sediment is not significantly different from each other. However, the concentrations of Ca in the overbank sediment is widely spread ranging from 14,400 µg/g to 156,000 µg/g (Table 5.5), and can be the reason for the test concluding with significant difference. The concentrations in sample 21 and 22 are marked as outliers with the highest concentrations. These samples are collected at the delta at the outlet of the river and the high concentrations is probably due to seawater input.

With that said, the concentrations of As, Cr and Zn in the overbank sediment is within the range of the concentrations reported in overbank sediment in the

geochemical atlas (Table 5.7) [139] which is considered as background levels in the area [139]. The same conclusion is made from the limits set by the Norwegian Environmental Agency (2020) for levels of elements in sediments [146]. All concentrations of As, Cr and Zn falls under the category "very good" or background levels. The mean concentration of Pb exceeds the range of 0.5-8.8 reported in the geochemical atlas but falls under the category of background level from the limits. The levels of Fe and Al does not exceed the crustal contribution levels found from crustal levels in Western Europe and Canada [136–138]. Whereas the same cannot be said for Cd. The mean and the median exceed 0.1 µg/g from the crustal composition levels but are within the limit of background levels set by the Norwegian Environmental Agency of < 0.2 µg/g. However, three samples, sample 37, 38 and 39 exceeds this limit with concentrations of 0.276, 0.301 and 0.223 µg/g respectively where the two first fall under the category "moderately polluted". Sample 37 and 38 are collected at point P14 which is from the river emerging from Vestre Brøggerbreen. This may indicate that elevated levels of Cd are found on or in the area of Vestre Brøggerbreen. Since samples where not collected on or closer to Vestre Brøggerbreen this needs to be further investigated.

The levels found in this thesis corresponds with levels found in a master's thesis by Kveli (2015) that sampled overbank sediment along Bayelva [147], as seen in Table 5.7. The mean concentration of Cd in Bayelva in this thesis (0.174 µg/g) was within the range of the mean concentrations of 0.155-0.188 µg/g reported by Kveli. The mean concentration of Pb, As and Zn were slightly higher in this thesis but not notably. The levels for Fe and Al were within the same levels from Kveli [147].

For the marine sediments, the mean concentrations of Cr, Zn, Fe and Al are significantly higher than in overbank sediment and significantly lower than in supraglacial material. For Pb and As, the mean concentrations are significantly lower than in supraglacial material but is not significantly different from overbank sediment.

The Norwegian Geological Survey (NGU) published a comprehensive mapping of the levels of trace elements in marine sediment in fjords of Spitsbergen in 2019 to outline possible pollution [148]. The inner Kongsfjorden was included and the levels reported is presented in Table 5.7. The mean concentrations of Pb, As, Cd, Cr and Zn did not exceed the levels from the NGU report. Though the levels of As was much higher in the NGU report which was 18-71 µg/g compared to the mean concentration of 6.88 µg/g found in this thesis. All the concentrations also fall under the category of background levels, except for one sample that falls in the "good" category for Pb, in the limits set by the Norwegian Environmental Agency for levels of trace elements in sediments [146]. However the mean concentration for

Pb and Zn does exceed the considered background levels in the geological atlas, indicating possible input from other sources than the crustal contribution. The levels of Fe and Al does not exceed the crustal composition levels [139].

The large differences in the natural environment, parameters and properties of the different matrices makes them difficult to compare. The differences in the levels of the selected trace elements in supraglacial material from Austre Brøggerbreen, overbank sediment from Bayelva and marine sediment from Kongsfjorden are dependent on many factors such as differences in input sources, transport and erosion processes and differences in physical and chemical properties. However, the significant higher levels of Fe and Al and significant lower level of Ca in supraglacial material on Austre Brøggerbreen, indicate a lower input of carbonate rocks than in sediment in Bayelva and Kongsfjorden. Higher accumulation rates of most of the trace elements on Austre Brøggerbreen are evident. The in general lower concentrations of the selected trace elements in the overbank sediment in Bayelva and that the levels are within the levels of considered background levels, imply low accumulation from particulate matter from Austre Brøggerbreen in the river sediments. The transport of particulate matter and trace elements released from Austre Brøggerbreen to Kongsfjorden are further discussed in the next section.

Table 5.5.: The mean, relative standard deviation in percentage (RSD%), the median, the minimum and the maximum concentration (µg/g) of lead (Pb), cadmium (Cd), arsenic (As), chromium (Cr), zinc (Zn), iron (Fe), aluminum (Al) and calcium (Ca) in supraglacial material from Austre Brøggerbreen, overbank sediment from Bayelva and marine sediment from Kongsfjorden.

Site		Pb	Cd	As	Cr	Zn	Fe	Al	Ca
Austre Brøggerbreen	Mean	55.8	0.0946	6.79	63.9	105	45500	45400	4090
	RSD%	52.8	28.5	44.5	10.2	8.6	9.9	13.1	24.0
	Median	40.5	0.0912	5.62	61.9	105	45500	43500	4010
	Min.	34.6	0.0529	3.68	56.9	88.1	37200	39100	2580
	Max.	122	0.147	13.0	79.3	123	52200	55800	5610
Bayelva	Mean	12.4	0.174	4.35	35.3	47.5	18300	20500	49300
	RSD%	31.9	37.0	17.0	14.7	14.7	43.3	41.7	109.9
	Median	13.7	0.166	4.33	36.0	50.1	22300	23500	21100
	Min.	5.50	0.0971	3.35	26.8	32.5	1030	1220	14400
	Max.	17.8	0.301	5.89	45.3	56.0	24900	28600	155500
Kongsfjorden	Mean	13.9	0.0947	6.88	45.3	61.7	25500	32900	44200
	RSD%	10.8	23.4	35.8	13.3	15.7	12.1	14.3	13.0
	Median	14.0	0.0983	6.64	44.2	63.4	25600	32100	46400
	Min.	11.3	0.0571	3.23	37.1	42.9	20900	26100	33100
	Max.	16.2	0.131	11.4	56.3	78.9	30300	41000	49600

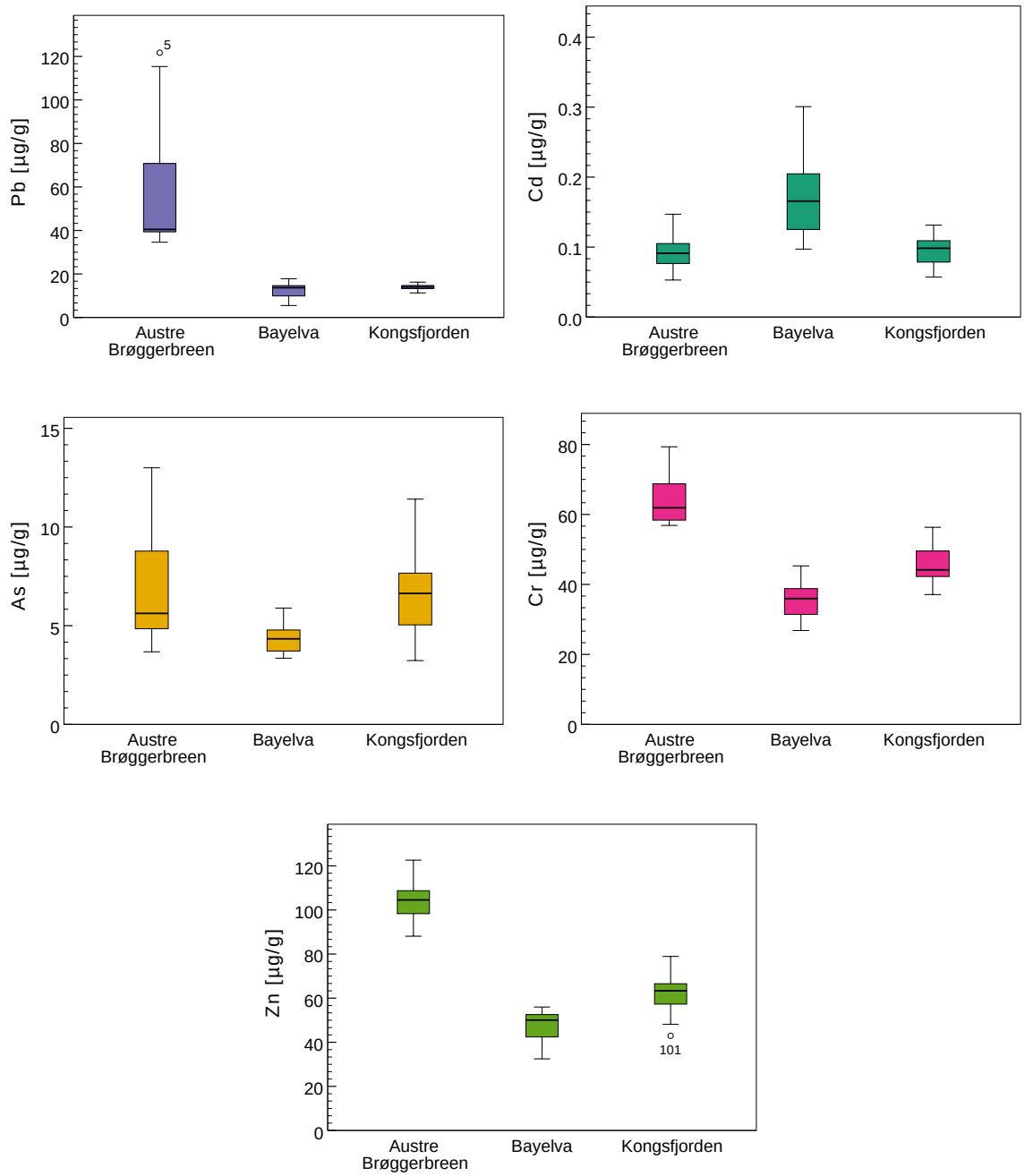

Figure 5.10.: Concentrations (µg/g) of lead (Pb), cadmium (Cd), arsenic (As), chromium (Cr) and zinc (Zn) in supraglacial material from Austre Brøggerbreen, overbank sediment from Bayelva and marine sediment from Kongsfjorden presented as box plots. Outliers are labeled (o).

,

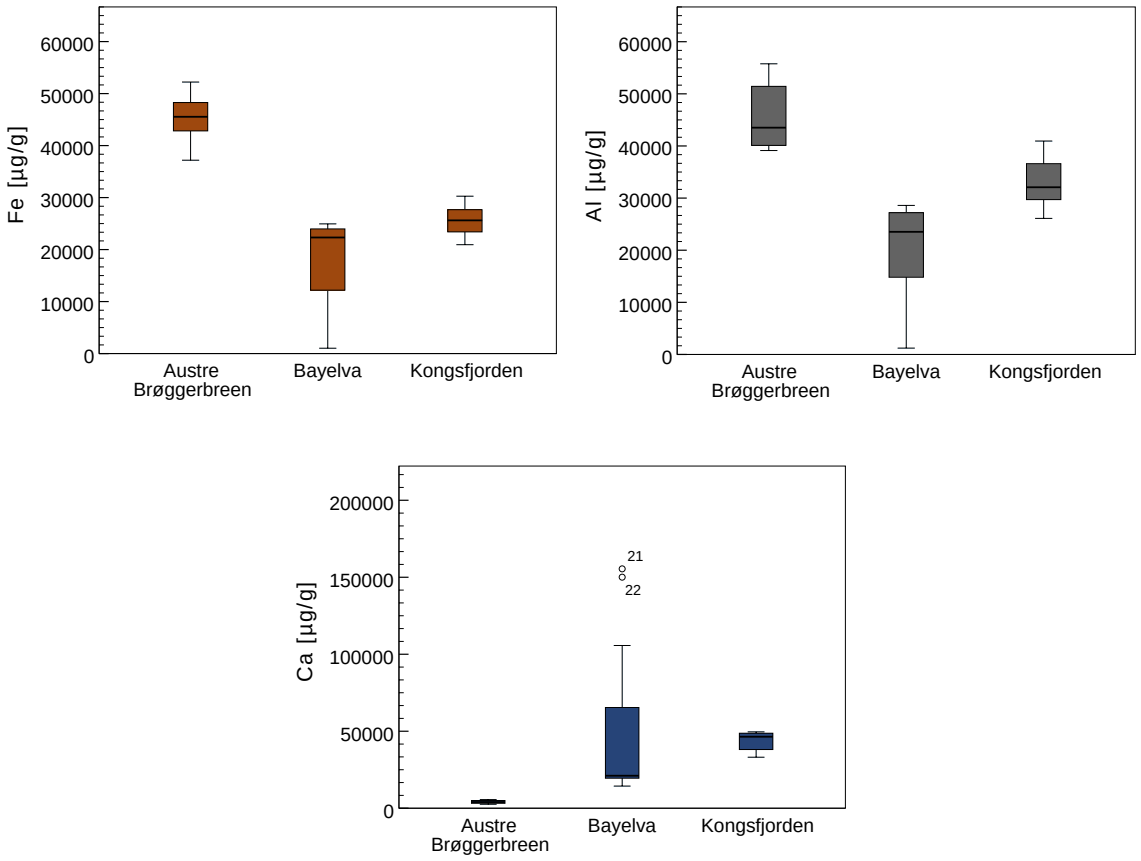

Figure 5.11.: Concentrations (µg/g) of iron (Fe), aluminum (Al) and calcium (Ca) in supraglacial material from Austre Brøggerbreen, overbank sediment from Bayelva and marine sediment from Kongsfjorden presented as box plots.

5.3. Possible transport pattern of particulate matter from glacier to fjord

A principal component analysis (PCA) was applied for determining possible correlations between the marine sediment composition in Kongsfjorden and the transport of particulate matter from Austre Brøggerbreen to Bayelva. The PCA score- and loading-plot for PC1 and PC2 for correlations between samples of marine sediment and selected elements are presented in Figure 5.12 and 5.13 respectively. The numbers denote the distance in meter from the Bayelva outlet into the fjord. NE, E and SW denotes the direction: north-east, east and south-west respectively for the river outlet.

The horizontal PC1 explains 58% of the variance in the data set and are related to the distance from the river outlet (Figure 5.12). The samples closest to the river outlet (750mNE), see Figure 3.6, are placed far to the left in the plot and the samples furthest away fro the outlet (1900mE) are placed far to the right. The sediments furthest out are, among several, rich in Fe, Al, Pb and Cr (Figure 5.13). The samples closest to the river outlet have lower concentrations of the mentioned elements, and have higher levels of Ba, Si, Sb and Ca. These results indicate that there is a correlation between the transport of elements and the river flow. It is previously observed that there is a relationship between the color of the river and the river flow. Moe (2018) observed in her master's thesis a change in the color of Bayelva from red to light grey with decreasing intensity of the river flow, with decreasing temperatures in the autumn [13]. This suggests a change in the sediment flux in the river with the river flow. There is also observed an increase in suspended sediment in the river water with increasing water flow [149]. That the sediments furthest out are rich in iron, implies that these are more impacted by sediments transported from the reddish river water that are observed emerging from Austre Brøggerbreen. When the river flow is high, water and suspended sediment will reach the river outlet at a higher velocity than at lower flows and will be transported further out into the fjord. That the sediments closest to the river outlet are lower in Fe, indicates that they have higher contribution from the grey part of the river, observed emerging from Vestre Brøggerbreen. This agrees with the observations that the river is light grey at low flow rates.

This can also be supported by studying the river water samples. Moe (2018) observed and reported that the water emerging from Austre Brøggerbreen had significantly higher concentrations of Fe, Al and Mn whilst the water emerging from Vestre Brøggerbreen had significantly higher concentrations of Ca and Mg [13]. Moreover, this was also reported in two other previous master's theses by Hald (2014) [150] and Nordum (2012) [151]. This is the case for the river water

samples collected in this thesis as well. The concentration of Ca, Fe, Mg and Mn in river water samples collected from the water emerging from Austre (point P15) and Vestre (point P14) Brøggerbreen are presented in Table 5.6. The concentration of Ca is 2.1 times higher, and the concentration of Mg is 1.9 times higher in the water from Vestre than from Austre. Similarly, the concentration of Ca and Mg was approximately two times higher on the Vestre side than in Austre in both Moe's and Hald's study.

Notably, the concentration of Fe is not significantly different in the two meltwater streams from this thesis. This can be due to diurnal variations. The samples at the different points were not sampled at the same day nor at the same time of day. The samples from Austre were collected two days prior to the samples at Vestre. In addition, the samples at Austre were sampled late in the day where the temperature had dropped for the day and melting rates are lower. Diurnal changes in pH, turbidity, conductivity and dissolved oxygen, are all factors affecting the concentration of dissolved ions in water [15]. Large diurnal variations in the Fe concentration in Bayelva was discovered by Hald (2015) and Nordum (2012) in their theses [150, 151].

On the other hand, higher concentrations of Fe in water from Austre was reported in all three master's theses mentioned above [13, 150, 151]. Nordum (2012) reported a mean concentration of 0.67 µg/L in the meltwater stream from Vestre and a mean concentration of 12 µg/L in the meltwater stream from Austre being 17.9 times higher. The same trend was both observed in 2018 by Moe and in 2015 by Hald with Fe concentrations several times higher in water from Austre. The concentrations of Mn and Al was also several magnitudes higher in the water from Austre than Vestre in all three theses, with concentrations 5.0-14.1 times higher for Mn and 4.2-9.5 times higher for Al. This was also the case in this thesis with a mean concentration of 4.37 µg/L at Austre and 0.00443 µg/L at Vestre for Mn and 18.2 and 4.31 µg/L for Al in Austre and Vestre, respectively.

With Pb and Cr being clustered together with Fe and Al in the PCA loading-plot, indicate that they originate from the same source, Austre Brøggerbreen. As previously discussed, the levels of Pb and Cr are significantly higher in supraglacial material than in overbank sediment and this might imply that they are being transported out into the fjord with the particulate matter from Austre Brøggerbreen. Zn is also placed relatively far to the right in the PC1 and has a significantly higher concentration in supraglacial material. Especially Pb and Zn was shown, in both Hald (2015) and Moe (2018), to have significant positive correlations in the river water which can indicate common source. In Nordum's (2012) study significant positive correlations was found between Fe and Pb, and especially strong at the sampling point at Austre Brøggerbreen. For the water samples (Table 5.6) in this

thesis Pb was only detected in one sample in the meltwater stream from Austre. Several magnitudes (4-28 times) higher concentrations of Pb on the Austre side was detected in Nordum (2011), Hald (2015) and Moe (2018) [13, 150, 151]. This was also the trend for Zn in all three theses, the concentration was higher in the water emerging from Austre. This was not found in this thesis, as seen in Table 5.6. The Zn concentration in the meltwater fra Austre was lower than in the meltwater from Vestre. This can be, as previously discussed, due to diurnal differences since the samples from Austre and Vestre was not sampled on the same day. Since the concentration of Fe in the river water from Austre also was generally low, this might be the case.

The clustering of Fe, Al, Pb, Cr and Zn in the PCA plot might also indicate similar transport mechanisms in the river water. However, this is all speculations and need to be further investigated. Another thing to consider is that the water samples investigated in all four data sets are filtered water and the concentrations presented are considered as the dissolved load. Since trace elements strongly bind to particles, the concentration would be higher in unfiltered water and they might show different trends.

Moe (2018) also studied the differences in the water chemistry in Bayelva between early and late in the melting season, spring and autumn [13]. They measured a difference in the turbidity between the seasons and observed a link between the turbidity and the river flow. The turbidity was higher in the beginning of the autumn period than in the spring. This corresponds with the observed increased flow rate in the beginning of the autumn. As the river flow decreased at the end of the period in the autumn, changing the color from red to grey, and from being dominated by the runoff from Austre Brøggerbreen to the runoff from Vestre Brøggerbreen, the turbidity in the river decreased. This indicates a decrease in particulate matter in the river water with decreasing flows. Additionally, a significant negative correlation was found between the turbidity and the conductivity in the river. This implying that the more particulate matter in the river, the more ions are absorbed to particles and transported with the particulate matter. This can be strengthened by the increase in concentrations of the dissolved metal ions in the river samples of Moe at the end of the autumn period. Hald (2015) measured a higher turbidity from the meltwater stream from Austre Brøggerbreen than from Vestre Brøggerbreen suggestion that more particulate matter is released from Austre Brøggerbreen than from Vestre Brøggerbreen.

The PC2 is more uncertain and only explains 15% of the variance in the data set. Nevertheless, this variance seems to be related to the direction out from the river outlet, north-east (NE) or south-west (SW). The sediments related to the direction north-east, hence the sediments closest to Ny-Ålesund (Figure 3.6), are associated

with As, Ti, Ca and S while the sediments in the south-west direction are lower in these and have higher concentrations of Cu and Mo. The elements associated with the sediments closest to Ny-Ålesund can stem from pollution sources related to the establishment. Before the construction of a sewage treatment system in 2015, wastewater and sewage from Ny-Ålesund was directly release into the fjord [152]. The bay close to the sampling point in the fjord, was also used as a dumpsite. There are previously reported high concentrations of arsenic in the sediments related to the dumpsite [152]. In addition, the higher levels of these elements can be related to the airport and aviation that are situated relatively close to the river outlet area.

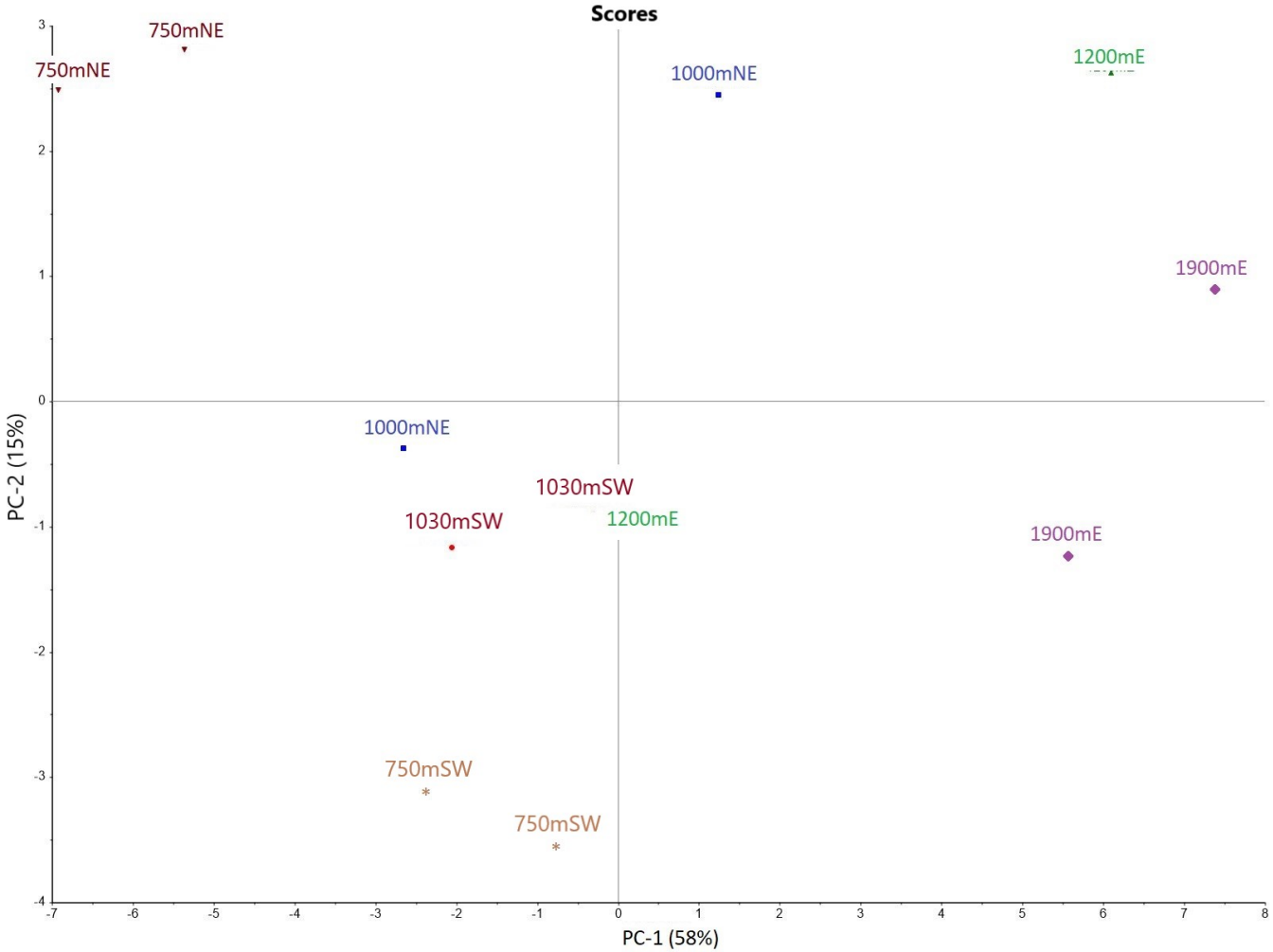

Figure 5.12.: Principal component analysis (PCA) score-plot for marine sediment for PC1 and PC2 with sample point as displayed property. The numbers denote the distance in meter from the river outlet into the fjord. NE: north-east; E: east; SE: south-east.

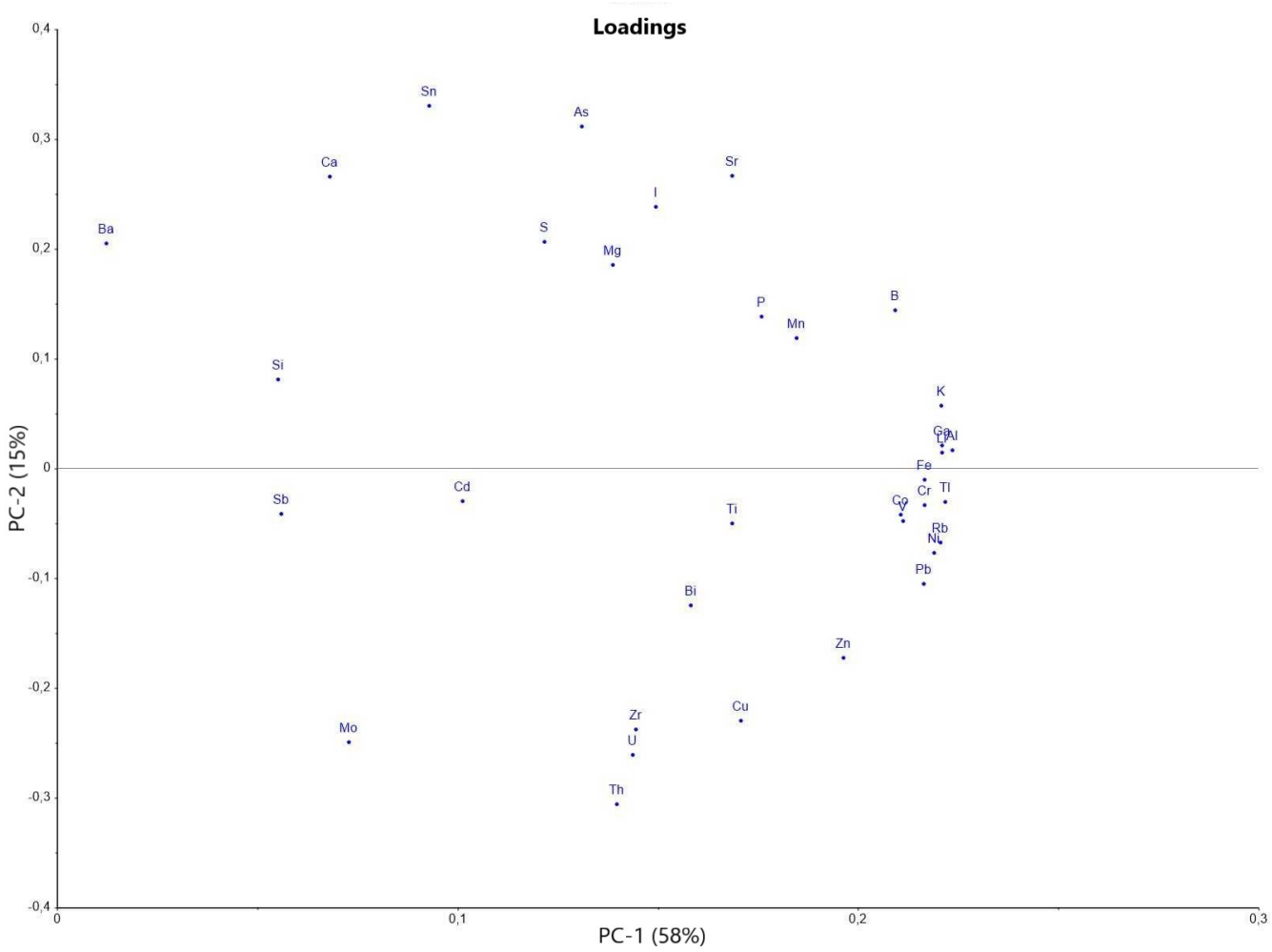

Figure 5.13.: Principal component analysis (PCA) loading-plot for PC1 and PC2 for selected elements in marine sediment.

Table 5.6.: Mean concentration (µg/L) ± RSD% of aluminum (Al) calcium (Ca), iron (Fe), magnesium (Mg), manganese (Mn) lead (Pb), chromium (Cr) and zinc (Zn) in meltwater from Austre and Vestre Brøggerbreen.

	Austre	**Vestre**
Al	18.2 ± 115.2	4.31 ± 6.2
Ca	9220 ± 1.0	19100 ± 4.3
Fe	1.14 ± 65.9	1.11 ± 66.0
Mg	2280 ± 8.5	4420 ± 4.1
Mn	4.37 ± 101.9	0.0443 ± 27.3
Pb	0.00227	-
Cr	0.0262 ± 0.1	0.0906 ± 6.7
Zn	0.213 ± 0.01	0.455 ± 67.8

5.3.1. Possible future consequences of particulate matter release from a melting glacier

From the previous discussion it can be implied that Austre Brøggerbreen dominate the sediment yield to Bayelva during the melting season, releasing higher amounts of particulate matter to Bayelva than from Vestre Brøggerbreen. It is also evident that the chemical composition of the particulate matter released from the two glaciers are different and have different elemental inputs to the glacier-fed river system. Edwards *et al.* found that the supraglacial material on Austre Brøggerbreen composed of finer particles than the particles in Vestre [134]. This can suggest that particles from the Austre Brøggerbreen runoff are kept longer in the suspended load and are not easily subjected to sedimentation. Trace elements have a stronger affinity to finer particles because of the considerably higher surface to charge area [55]. This, in addition to the higher amount of particles released from Austre Brøggerbreen with increasing river flow, can be the reason for the higher levels of Pb, Cr and Zn in the marine sediments further out in Kongsfjorden. The levels for Pb and Zn is also slightly higher than Pb and Zn levels from the geochemical atlas [139]. It is though possible that the elevated concentrations is due to other local sources, such as anthropogenic activity, sea ice and melting of other glacier in the area, and/or long-range oceanic transport.

As the mass balance of glaciers continue to decrease, a change in thermal regimes has been reported [153]. Studies have reported the change in the thermal regime of Austre Brøggerbreen since the first half of the 90's from polythermal to gradually containing more and more cold-based ice [154]. Thermal regimes affect

the englacial (inside a glacier) deformation of the ice and thus the pathways of supraglacial meltwater. Meltwater pathways in polythermal glaciers are dominated by englacial and subglacial drainage systems. This is due to the high englacial deformation of warm-based ice especially during the melting season. This can make meltwater and runoff trapped in the ice instead of reaching the glacier snout and the glacier-fed river. Cold-based glaciers are less susceptible to englacial deformation and tend to form larger supraglacial meltwater channels. It is therefore suggested that with the changes in thermal regimes and thus meltwater drainage systems that this will change the sediment yield to Bayelva, possibly bringing more of the supraglacial material to Bayelva [110, 153]. This possibly leading to a higher release of the hazardous trace elements from Austre Brøggerbreen to Bayelva and Kongsfjorden from meltwater and supraglacial material.

In addition, as the temperature in the Arctic keeps increasing, leading to longer melting seasons and higher melting rates, erosion and transport of sediments from Austre Brøggerbreen to the river and fjord will increase in the short term. The results from the PCA-plots showing that the transport of particulate matter, and thus trace elements, are dependent on flow rates in the river, can imply a large change in the chemical composition of marine sediments in the fjord. This will also affect the concentrations and speciation of trace elements in the water. These changes can lead to drastic impacts on Arctic biota, since they are highly sensitive to small changes in the environment.

Table 5.7.: Mean concentrations (µg/g ± RSD%) of lead (Pb), cadmium (Cd), arsenic (As), chromium (Cr), zinc (Zn), iron (Fe) and aluminum (Al) in supraglacial material, overbank sediment and marine sediment in this thesis and levels found in comparable studies.

Source	Site	Sample type	Pb	Cd	As	Cr	Zn	Fe	Al
This thesis	Austre Brøggerbreen	Supraglacial material	55.8±52.8	0.0946±28.5	6.79±44.5	63.9±10.2	105±8.6	45500±9.9	45400±13.1
	Bayelva	Overbank sediment	12.4±31.9	0.174±37.0	4.35±17.0	35.3±14.7	47.5±14.7	18300±43.3	20500±41.7
	Kongsfjorden	Marine sediment	13.9±10.8	0.0947±23.4	6.88±35.8	45.3±13.3	61.7±15.7	25500±12.1	32900±14.3
Shaw *et al.* (1967, 1976), Wedepohl (1995) [136–138]	Western Europe and Canada	Crustal composition	14.8	0.1	1.7	126	65	43200	79600
Geochemical atlas (2010) [139]	Brøggerdalen	Overbank sediment	0.5-8.8		0-9	10-70	11.0-58.8	0.063-1.776%	0.176-0.828 %
Singh *et al.* (2013) [9]	Midre Lovenbreen	Cryoconite	73.88±1.38	0.060±0.015	14.22±0.32	52.37±1.27	150±11.11	28186±437	38603±405
			85.08±0.009	0.080±0.015	13.73±0.51	58.72±0.23	138±0.12	30400±97.1	42633±194
			57.18±0.11	0.145±0.017	12.05 ± 0.19	60.68 ± 0.5	146±2.26	32413±55.7	41763±172
			49.87±0.4	0.043±0.008	11.01±0.35	59.57±0.26	132±1.15	31496±155	42870±154
Lokas *et al.* (2016) [10]	Hansbreen, Hornsund	Cryoconite	54.38	0.420			84.31	54280	
Kveli (2015) [147]	Bayelva	Overbank sediment	8.69	0.188	3.26	33.9	30.4	15600	19500
			11.5	0.179	3.75	37.5	44.9	20200	22700
			10.8	0.155	3.95	31.4	40.3	20400	20900
NGU report (2019) [148]	Kongsfjorden	Marine sediment	19.2-25.0	0.05-0.1	18-71	40.0-50.0	70-90		

5.4. Sources of error

Sources of error and sources of contamination can be present from sampling to data treatment even though quality assurance and quality control measures are included. Due to limitations in the scale of the project, time and resources, some quality control measures were not included or conducted. The inclusion of these could probably strengthen the reliability of the data.

Field blanks and blanks for transportation was not included. This would have determined possible contamination in the field and through the transportation from Ny-Ålesund to NTNU. However, contamination from air are considered to be low in the sampling area. Quality assurance and control measures from ISO-standards for collection and handling of samples are followed as close as possible. Method blanks were included in the ICP-MS analysis and had levels under the limit of quantification (LOQ) for all elements, except for Al, Fe, Cl, Ca, Ti, Cr and Cu. These levels were though several magnitudes lower than in the samples and were almost at the level of the LOQ, thus results were not adjusted for the blanks. To determine accuracy in the microwave digestion and the ICP-MS analysis, certified reference material (CRM) was included. The samples were not adjusted for the recovery of the CMR. Some deviation was seen in the levels measured compared to the levels from the manufacturer. However, these differences was not notably big and for the selected trace elements (Pb, Cd, As, Cr, Zn, Fe and Al) the values were close to the given value. Measured concentrations of the elements in the CRM and the levels from the manufacturer are presented in the supplementary Excel sheet.

An important factor to consider for the elemental results conducted by ICP-MS is the additional dilution step upon analysis. Supraglacial material and sediment samples where diluted 25 times due to instrument malfunctions. This is can have caused several elements to be under the limit of quantification (LOQ), such as mercury. Due to limitations in capacity, the samples were also analyzed later than planned and this can have caused volatile compounds to evaporate, e.g Hg.

As previously discussed, precipitation was observed in all vials after the microwave digestion and is believed to be residue of undissolved silicates. This is due to the use of nitric acid that does not dissolve silicates. The use of hydrofluoric acid (HF) would have dissolved SiO_2 but can cause damages to the plasma in the ICP-MS instrument. Since HNO_3 does not dissolve SiO_2, metals can be contained in the crystal structure of silicate and therefore be retained in the precipitation [61]. This can have lead to lower concentrations of some elements. The concentrations for the selected elements are though comparable to other studies and was close to the given values for the CRM. The concentration of silicone in the CRM was not included in the values from the manufacturer and the possible mechanical loss of

silicates from the microwave digestion could not be calculated.

Although ICP-MS is one of the most effective techniques for analysing trace elements, errors due to spectroscopic interferences can occur. As mentioned in the theory section, spectroscopic interferences can cause non-analyte species to have the same m/z ratio as an analyte species which leads them to be detected together. This can cause deviations from the true concentration of the analyte in the sample. The formation of MoO can cause interference with Cd. This was though adjusted for by correcting the Cd concentration according to the Mo content. Other examples of spectroscopic interferences that can have affected the concentration of the selected elements are the formation of ArO^+ which has the same m/z ratio as $^{56}Fe^+$ at 58 amu [69] and the formation of $^{35}Cl^{16}O$ and $^{40}Ar^{35}Cl$ that have the same m/z ratio as ^{75}As [68].

5.5. Shortcomings and further research

The above discussion leaves many questions unanswered and involves many assumptions that need further research and backup from field data. Due to the limitations in the scale of a master's project, priorities and decisions were made to focus on the supraglacial material and sediment collected. This leaves some shortcomings to the research. The glacier-fed river system and sediment transport transport from glacier to fjord are complex and many factors are involved. There are many factors that are not accounted for in this thesis that need further investigation. Field work was carried out and several samples were collected that are outside the scope of this project. The methodology and results were still included for additional knowledge on the glacier-fed river system and for possible future studies.

Several assumptions are made on a small number of samples. A higher number of samples was not collected due to limitations in transport capacity from Ny-Ålesund til Trondheim. A higher number of samples would strengthen the reliability of the results. This is especially prominent for the supraglacial material where the sample size was to small to test for statistical significance. A more comprehensive study of the chemistry of the supraglacial material on Austre Brøggerbreen is needed to support the indications on differences in color and possible pollution sources of trace elements.

It is evident that the sediment supply and input of trace elements to Bayelva is also affected by the runoff from Vestre Brøggerbreen. Samples of supraglacial material from Vestre Brøggerbreen was not collected and would contribute to the observed differences in the meltwater streams from the two glaciers. More samples

and a more comprehensive study on the difference between the two glacier would also increase the knowledge on the supply and transport of trace elements with particulate matter to Bayelva and Kongsfjorden.

Results from the river water samples were used to strengthen the observations of the difference in the runoff from the two glaciers, and for the observations in the PCA plot for the marine sediment. The results for several water samples was not included but further studies on the transport of particulate matter in the river water and trace elements from glacier snout to the outlet to Kongsfjorden are needed.

For down scaling purposes of this project, the results for the seawater samples were not included. Studies on the levels of the selected trace elements in the seawater as a function of distance from the river outlet and depth would gain knowledge on the transport and fates of particulate matter.

The concentrations of elements studied in this thesis are the total concentration and does not give information on trace element speciation. Outlining of element speciation in all matrices will give a better picture on the transport and fate of the trace elements from glacier to fjord.

From the results conducted in this thesis, it is evident that a continuous monitoring of the changes in runoff patterns, sediment flux and levels of trace elements in all parts of the glacier-fed river system, from glacier to fjord, is needed.

6. Conclusions

The Bayelva basin and Kongsfjorden, situated close to Ny-Ålesund on Svalbard, was studied to determine potential impact on the release of fine particulate matter from a melting glacier to a glacier-fed river system. This was done by studying the chemical composition of supraglacial material from the glacier Austre Brøggerbreen, overbank sediment from the river Bayelva, and marine sediment from the fjord Kongsfjorden.

The supraglacial material was dominated by inorganic material, with generally low Total Carbon and Nitrogen content. The major elemental components were Fe, Al, Mg and K. The chemical composition of different colored supraglacial material, black, brown, red-brown and red, was compared, and the chemical composition varied markedly despite the sampling point being relatively close to each other. Red and red-brown supraglacial material contained higher levels of Fe and Al probably due to the input of reddish sandstone. The black material had elevated Pb and As concentrations that exceeded the crustal background levels. The levels of Pb and Zn in all supraglacial samples exceeded the crustal background levels, indicating possible external local sources and/or long-range transport.

The overbank and marine sediments were dominated by Ca, Fe, Al and Mg. The levels of several trace elements were higher in supraglacial material than in overbank and marine sediment. Levels of Cr, Zn, Fe and Al where highest in supraglacial material followed by marine sediment and overbank sediment. Elevated concentrations of Pb and Zn relative to background levels were found in marine sediments.

Results from a principal component analysis (PCA) of elements in marine sediment from Kongsfjorden had PC1 explaining 58% of the variances in the data set, which seemed to be explained by the distance from the river outlet. Sediments furthest out in the fjord showed higher concentrations of, among others, Fe, Al, Pb, Cr and Zn while the sediments closest to the river outlet had higher concentrations of Ba, Si and Ca. That the sediments furthest out were rich in iron, implies that these are more impacted by sediments transported from the reddish river water that are observed emerging from Austre Brøggerbreen at high flow rates. That the sediments closest to the river outlet are lower in Fe and higher in Ca, indicates that

they have higher contribution from the grey part of the river, observed emerging from Vestre Brøggerbreen, which agrees with earlier observations that the river is light grey at low flow rates.

The association of Pb, Cr and Zn with Fe and Al in the PCA, combined with the higher levels of these elements further out from the river outlet, can imply higher transport rates of these elements via particles from Austre Brøggerbreen. As the temperature in the Arctic keeps increasing, leading to changes in meltwater runoff patterns, longer melting seasons and higher melting rates, erosion and transport of sediments from Austre Brøggerbreen to the river and fjord will increase in the short term. This can imply a large change in the chemical composition of marine sediments in Kongsfjorden. These changes could further lead to drastic impacts on biota, since the Arctic ecosystem is highly sensitive to small changes in the environment.

Bibliography

1. Box, J. E., Colgan, W. T., Christensen, T. R., Schmidt, N. M., Lund, M., Parmentier, F.-J. W., Brown, R., Bhatt, U. S., Euskirchen, E. S., Romanovsky, V. E., Walsh, J. E., Overland, J. E., Wang, M., Corell, R. W., Meier, W. N., Wouters, B., Mernild, S., Mård, J., Pawlak, J. & Olsen, M. S. Key indicators of Arctic climate change: 1971–2017. *Environmental Research Letters* **14,** 045010 (2019).
2. Svendsen, H., Beszczynska-Møller, A., Hagen, J. O., Lefauconnier, B., Tverberg, V., Gerland, S., Børre Ørbæk, J., Bischof, K., Papucci, C., Zajaczkowski, M., Azzolini, R., Bruland, O. & Wiencke, C. The physical environment of Kongsfjorden–Krossfjorden, an Arctic fjord system in Svalbard. *Polar Research* **21,** 133–166 (2002).
3. *Massebalanse for isbreer på Svalbard* Miljøovervåking Svalbard og Jan Mayen (MOSJ).
   `https://www.mosj.no/no/klima/land/massebalanse-isbreer.html`
   (last accessed Apr. 12, 2021).
4. Milner, A. M., Brown, L. E. & Hannah, D. M. Hydroecological response of river systems to shrinking glaciers. *Hydrological Processes* **23,** 62–77 (2009).
5. Wharton, R. A., McKay, C. P., Simmons, G. M. & Parker, B. C. Cryoconite Holes on Glaciers. *BioScience* **35,** 499–503 (1985).
6. Säwström, C., Mumford, P., Marshall, W., Hodson, A. & Laybourn-Parry, J. The microbial communities and primary productivity of cryoconite holes in an Arctic glacier (Svalbard 79°N). *Polar Biology* **25,** 591–596 (2002).
7. Novotná Jaroměřská, T., Trubač, J., Zawierucha, K., Vondrovicová, L., Devetter, M. & Žárský, J. D. Stable isotopic composition of top consumers in Arctic cryoconite holes: revealing divergent roles in a supraglacial trophic network. *Biogeosciences* **18,** 1543–1557 (2021).
8. Zawierucha, K., Baccolo, G., Di Mauro, B., Nawrot, A., Szczuciński, W. & Kalińska, E. Micromorphological features of mineral matter from cryoconite holes on Arctic (Svalbard) and alpine (the Alps, the Caucasus) glaciers. *Polar Science* **22,** 100482 (2019).

9. Singh, S. M., Sharma, J., Gawas-Sakhalkar, P., Upadhyay, A. K., Naik, S., Pedneker, S. M. & Ravindra, R. Atmospheric deposition studies of heavy metals in Arctic by comparative analysis of lichens and cryoconite. *Environmental Monitoring and Assessment* **185,** 1367–1376 (2013).
10. Łokas, E., Zaborska, A., Kolicka, M., Różycki, M. & Zawierucha, K. Accumulation of atmospheric radionuclides and heavy metals in cryoconite holes on an Arctic glacier. *Chemosphere* **160,** 162–172 (2016).
11. Hodson, A. J. & Ferguson, R. I. Fluvial suspended sediment transport from cold and warm-based glaciers in Svalbard. *Earth Surface Processes and Landforms* **24,** 957–974 (1999).
12. Novigatskii, N., Klyuvitkin, A. & Lisitzin, A. P. The speed of sedimentation, vertical flow of matter, and the absolute mass of precipitation in the shelf region of Russian Arctic. *Journal of Oceanological Research* **46,** 167–179 (2018).
13. Moe, B. *Trace elements in Arctic river water during seasonal transitions* Master's thesis (NTNU, 2018).
14. Mao, L., Comiti, F., Carrillo, R. & Penna, D. *Sediment Transport in Proglacial Rivers* in *Geomorphology of Proglacial Systems. Geography of the Physical Environment* (eds Heckmann, T. & Morche, D.) 199–217 (Springer International Publishing, Cham, 2019).
15. Gregory, J. *Particles in Water. Properties and Processes.* (CRC Press. Taylor & Francis Group, 2007).
16. Sund, M. *Polar hydrology - Norwegian Water Resources and Energy Directorate's work in Svalbard* tech. rep. (Norwegian Water Resources and Energy Directorate, Oslo, Norway, 2008).
17. Umbreit, A. *Spitsbergen. Svalbard, Franz Josef Land, Jan Mayen* Third (Bradt Travel Guides Ltd, Chalfont St Peter, Bucks, England, 2008).
18. *Svalbard* Norwegian Polar Institute. `https://web.archive.org/web/20120415125926/http://www.npolar.no/en/the-arctic/svalbard/index.html` (last accessed May 6, 2021).
19. Shears, J., Theisen, F., Bjørdal, A. & Norris, S. Environmental impact assesment: Ny-Ålesund international scientific research and montoring station, Svalbard. *Meddelelser* (1998).
20. *Environment and climate in the arctic* Norwegian Polar Institute. `https://web.archive.org/web/20120427162622/http://www.npolar.no/en/the-arctic/environment-and-climate/` (last accessed May 6, 2021).

21. Clunies-Ross, P. *Glacial suspended particulate matter : character, composition and adsorption potential in freshwater environments* PhD thesis (University of Canterbury, 2017).

22. Wharton, R. A., Vinyard, W. C., Parker, B. C., Simmons, G. M. & Seaburg, K. G. Algae in cryoconite holes on Canada Glacier in Southern Victorialand, Antarctica. *Phycologia* **20,** 208–211 (1981).

23. Hambrey, M. J. & Glasser, N. F. *Sediment Entrainment, Transport, and Deposition* in *Encyclopedia of Snow, Ice and Glaciers* (eds Singh, V. P., Singh, P. & Haritashya, U. K.) 984–1003 (Springer Nature, Dordrecht, 2011).

24. Brittain, J. E., Bogen, J., Khokhlova, L. G., Melvold, K., Steinina, A. S., Gíslson, G. M., Brørs, S., Kochanov, S. K., Ólafson, J. S., Ponomerv, V. I., Jensen, A. J., Kokovkin, A. V. & Petterson, L.-E. *Artic Rivers* in *Rivers of Europe* (eds Tockner, K., Uehlinger, U. & Robinson, C. T.) 337–379 (Academic Press, 2009).

25. Mayr, E. & Hagg, W. *Debris-Covered Glaciers* in *Geomorphology of Proglacial Systems. Geography of the Physical Environment* (eds Heckmann, T. & Morche, D.) 59–71 (Springer International Publishing, 2019).

26. Takeuchi, N., Kohshima, S. & Seko, K. Structure, Formation, and Darkening Process of Albedo-reducing Material (Cryoconite) on a Himalayan Glacier: A Granular Algal Mat Growing on the Glacier. *Arctic, Antarctic, and Alpine Research* **33,** 115–122 (2001).

27. Takeuchi, N. Optical characteristics of cryoconite (surface dust) on glaciers: the relationship between light absorbency and the property of organic matter contained in the cryoconite. *Annals of Glaciology* **34,** 409–414 (2002).

28. De Smet, W. H. & Van Rompu, E. A. Rotifera and Tardigrada from some cryoconite holes on a Spitsbergen (Svalbard) glacier. *Belgian Journal of Zoology* **124,** 27–37 (1994).

29. Anesio, A. M., Mindl, B., Laybourn-Parry, J., Hodson, A. J. & Sattler, B. Viral dynamics in cryoconite holes on a high Arctic glacier (Svalbard). *Journal of Geophysical Research: Biogeosciences* **112** (2007).

30. Tsai, C. W. & Lai, K.-C. Three-State Continuous-Time Markov Chain Model for Mixed-Size Sediment Particle Transport. *Journal of Hydraulic Engineering* **140** (2014).

31. *Sediment Transport* in *Open-Channel Flow* (ed Chaudhry, M. H.) 453–477 (Springer US, Boston, MA, 2008).

32. Stumm, W. & Morgan, J. J. *Precipitation and dissolution* in *Aquatic Chemistry : Chemical Equilibria and Rates in Natural Waters* Third, 349–424 (John Wiley & Sons Inc, New York, United States, 1995).

33. Ouillon, S. Why and How Do We Study Sediment Transport? Focus on Coastal Zones and Ongoing Methods. *Water* **10** (2018).

34. Fifeld, F. & Haines, P. *Trace elements* in *Environmental Analytical Chemistry* Second, 360–392 (London, 2000).

35. Manahan, S. *Environmental chemistry and the five spheres of the environment* in *Environmental Chemistry* Tenth Edit. Chap. Chapter 1 (CRC Press. Taylor & Francis Group, Boca Raton, 2017).

36. Larocque, A. C. L. & Rasmussen, P. E. An overview of trace metals in the environment, from mobilization to remediation. *Environmental Geology* **33,** 85–91 (1998).

37. Kolarova, N. & Napiórkowski, P. Trace elements in aquatic environment. Origin, distribution, assessment and toxicity effect for the aquatic biota. *Ecohydrology & Hydrobiology* (2021).

38. Walker, C., Sibly, R., Hopkin, S. & Peakall, D. *Major Classes of Pollutants* in *Principles of Ecotoxicology* Forth edit, 3–26 (CRC Press. Taylor & Francis Group, 2012).

39. Meillère, A., Brischoux, F., Bustamante, P., Michaud, B., Parenteau, C., Marciau, C. & Angelier, F. Corticosterone levels in relation to trace element contamination along an urbanization gradient in the common blackbird (Turdus merula). *Science of The Total Environment* **566-567,** 93–101 (2016).

40. Poikolainen, J., Kubin, E., Piispanen, J. & Karhu, J. Estimation of the Long-range Transport of Mercury, Cadmium, and Lead to Northern Finland on the Basis of Moss Surveys. *Arctic, Antarctic, and Alpine Research* **36,** 292–297 (2004).

41. Kozak, K., Polkowska, Ż., Stachnik, Ł., Luks, B., Chmiel, S., Ruman, M., Lech, D., Kozioł, K., Tsakovski, S. & Simeonov, V. Arctic catchment as a sensitive indicator of the environmental changes: distribution and migration of metals (Svalbard). *International Journal of Environmental Science and Technology* **13,** 2779–2796 (2016).

42. Hop, H., Borgå, K., Gabrielsen, G. W., Kleivane, L. & Skaare, J. U. Food Web Magnification of Persistent Organic Pollutants in Poikilotherms and Homeotherms from the Barents Sea. *Environmental Science & Technology* **36,** 2589–2597 (2002).

43. Le Roux, G., Hansson, S. V. & Claustres, A. *Inorganic Chemistry in the Mountain Critical Zone: Are the Mountain Water Towers of Contemporary Society Under Threat by Trace Contaminants?* in *Mountain Ice and Water* (eds Greenwood, G. B. & Shroder, J. F. B. T. .-. D. i. E. S. P.) 131–154 (Elsevier, 2016).

44. Manahan, S. *The geosphere and geochemistry* in *Environmental Chemistry* Eight edit, 405–439 (CRC Press LLC, Boca Raton, USA, 2005).

45. Manahan, S. *Soil and agricultural environmental chemistry* in *Environmental Chemistry* Eigth edit, 441–472 (CRC Press LLC, Boca Raton, USA, 2005).

46. *Arctic Pollution Issues: A State of the Arctic Environment Report* tech. rep. (Arctic monotoring and Assessment Programme (AMAP), Oslo, Norway, 1997).

47. Gouin, T., Mackay, D., Jones, K. C., Harner, T. & Meijer, S. N. Evidence for the "grasshopper" effect and fractionation during long-range atmospheric transport of organic contaminants. *Environmental Pollution* **128,** 139–148 (2004).

48. Wania, F. & MacKay, D. Peer Reviewed: Tracking the Distribution of Persistent Organic Pollutants. *Environmental Science & Technology* **30,** 390A–396A (1996).

49. Hill, D. M. & Aplin, A. C. Role of colloids and fine particles in the transport of metals in rivers draining carbonate and silicate terrains. *Limnol. Oceanography* **46,** 331–344 (2001).

50. Fifeld, F. & Haines, P. *Speciation* in *Environmental Analytical Chemistry* Second, 309–325 (Blackwell Science Ltd., London, 2000).

51. Stumm, W. & Morgan, J. J. *Metal ions in aqueous solution: Aspects of coordination chemistry* in *Aquatic Chemistry : Chemical Equilibria and Rates in Natural Waters* Third, 252–348 (John Wiley & Sons Inc, New York, United States, 1995).

52. Hartnett, H. E. *Dissolved Organic Matter (DOM)* in *Encyclopedia of Geochemistry: A Comprehensive Reference Source on the Chemistry of the Earth* (ed White, W.) `https://doi.org/10.1007/978-3-319-39193-9_155-1` (Springer International Publishing, Cham, 2018).

53. Mostofa, K., Liu, C.-Q., Feng, X., Yoshioka, T., Vione, D., Pan, X. & Wu, F. *Complexation of Dissolved Organic Matter with Trace Metal Ions in Natural Waters* in *Photobiogeochemistry of Organic Matter: Principles and Practices in Water Environments* 769–849 (Environmental Science and Engineering, 2013).

54. Law, J. & Brar, A. *Colloids* LibreTexts Chemistry. https://chem.libretexts.org/@go/page/1595 (last accessed June 30, 2021).

55. Sigg, L., Xue, H., Kistler, D. & Sshönenberger, R. Size Fractionation (Dissolved, Colloidal and Particulate) of Trace Metals in the Thur River, Switzerland. *Aquatic Geochemistry* **6,** 413–434 (2000).

56. Averill, B. & Eldredge, P. *Solutions* in *General Chemistry: Principles, Patterns, and Applications* chap. Chapter 13 (Saylor Foundation, 2011).

57. Fawell, J. *pH in drinking water* tech. rep. (World Health Organisastion (WHO), 2007).

58. Mason, R. P. *Trace elements in aquatic systems* (John Wiley & Sons, 2013).

59. Morrison, G. M. P. *Trace element speciation and its relationship to bioavailablity and toxicity in natural waters* in *Trace element speciation analytical methods and problems* (ed Batley, G. E.) chap. Chapter 2 (CRC Press, Inc., Boca Raton, USA, 1989).

60. Barley, J. *Basic Principles of Freeze Drying* SP Scientific. https://www.spscientific.com/freeze-drying-lyophilization-basics/ (last accessed Apr. 12, 2021).

61. Barnes, R. M., Júnior, D. S. & Krug, F. J. *Introduction to Sample Preparation for Trace Element Determination* in *Microwave-Assisted Sample Preparation for Trace Element Determination* 1–58 (Elsevier B.V., 2014).

62. Hu, Z. & Qi, L. *Sample Digestion Methods* in *Treatise on Geochemistry: Second Edition* 87–109 (Elsevier Inc., 2013).

63. Depalma, A. *How to Achieve Consistency with Microwave Digestion* Lab Manager. https://www.labmanager.com/product-focus/how-to-achieve-consistency-with-microwave-digestion-21854 (last accessed Apr. 21, 2021).

64. Bizzi, C. A., Marlon De Moraes Flores, É., Sogari Picoloto, R., Smanioto Barin, J. & Araújo Nóbrega, J. Microwave-assisted digestion in closed vessels: Effect of pressurization with oxygen on digestion process with diluted nitric acid. *Analytical Methods* **2,** 734–738 (2010).

65. Müller, E. I., Mesko, M. F., Moraes, D. P., Korn, M. d. G. A. & Flores, É. M. *Wet Digestion Using Microwave Heating* in *Microwave-Assisted Sample Preparation for Trace Element Determination* 99–142 (Elsevier B.V., 2014).

66. Nóbrega, J. A., Pirola, C., Fialho, L. L., Rota, G., De Campos Jordão, C. E. & Pollo, F. Microwave-assisted digestion of organic samples: How simple can it become? *Talanta* **98,** 272–276 (2012).

67. Skoog, D. A., West, D. M., Holler, F. J. & Crouch, S. R. *Atomic Spectroscopy* in *Fundementals of analytical chemistry* Ninth, 723–797 (Cengage Learning EMEA, Hampshire, United Kingdom, 2013).

68. Wilschefski, S. C. & Baxter, M. R. Inductively Coupled Plasma Mass Spectrometry: Introduction to Analytical Aspects. *Clin Biochem Rev.* **40,** 115–133 (2019).

69. Robert, T. *Practical Guide to ICP-MS* (Marcel Dekker, Inc., New York, USA, 2004).

70. Lausanne, A. & Kiad6, A. NAA and ICP-MS: A comparison between two methods for trace and ultra-trace element analysis. *Budapest Journal of Radioanalytical and Nuclear Chemistry, Articles* **192,** 29–38 (1995).

71. International Organization for Standardization (ISO). ISO 10694:1995(E) Soil quality - Determination of organic and total carbon after dry combustion (elementary analysis). (1995).

72. Barron, A. & Simon, B. *Physical Methods in Chemistry and Nano Science. Volume 1: Elemental Analysis* chap. Chapter 1 (Midas Green Innovations, Ltd, 2020).

73. *DIN 19539:2016-12 Investigation of solids - Temperature-dependent differentiation of total carbon (TOC_{400}, ROC, TIC_{900})* 2016.

74. Lundanes, E., Reubsaet, L. & Greibrokk, T. *Quantitation* in *Chromoatography. Basic Principles, Sample Preparations and Related Methods* 189–199 (Wiley-VCH Verlag GmbH & Co., Weinheim, Germany, 2014).

75. Skoog, D. A., West, D. M., Holler, F. J. & Crouch, S. R. *Inroduction to Spectrochemical Methods* in *Fundementals of analytical chemistry* Ninth, 250–680 (Cengage Learning EMEA, Hampshire, United Kingdom, 2013).

76. Fifeld, F. & Haines, P. *Separation techniques* in *Environmental Analytical Chemistry* Second Edi, 103–106 (Blackwell Science Ltd., London, 2000).

77. Lundanes, E., Reubsaet, L. & Greibrokk, T. *High-Performance Liquid Chromatography (HPLC)* in *Chromoatography. Basic Principles, Sample Preparations and Related Methods* 73–74 (Wiley-VCH Verlag GmbH & Co., Weinheim, Germany, 2014).

78. Batley, G. E. Quality Assurance in Environmental Monitoring. *Marine Pollution Bulletin* **39,** 23–31 (1999).

79. Fifeld, F. & Haines, P. *Introduction* in *Environmental Analytical Chemistry* Second, 3–12 (Blackwell Science Ltd., London, 2000).

80. *Standards* ISO. `https://www.iso.org/standards.html` (last accessed June 27, 2021).

81. ISO. *ISO 5667-1:2020(E) Water quality — Sampling — Part 1: Guidance on the design of sampling programmes and sampling techniques* (2020).

82. ISO. *ISO 5667-6:2014(E) Water quality Sampling Part 6: Guidance on sampling of rivers and streams* (2014).

83. ISO. *ISO 5667-12:2017(E) Water quality — Sampling — Part 12: Guidance on sampling of bottom sediments from rivers, lakes and estuarine areas* (2017).

84. ISO. *ISO 5667-9:1992(E) Water quality - Sampling - Part 9: Guidance on sampling from marine waters* (1992).

85. ISO. *ISO 5667-19:2004(E) Water quality — Sampling — Part 19: Guidance on sampling of marine sediments* (2004).

86. ISO. *ISO 5667-3:2018(E) Water quality — Sampling — Part 3: Preservation and handling of water samples* (2018).

87. ISO. *ISO 5667-15:2009(E) Water quality — Sampling — Part 15: Guidance on the preservation and handling of sludge and sediment samples* (2009).

88. ISO. *ISO 5667-14:2014(E) Water quality — Sampling — Part 14: Guidance on quality assurance and quality control of environmental water sampling and handling* (2014).

89. *Blanks in Method Validation - Supplement to Eurachem Guide The Fitness for Purpose of Analytical Methods* First (ed Cantwel, H.) (Eurachem, 2019).

90. Raynie, D. E. The Vital Role of Blanks in Sample Preparation. *LCGC North America* **36,** 494–497 (2018).

91. *Certificate of Certified Reference Material Soil* Institute of Geophysical and Geochemical Exploration. `https://www.ncrm.org.cn/Web/OrderingEn/MaterialDetail?autoID=7416` (last accessed July 22, 2021).

92. Armbruster, D. A. & Pry, T. Limit of blank, limit of detection and limit of quantitation. eng. *The Clinical biochemist. Reviews* **29,** S49–S52 (2008).

93. Fifeld, F. & Haines, P. *Analytical environmental data: Assessment and interpretation* in *Environmental Analytical Chemistry* Second Edi, 13–35 (Blackwell Science Ltd., London, 2000).

94. Wattles, W., Dean, S., Duranczyk, I. M., Illowsky, B., Lane, D., Loch, S., Stottlemyer, J. & Wildman, L. *Collaborative Statistics* (ed Wattles, W.) (2014).

95. *Shapiro Wilk Test* Statistics Kingdom. `https://www.statskingdom.com/doc_shapiro_wilk.html` (last accessed June 25, 2021).

96. Zhang, Z. & Shafer, D. *Correlation and regression* in *Introductory Statistic* chap. Chapter 10 (Saylor Foundation, 2012).

97. Kim, T. K. Understanding one-way ANOVA using conceptual figures. *Korean Journal of Anesthesiology* **70,** 22–26 (2017).

98. Stangroom, J. *One-Way ANOVA Calculator, Including Tukey HSD* Social Science Statistics. `https://www.socscistatistics.com/tests/anova/default2.aspx` (last accessed June 25, 2021).

99. *Mann-Whitney U Test* Statistics Kingdom. `https://www.statskingdom.com/test_mann_whitney.html` (last accessed June 25, 2021).

100. Lee, S. & Lee, D. K. What is the proper way to apply the multiple comparison test? *Korean Journal of Anesthesiology* **71,** 353–360 (2018).

101. *Spearman's Rank-Order Correlation* Lund Research Ltd. `https://statistics.laerd.com/statistical-guides/spearmans-rank-order-correlation-statistical-guide-2.php` (last accessed June 25, 2021).

102. Smith, L. I. *A tutorial on Principal Component Analysis* tech. rep. (University of Otago, Otago, New Zealand, 2002).

103. Lever, J., Krzywinski, M. & Altman, N. Points of Significance: Principal Component Analysis. *Nature Methods* **14,** 641–642 (2017).

104. Bruland, O. & Hagen, J. O. Glacial mass balance of Austre Brøggerbreen (Spitsbergen), 1971–1999, modelled with a precipitation-run-off model. *Polar Research* **21,** 109–121 (2002).

105. Krawczyk, W. E., Lefauconnier, B. & Pettersson, L. E. Chemical denudation rates in the Bayelva Catchment, Svalbard, in the Fall of 2000. *Physics and Chemistry of the Earth* **28,** 1257–1271 (2003).

106. Nowak, A. & Hodson, A. Hydrological response of a High-Arctic catchment to changing climate over the past 35 years: a case study of Bayelva watershed, Svalbard. *Polar Research* **32** (2013).

107. *Austre Broeggerbreen, Svalbard* World Glacier Monitoring Service (WGMS). https://wgms.ch/products_ref_glaciers/austre-broeggerbreen-svalbard/ (last accessed Apr. 15, 2021).

108. Zhang, R., John, S. G., Zhang, J., Ren, J., Wu, Y., Zhu, Z., Liu, S., Zhu, X., Marsay, C. M. & Wenger, F. Transport and reaction of iron and iron stable isotopes in glacial meltwaters on Svalbard near Kongsfjorden: From rivers to estuary to ocean. *Earth and Planetary Science Letters* **424,** 201–211 (2015).

109. Alean, J. & Hambrey, M. *Austre Brøggerbreen* SwissEduc. https://www.swisseduc.ch/glaciers/svalbard/austre_broggerbreen/index-en.html (last accessed Apr. 12, 2021).

110. Myreng, S. M. *Characteristics and long-term evolution of an englacial meltwater channel in a cold-based glacier, Austre Brøggerbreen, Svalbard* Master's thesis (NTNU and UNIS, 2015).

111. Zajaczkowski, M. Sediment supply and fluxes in glacial and outwahs fjords, Kongsfjorden and Adventfjorden, Svalbard. *Polish Polar Research* **29,** 59–72 (2008).

112. Henriksen, J., Johansen, B. F., Prestvold, K. & Overrein, Ø. *Ny-Ålesund [78° 55' N 11° 55' Ø]* Norsk Polarinstitutt. http://cruise-handbook.npolar.no/no/kongsfjorden/ny-alesund.html (last accessed Apr. 7, 2021).

113. *TopoSvalbard* Norwegian Polar Institute. https://toposvalbard.npolar.no/ (last accessed Apr. 8, 2021).

114. Haldar, S. & Tišljar, J. *Rocks and Minerals* in *Introduction to Mineralogy and Petrology* 1–37 (Elsevier, 2014).

115. Hodson, A., Tranter, M., Gurnell, A., Clark, M. & Hagen, J. O. The hydrochemistry of Bayelva, a high Arctic proglacial stream in Svalbard. *Journal of Hydrology* **257,** 91–114 (2002).

116. *Geological Map Svalbard* Norwegian Polar Institute, Norwegian Polar Geological Sample Archive. https://geokart.npolar.no/geologi/GeoSvalbard/#12/78.9338/11.7239 (last accessed May 1, 2021).

117. Alloway, B. J. *Sources of heavy metals and metalloids in soil* in *Heavy Metals in Soil* (ed Springer) 11–50 (2013).

118. Barrie, L. A., Gregor, D., Hargrave, B., Lake, R., Muir, D., Shearer, R., Tracey, B. & Bidleman, T. Arctic contaminants: sources, occurrence and pathways. *Science of The Total Environment* **122,** 1–74 (1992).

119. King, H. M. *Anhydrite* Geology.com. https://geology.com/minerals/anhydrite.shtml (last accessed July 22, 2021).

120. *Clay Minerals* in *Encyclopedia of Geology (Second Edition)* (eds Alderton, D. & Elias, S. A.) 341–349 (Academic Press, Oxford, 2021).

121. Brigatti, M. F., Galán, E. & Theng, B. K. *Structure and Mineralogy of Clay Minerals* in *Developments in Clay Science* 21–81 (Elsevier B.V., 2013).

122. King, H. M. *Kyanite* Geology.com. https://geology.com/minerals/kyanite.shtml (last accessed Apr. 15, 2021).

123. Zhou, C., Tong, D. & Yu, W. *Smectite nanomaterials: Preparation, properties, and functional applications* in *Nanomaterials from Clay Minerals: A New Approach to Green Functional Materials* 335–364 (Elsevier, 2019).

124. Bleam, W. F. *Clay Mineralogy and Clay Chemistry* in *Soil and Environmental Chemistry* 85–116 (Elsevier, 2012).

125. Schulze, D. G. *Clay Minerals* in *Encyclopedia of Soils in the Environment* 246–254 (Elsevier Inc., 2004).

126. King, H. M. *Chert* Geology.com. https://geology.com/rocks/chert.shtml (last accessed Apr. 14, 2021).

127. Raade, G. & Solberg, B. *Flint* Store Norske Leksikon. https://snl.no/flint (last accessed July 22, 2021).

128. *MS Teisten* Ny-Ålesund Research Station. https://nyalesundresearch.no/infrastructures/ms-teisten/ (last accessed Apr. 8, 2021).

129. Potter, B. & Wimsatt, J. *Method 415.3, Rev. 1.2: Determination of Total Organic Carbon and Specific UV Absorbance at 254 nm in Source Water and Drinking Water* U.S. Environmental Protection Agency (EPA). https://cfpub.epa.gov/si/si_public_record_report.cfm?Lab=NERL&dirEntryId=214406&simpleSearch=1&searchAll=415.3.

130. ISO. *ISO 10390:2005(E): Soil quality - Determination of pH* (2005).

131. Heistad, M. *Mercury release from thawing permafrost in the Arctic* Master's thesis (NTNU, 2021).

132. Zethof, J., Leue, M., Vogel, C., Stoner, S. & Kalbitz, K. Identifying and quantifying geogenic organic carbon in soils – the case of graphite. *SOIL Discussions,* 1–28 (2019).

133. Anesio, A. M., Hodson, A. J., Fritz, A., Psenner, R. & Sattler, B. High microbial activity on glaciers: importance to the global carbon cycle. *Global Change Biology* **15,** 955–960 (2009).

134. Edwards, A., Anesio, A. M., Rassner, S. M., Sattler, B., Hubbard, B., Perkins, W. T., Young, M. & Griffith, G. W. Possible interactions between bacterial diversity, microbial activity and supraglacial hydrology of cryoconite holes in Svalbard. *The ISME Journal* **5,** 150–160 (2011).

135. Statens forurensningstilsyn. *Helsebasert tilstandsklasser for forurenset grunn* tech. rep. (Statens forurensningstilsyn, 2010).

136. Shaw, D. M., Reilly, G. ., Muysson, J. R., Pattenden, G. E. & Campbell, F. E. An estimate of the chemical composition of the Canadian Precambrian shield. *Canadian Journal of Earth Sciences* **4,** 829–853 (1967).

137. Shaw, D. M., Dostal, J. & Keays, R. R. Additional estimates of continental surface Precambrian shield composition in Canada. *Geochimica et Cosmochimica Acta* **40,** 73–83 (1976).

138. Wedepohl, H. K. The composition of the continental crust. *Geochimica et Cosmochimica Acta* **59,** 1217–1232 (1995).

139. Ottesen, R. T., Bogen, J., Finne, T. E., Andersson, M., Dallmann, W. K., Eggen, O. A., Jartun, M., Lundkvist, Q., Pedersen, H. R. & Volden, T. *Geochemical atlas of Norway Part 2: Geochemical atlas of Spitsbergen. Chemical compositon of overbank sediment* (Geological Survey of Norway (NGU) and Norges Vassdrags- og energidirektorat (NVE), Trondheim, 2010).

140. Moroni, B., Cappelletti, D., Ferrero, L., Crocchianti, S., Busetto, M., Mazzola, M., Becagli, S., Traversi, R. & Udisti, R. Local vs. long-range sources of aerosol particles upon Ny-Ålesund (Svalbard Islands): mineral chemistry and geochemical records. *Rendiconti Lincei* **27,** 115–127 (2016).

141. *AMAP Assessment 2002: Heavy Metals in the Arctic* tech. rep. (Arctic Monitoring and Assessment Programme (AMAP), Oslo, Norway, 2005).

142. Andersson, M., Eggen, O. A., Finne, T. E. & Ottesen, R. T. *Områder i Norge med naturlig hoyt bakgrunnsnivil (over norm verdi) - betydning for disponering av masser* tech. rep. (Norges Geologiske Undersøkelse (NGU), 2011).

143. Horrocks, R. D. & Vallentine, J. F. *Soil fertility and forage production* in *Harvest Forages* (eds Horrocks, R. D. & Vallentine, J. F. B. T. .-. H. F.) 187–224 (Academic Press, San Diego, 1999).

144. Stibal, M., Sabacká, M. & Kaštovská, K. Microbial Communities on Glacier Surfaces in Svalbard: Impact of Physical and Chemical Properties on Abundance and Structure of Cyanobacteria and Algae. *Microbial Ecology* **52,** 644–654 (2006).

145. Hodson, A. J., Tranter, M., Dowdeswell, J. A., Gurnell, A. M. & Hagen, J. O. Glacier thermal regime and suspended-sediment yield: a comparison of two high-Arctic glaciers. *Annals of Glaciology* **24,** 32–37 (1997).

146. Norwegian Environmental Agency. *Grenseverdier for klassifisering av vann, sediment og biota* tech. rep. (2020).

147. Kveli, S. M. *Studie av totalt organisk materiale, kvikksølv og andre sporelementer i sedimenter/elveavsetninger i Bayelva og andre elver i Ny Ålesund (Svalbard)* Master's thesis (NTNU, 2015).

148. Jensen, H. K. *Miljøgeokjemiske data og dateringsresultater fra indre Kongsfjorden og indre Rijpfjorden samt områdene SK01 og SK02 vest for Svalbard* tech. rep. (Norwegian Geological Survey (NGU), 2019).

149. Bogen, J. & Bønsnes, T. E. Erosion and sediment transport in High Arctic rivers, Svalbard. *Polar Research* **22,** 175–189 (2003).

150. Hald, S. J. K. *Kartlegging og studie av metaller og naturlig organisk materiale i elver på Svalbard* Master's thesis (NTNU, 2014).

151. Nordum, M. *Metaller og naturlig organisk materiale i arktiske elver på Svalbard* Master's thesis (NTNU, 2012).

152. Granberg, M. E., Ask, A. & Gabrielsen, G. W. *Local contamination in Svalbard. Overview and suggestions fro remediation actions* tech. rep. (Norwegian Polar Institute, Tromsø, Norway, 2017).

153. Hodgkins, R. Glacier hydrology in Svalbard, Norwegian high arctic. *Quaternary Science Reviews* **16,** 957–973 (1997).

154. Björnsson, H., Gjessing, Y., Hamran, S.-E., Hagen, J. O., LiestøL, O., Pálsson, F. & Erlingsson, B. The thermal regime of sub-polar glaciers mapped by multi-frequency radio-echo sounding. *Journal of Glaciology* **42,** 23–32 (1996).

A. Field work

Respective coordinates in DDM for the sampling points for samples collected from the glacier Austre Brøggerbreen, the river Bayelva and the fjord Kongsfjorden is given in Table A.1. Maps showing the sampling sites and points are presented in Figure 3.3-3.6.

Table A.1.: Sampling points for samples collected from the glacier Austre Brøggerbreen, the river Bayelva and the fjord Kongsfjorden and their respective coordinates [DDM].

Point	Latitude	Longitude	Sampling site
P1	78°53.977'N	11°49.896'E	Austre Brøggerbreen
P2	78°53.934'N	11°49.813'E	Austre Brøggerbreen
P3	78°53.784'N	11°49.848'E	Austre Brøggerbreen
P4	78°53.661'N	11°50.411'E	Austre Brøggerbreen
P5	78°53.652'N	11°50.449'E	Austre Brøggerbreen
P6	78°53.637'N	11°50.440'E	Austre Brøggerbreen
P7	78°53.588'N	11°50.439'E	Austre Brøggerbreen
P8	78°56.095'N	11°50.863'E	Bayelva
P9	78°56.042'N	11°50.544'E	Bayelva
P10	78°55.929'N	11°50.036'E	Bayelva
P11	78°55.499'N	11°49.222'E	Bayelva
P12	78°55.553'N	11°49.748'E	Bayelva
P13	78°55.717'N	11°50.483'E	Bayelva
P14	78°55.457'N	11°48.803'E	Bayelva
P15	78°54.853'N	11°50.640'E	Bayelva
P16	78°56.083'N	11°53.673'E	Kongsfjorden
P17	78°56.081'N	11°54.193'E	Kongsfjorden
P18	78°56.081'N	11°55.331'E	Kongsfjorden
P19	78°56.079'N	11°57.300'E	Kongsfjorden
P20	78°55.973'N	11°54.821'E	Kongsfjorden
P21	78°55.973'N	11°54.040'E	Kongsfjorden
P22	78°56.257'N	11°53.893'E	Kongsfjorden
P23	78°56.217'N	11°54.667'E	Kongsfjorden

B. Sample information

Sample data on sample ID, sample type, sampling site, sampling point, sampling container and sampling depth are given in Table B.1. Summary of sample preparation and analysis used in this thesis are given in B.2. Applied technique is labeled with x.

Table B.1.: Sample data of supraglacial material, glacier water, river water, overbank sediment, seawater, and marine sediment samples. Table continues over multiple pages.

Sample ID	Sample type	Sample site	Sample point	Latitude	Longitude	Sample container	Depth [m]
1	Supraglacial material	Austre Brøggerbreen	P1	78°53.977'N	11°49.896'E	50 mL HDPP	-
2	Supraglacial material	Austre Brøggerbreen	P1	78°53.977'N	11°49.896'E	50 mL HDPP	-
3	Supraglacial material	Austre Brøggerbreen	P2	78°53.934'N	11°49.813'E	50 mL HDPP	-
4	Supraglacial material	Austre Brøggerbreen	P2	78°53.934'N	11°49.813'E	50 mL HDPP	-
5	Supraglacial material	Austre Brøggerbreen	P3	78°53.784'N	11°49.848'E	50 mL HDPP	-
6	Supraglacial material	Austre Brøggerbreen	P3	78°53.784'N	11°49.848'E	50 mL HDPP	-
7	Supraglacial material	Austre Brøggerbreen	P4	78°53.661'N	11°50.411'E	50 mL HDPP	-
8	Supraglacial material	Austre Brøggerbreen	P4	78°53.661'N	11°50.411'E	50 mL HDPP	-
9	Supraglacial material	Austre Brøggerbreen	P5	78°53.652'N	11°50.449'E	50 mL HDPP	-
10	Supraglacial material	Austre Brøggerbreen	P5	78°53.652'N	11°50.449'E	50 mL HDPP	-
11	Supraglacial material	Austre Brøggerbreen	P6	78°53.637'N	11°50.440'E	50 mL HDPP	-
12	Supraglacial material	Austre Brøggerbreen	P6	78°53.637'N	11°50.440'E	50 mL HDPP	-
13	Supraglacial material	Austre Brøggerbreen	P7	78°53.588'N	11°50.439'E	50 mL HDPP	-
14	Supraglacial material	Austre Brøggerbreen	P7	78°53.588'N	11°50.439'E	50 mL HDPP	-
1W	Glacier water	Austre Brøggerbreen	P1	78°53.977'N	11°49.896'E	50 mL HDPP	-
2W	Glacier water	Austre Brøggerbreen	P1	78°53.934'N	11°49.813'E	50 mL HDPP	-
3W	Glacier water	Austre Brøggerbreen	P2	78°53.977'N	11°49.896'E	50 mL HDPP	-
7W	Glacier water	Austre Brøggerbreen	P4	78°53.661'N	11°50.411'E	50 mL HDPP	-
9W	Glacier water	Austre Brøggerbreen	P5	78°53.652'N	11°50.449'E	50 mL HDPP	-
10W	Glacier water	Austre Brøggerbreen	P5	78°53.652'N	11°50.449'E	50 mL HDPP	-
11W	Glacier water	Austre Brøggerbreen	P6	78°53.637'N	11°50.440'E	50 mL HDPP	-

Sample ID	Sample type	Sample site	Sample point	Latitude	Longitude	Sample container	Depth [m]
13W	Glacier water	Austre Brøggerbreen	P7	78°53.588'N	11°50.439'E	50 mL HDPP	-
14W	Glacier water	Austre Brøggerbreen	P7	78°53.588'N	11°50.439'E	50 mL HDPP	-
15	River water	Bayelva	P8	78°56.095'N	11°50.863'E	50 mL HDPP	-
16	River water	Bayelva	P8	78°56.095'N	11°50.863'E	50 mL HDPP	-
17	River water	Bayelva	P9	78°56.042'N	11°50.544'E	50 mL HDPP	-
18	River water	Bayelva	P9	78°56.042'N	11°50.544'E	50 mL HDPP	-
19	River water	Bayelva	P10	78°55.929'N	11°50.036'E	50 mL HDPP	-
20	River water	Bayelva	P10	78°55.929'N	11°50.036'E	50 mL HDPP	-
21	River water	Bayelva	P14	78°55.720'N	11°47.826'E	50 mL HDPP	-
22	River water	Bayelva	P14	78°55.720'N	11°47.826'E	50 mL HDPP	-
23	River water	Bayelva	P13	78°55.688'N	11°48.140'E	50 mL HDPP	-
24	River water	Bayelva	P13	78°55.688'N	11°48.140'E	50 mL HDPP	-
25	River water	Bayelva	P12	78°55.635'N	11°49.556'E	50 mL HDPP	-
26	River water	Bayelva	P12	78°55.635'N	11°49.556'E	50 mL HDPP	-
27	River water	Bayelva	P11	78°55.612'N	11°50.901'E	50 mL HDPP	-
28	River water	Bayelva	P11	78°55.612'N	11°50.901'E	50 mL HDPP	-
29	River water	Bayelva	P15	78°54.853'N	11°50.640'E	50 mL HDPP	-
30	River water	Bayelva	P15	78°54.853'N	11°50.640'E	50 mL HDPP	-
31	Overbank sediment	Bayelva	P8	78°56.095'N	11°50.863'E	Cc-cup	-
32	Overbank sediment	Bayelva	P8	78°56.095'N	11°50.863'E	Cc-cup	-
33	Overbank sediment	Bayelva	P9	78°56.042'N	11°50.544'E	Cc-cup	-
34	Overbank sediment	Bayelva	P9	78°56.042'N	11°50.544'E	Cc-cup	-
35	Overbank sediment	Bayelva	P10	78°55.929'N	11°50.036'E	Cc-cup	-
36	Overbank sediment	Bayelva	P10	78°55.929'N	11°50.036'E	Cc-cup	-
37	Overbank sediment	Bayelva	P14	78°55.720'N	11°47.826'E	Cc-cup	-

Sample ID	Sample type	Sample site	Sample point	Latitude	Longitude	Sample container	Depth [m]
38	Overbank sediment	Bayelva	P14	78°55.720'N	11°47.826'E	Cc-cup	-
39	Overbank sediment	Bayelva	P13	78°55.688'N	11°48.140'E	Cc-cup	-
40	Overbank sediment	Bayelva	P12	78°55.635'N	11°49.556'E	Cc-cup	-
41	Overbank sediment	Bayelva	P11	78°55.612'N	11°50.901'E	Cc-cup	-
42	Overbank sediment	Bayelva	P11	78°55.612'N	11°50.901'E	Cc-cup	-
43	Seawater	Kongfjorden	P16	78°56.083'N	11°53.673'E	15 mL HDPP	1
44	Seawater	Kongfjorden	P16	78°56.083'N	11°53.673'E	15 mL HDPP	2
45	Seawater	Kongfjorden	P16	78°56.083'N	11°53.673'E	15 mL HDPP	5
46	Seawater	Kongfjorden	P17	78°56.081'N	11°54.193'E	15 mL HDPP	1
47	Seawater	Kongfjorden	P17	78°56.081'N	11°54.193'E	15 mL HDPP	2
48	Seawater	Kongfjorden	P17	78°56.081'N	11°54.193'E	15 mL HDPP	5
49	Seawater	Kongfjorden	P18	78°56.081'N	11°55.331'E	15 mL HDPP	1
50	Seawater	Kongfjorden	P18	78°56.081'N	11°55.331'E	15 mL HDPP	2
51	Seawater	Kongfjorden	P18	78°56.081'N	11°55.331'E	15 mL HDPP	5
52	Seawater	Kongfjorden	P18	78°56.081'N	11°55.331'E	15 mL HDPP	10
53	Seawater	Kongfjorden	P18	78°56.081'N	11°55.331'E	15 mL HDPP	48
54	Seawater	Kongfjorden	P19	78°56.079'N	11°57.300'E	15 mL HDPP	1
55	Seawater	Kongfjorden	P19	78°56.079'N	11°57.300'E	15 mL HDPP	2
56	Seawater	Kongfjorden	P19	78°56.079'N	11°57.300'E	15 mL HDPP	5
57	Seawater	Kongfjorden	P19	78°56.079'N	11°57.300'E	15 mL HDPP	10
58	Seawater	Kongfjorden	P19	78°56.079'N	11°57.300'E	15 mL HDPP	140
59	Seawater	Kongfjorden	P20	78°55.973'N	11°54.821'E	15 mL HDPP	1
60	Seawater	Kongfjorden	P20	78°55.973'N	11°54.821'E	15 mL HDPP	2
61	Seawater	Kongfjorden	P20	78°55.973'N	11°54.821'E	15 mL HDPP	5
62	Seawater	Kongfjorden	P20	78°55.973'N	11°54.821'E	15 mL HDPP	10

Sample ID	Sample type	Sample site	Sample point	Latitude	Longitude	Sample container	Depth [m]
63	Seawater	Kongfjorden	P20	78°55.973'N	11°54.821'E	15 mL HDPP	25
64	Seawater	Kongfjorden	P21	78°55.973'N	11°54.040'E	15 mL HDPP	1
65	Seawater	Kongfjorden	P21	78°55.973'N	11°54.040'E	15 mL HDPP	2
66	Seawater	Kongfjorden	P21	78°55.973'N	11°54.040'E	15 mL HDPP	5
67	Seawater	Kongfjorden	P22	78°56.257'N	11°53.893'E	15 mL HDPP	1
68	Seawater	Kongfjorden	P22	78°56.257'N	11°53.893'E	15 mL HDPP	2
69	Seawater	Kongfjorden	P22	78°56.257'N	11°53.893'E	15 mL HDPP	5
70	Seawater	Kongfjorden	P22	78°56.257'N	11°53.893'E	15 mL HDPP	10
71	Seawater	Kongfjorden	P22	78°56.257'N	11°53.893'E	15 mL HDPP	18
72	Seawater	Kongfjorden	P23	78°56.217'N	11°54.667'E	15 mL HDPP	1
73	Seawater	Kongfjorden	P23	78°56.217'N	11°54.667'E	15 mL HDPP	2
74	Seawater	Kongfjorden	P23	78°56.217'N	11°54.667'E	15 mL HDPP	5
75	Seawater	Kongfjorden	P23	78°56.217'N	11°54.667'E	15 mL HDPP	10
76	Seawater	Kongfjorden	P23	78°56.217'N	11°54.667'E	15 mL HDPP	43
77	Seawater	Kongfjorden	P16	78°56.083'N	11°53.673'E	50 mL HDPP	1
78	Seawater	Kongfjorden	P16	78°56.083'N	11°53.673'E	50 mL HDPP	2
79	Seawater	Kongfjorden	P16	78°56.083'N	11°53.673'E	50 mL HDPP	5
80	Seawater	Kongfjorden	P17	78°56.081'N	11°54.193'E	50 mL HDPP	1
81	Seawater	Kongfjorden	P17	78°56.081'N	11°54.193'E	50 mL HDPP	2
82	Seawater	Kongfjorden	P17	78°56.081'N	11°54.193'E	50 mL HDPP	5
83	Seawater	Kongfjorden	P18	78°56.081'N	11°55.331'E	50 mL HDPP	1
84	Seawater	Kongfjorden	P18	78°56.081'N	11°55.331'E	50 mL HDPP	2
85	Seawater	Kongfjorden	P18	78°56.081'N	11°55.331'E	50 mL HDPP	5
86	Seawater	Kongfjorden	P18	78°56.081'N	11°55.331'E	50 mL HDPP	10
87	Seawater	Kongfjorden	P18	78°56.081'N	11°55.331'E	50 mL HDPP	48

Sample ID	Sample type	Sample site	Sample point	Latitude	Longitude	Sample container	Depth [m]
88	Seawater	Kongfjorden	P19	78°56.079'N	11°57.300'E	50 mL HDPP	1
89	Seawater	Kongfjorden	P19	78°56.079'N	11°57.300'E	50 mL HDPP	2
90	Seawater	Kongfjorden	P19	78°56.079'N	11°57.300'E	50 mL HDPP	5
91	Seawater	Kongfjorden	P19	78°56.079'N	11°57.300'E	50 mL HDPP	10
92	Seawater	Kongfjorden	P19	78°56.079'N	11°57.300'E	50 mL HDPP	140
93	Marine sediment	Kongfjorden	P17	78°56.081'N	11°54.193'E	Cc-cup	50
94	Marine sediment	Kongfjorden	P17	78°56.081'N	11°54.193'E	Cc-cup	50
95	Marine sediment	Kongfjorden	P18	78°56.081'N	11°55.331'E	Cc-cup	142
96	Marine sediment	Kongfjorden	P18	78°56.081'N	11°55.331'E	Cc-cup	142
97	Marine sediment	Kongfjorden	P19	78°56.079'N	11°57.300'E	Cc-cup	27,6
98	Marine sediment	Kongfjorden	P19	78°56.079'N	11°57.300'E	Cc-cup	27,6
99	Marine sediment	Kongfjorden	P20	78°55.973'N	11°54.821'E	Cc-cup	5,7
100	Marine sediment	Kongfjorden	P20	78°55.973'N	11°54.821'E	Cc-cup	5,7
101	Marine sediment	Kongfjorden	P21	78°55.973'N	11°54.040'E	Cc-cup	18,6
102	Marine sediment	Kongfjorden	P21	78°55.973'N	11°54.040'E	Cc-cup	18,6
103	Marine sediment	Kongfjorden	P22	78°56.257'N	11°53.893'E	Cc-cup	47,6
104	Marine sediment	Kongfjorden	P22	78°56.257'N	11°53.893'E	Cc-cup	47,6

Table B.2.: Summary of sample preparation and analysis carried out for samples in this thesis. Technique marked with x means used for the specific sample. The table continues on the next page. F/UF: Filtered/Unfiltered; HNO_3: Concentration of HNO_3; FD: Freeze dried; UC: Microwave digestion with UltraCLAVE; Dilu. factor: Dilution factor; ICP-MS: Inductively Coupled Plasma - Mass Spectrometry; TC/TN: Determination of Total Carbon and Total Nitrogen content; TOC/TIC/ROC: Determination of Total Organic, Total Inorganic and Residue Oxidizable Carbon content; UV: Determination of Total Organic Carbon with UV-spectrometry; IC: Anion analysis with Ion Chromatography; pH: pH measurement.

Sample	**Sample type**	**F/UF**	**FD**	**UC**	**HNO_3 [M]**	**Dilu. factor**	**ICP-MS**	**TC/TN**	**TOC/TIC/ROC**	**UV**	**IC**	**pH**
1-14	Supraglacial mat.	-	x	x	0.6	25x	x	x	x	-	-	x
1W	Glacier water	UF	-	-	-	-	-	-	-	x	x	-
2W	Glacier water	UF	-	-	-	-	-	-	-	x	x	-
3W	Glacier water	UF	-	-	-	-	-	-	-	x	x	-
7W	Glacier water	UF	-	-	-	-	-	-	-	x	x	-
9W	Glacier water	UF	-	-	-	-	-	-	-	x	x	-
10W	Glacier water	UF	-	-	-	-	-	-	-	x	x	-
11W	Glacier water	UF	-	-	-	-	-	-	-	x	x	-
13W	Glacier water	UF	-	-	-	-	-	-	-	x	x	-
14W	Glacier water	UF	-	-	-	-	-	-	-	x	x	-
15-30	River water	F	-	-	0.1	-	x	-	-	-	x	-
31-42	Overbank sed.	-	x	x	0.6	25x	x	-	-	-	-	-
43-76	Seawater	UF	-	-	0.1	30x	x	-	-	-	-	-

Sample	Sample type	F/UF	FD	UC	HNO_3 [M]	Dilu. factor	ICP-MS	TC/TN	TOC/TIC/ROC	UV	IC	pH
77-92	Seawater	F	-	-	0.1	30x	x	-	-	-	-	-
93-104	Marine sed.	-	x	x	0.6	25x	x	-	-	-	-	-

C. Sample preparation

C.1. Sample information

Mass in grams of samples before and after freeze drying, water loss in grams and percentage after freeze drying, mass of samples weighted out for microwave digestion with UltraCLAVE and mass in grams of diluted samples after digestion for supraglacial material (sample 1-14), overbank sediment (sample 33-42) and seafloor sediment (sample 93-104) samples, certified reference material (CRM) and blanks are given in C.1. Digestion were done in two rounds and are marked with 1 and 2. Samples containing precipitation after digestion are marked with "Yes".

Table C.1.: Mass in grams of samples before and after freeze drying, water loss in grams and percentage after freeze drying, mass of samples weighted out for microwave digestion with UltraCLAVE and mass in grams of diluted samples after digestion for supraglacial material (1-14), overbank sediment (sample 33-42) and marine sediment (sample 93-104) samples, certified reference material (CRM) and blanks. Rounds of digestion is marked with 1 and 2. Samples containing precipitation after digestion are marked with "Yes". Table continues over multiple pages.

	Freeze drying				**UltraClave**			
Sample	**Mass before [g]**	**Mass after [g]**	**Water loss [g]**	**Water loss [%]**	**Round**	**Mass before [g]**	**Mass after [g]**	**Precipitation**
1	9.6043	6.8292	2.7751	28.8943	1	0.2631	108.45	Yes
2	10.7805	6.6246	4.1559	38.5502	1	0.2522	110.11	Yes
3	32.2706	19.8320	12.4386	38.5447	1	0.2537	110.76	Yes
4	28.2008	16.7172	11.4836	40.7208	1	0.2772	108.80	Yes
5	20.0476	15.0429	5.0047	24.9641	1	0.2797	109.31	Yes
6	22.5042	16.9144	5.5898	24.8389	1	0.2698	108.10	Yes
7	15.3077	9.4848	5.8229	38.0390	1	0.3320	108.11	Yes
8	26.7836	16.8431	9.9405	37.1141	2	0.2805	108.15	Yes
9	7.8995	6.1242	1.7753	22.4736	2	0.2842	108.53	Yes
10	10.2613	7.6192	2.6421	25.7482	2	0.3099	110.96	Yes
11	31.3084	20.6300	10.6784	34.1071	2	0.2641	108.25	Yes
12	26.3367	16.4316	9.9051	37.6095	2	0.3031	111.25	Yes
13	10.7092	7.5752	3.1340	29.2646	2	0.2604	108.13	Yes
14	12.3516	8.4217	3.9299	31.8169	2	0.2950	108.86	Yes
31	50.3705	40.7468	9.6237	19.1058	1	0.3100	109.85	Yes
32	34.4566	28.7878	5.6688	16.4520	1	0.3204	124.09	Yes

	Freeze drying				UltraClave			
Sample	**Mass before [g]**	**Mass after [g]**	**Water loss [g]**	**Water loss [%]**	**Round**	**Mass before [g]**	**Mass after [g]**	**Precipitation**
33	46.5190	37.8173	8.7017	18.7057	1	0.3174	109.31	Yes
34	42.2608	33.7015	8.5593	20.2535	1	0.2505	109.30	Yes
35	33.6387	28.0907	5.5480	16.4929	1	0.2653	110.03	Yes
36	40.6931	31.8349	8.8582	21.7683	1	0.3222	108.42	Yes
37	33.4632	26.4829	6.9803	20.8596	1	0.2933	110.48	Yes
38	37.5072	28.5857	8.9215	23.7861	1	0.2686	110.03	Yes
39	29.2748	24.3044	4.9704	16.9784	1	0.3153	109.00	Yes
40	31.0910	26.9948	4.0962	13.1749	1	0.3065	110.44	Yes
41	30.2420	25.4862	4.7558	15.7258	1	0.2887	109.12	Yes
42	24.0627	20.3441	3.7186	15.4538	1	0.2704	109.42	Yes
93	29.0629	18.4975	10.5654	36.3536	1	0.2472	114.56	Yes
94	33.0762	24.8130	8.2632	24.9823	1	0.2747	111.78	Yes
95	30.1359	21.1401	8.9958	29.8508	1	0.2608	108.32	Yes
96	27.1356	19.5797	7.5559	27.8450	1	0.2527	112.18	Yes
97	26.3044	18.6278	7.6766	29.1837	1	0.3369	108.34	Yes
98	36.5682	25.2112	11.3570	31.0570	1	0.3127	108.49	Yes
99	24.5869	19.8448	4.7421	19.2871	1	0.3346	109.24	Yes
100	33.1061	26.7803	6.3258	19.1077	1	0.2883	108.69	Yes
101	38.7180	26.5990	12.1190	31.3007	1	0.2765	108.34	Yes
102	38.7997	27.8408	10.9589	28.2448	1	0.2701	108.16	Yes
103	35.8477	27.0006	8.8471	24.6797	1	0.3187	109.57	Yes
104	42.0257	26.0475	15.9782	38.0201	1	0.3099	108.56	Yes
CRM1	-	-	-	-	1	0.2623	108.34	Yes
Blank	-	-	-	-	1	-	114.59	-
Blank	-	-	-	-	1	-	108.42	-

	Freeze drying				UltraClave			
Sample	**Mass before [g]**	**Mass after [g]**	**Water loss [g]**	**Water loss [%]**	**Round**	**Mass before [g]**	**Mass after [g]**	**Precipitation**
Blank	-	-	-	-	1	-	108.41	-
CRM2	-	-	-	-	2	0.2844	108.59	Yes
Blank	-	-	-	-	2	-	111.10	-
Blank	-	-	-	-	2	-	111.81	-
Blank	-	-	-	-	2	-	108.58	-

C.2. Program

C.2.1. Microwave digestion with UltraCLAVE

Temperature, pressure and power program over time for microwave digestion with UltraCLAVE of supraglacial material, overbank sediment and marine sediment samples as described in Section 4.1.2 is presented in Figure C.1.

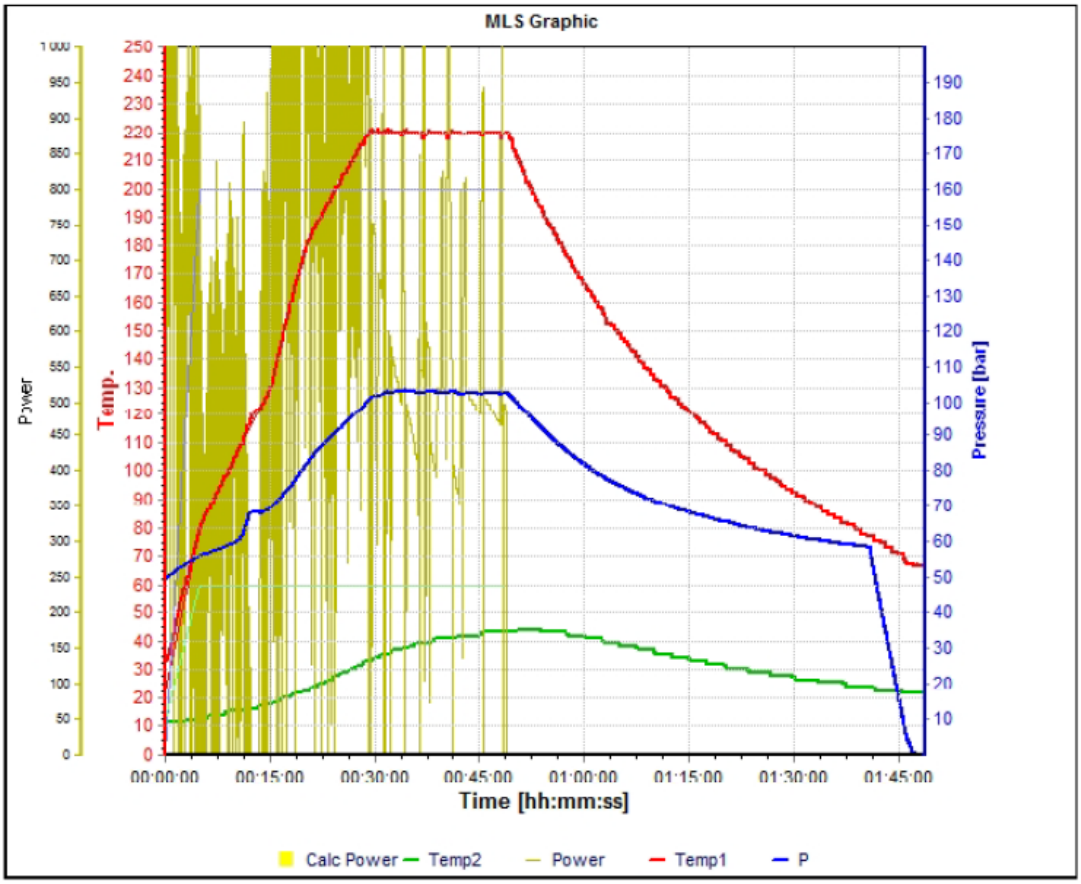

Figure C.1.: Temperature in Celsius, pressure in bar and power program over time for microwave digestion with UltraCLAVE.

D. Analysis

D.1. Element analysis with ICP-MS

Tuning parameters for high resolution Inductively Coupled Plasma - Mass Spectrometry (HP-ICP-MS) analysis with Agilent 8800 ICP-QQQ instrument for 64 elements performed at NTNU are presented in Table D.1 and Figure D.1-D.3.

Table D.1.: Tuning parameters for HP-ICP-MS analysis with Agilent 8800 ICP-QQQ instrument for 64 elements performed at NTNU. Table continues over multiple pages.

Tune Mode	Scan Type	Q1	Q2	Name	ISTD	R	b (blank)	DL	BEC	Units
NoGas	MS/MS	7	7	Li	103 → 103 Rh [NoGas]	0.99913	0.00035	0.00378	0.01510	µg/L
NoGas	MS/MS	9	9	Be	103 → 103 Rh [NoGas]	0.99901	0.00000	0.00143	0.00027	µg/L
O2	MS/MS	11	11	B	103 → 103 Rh [O2]	0.99987	0.00027	0.20683	0.85493	µg/L
O2	MS/MS	23	23	Na	103 → 103 Rh [O2]	0.99999	0.03706	0.19555	2.36575	µg/L
O2	MS/MS	24	24	Mg	103 → 103 Rh [O2]	1.00000	0.00045	0.02116	0.04064	µg/L
H2	MS/MS	27	27	Al	103 → 103 Rh [H2]	0.99797	0.00107	0.00445	0.03799	µg/L
H2	MS/MS	28	28	Si	103 → 103 Rh [H2]	1.00000	0.00678	0.02767	0.66308	µg/L
O2	MS/MS	31	47	P	185 → 217 Re [O2]	0.99918	0.00137	0.06342	0.15325	µg/L
O2	MS/MS	32	48	S	185 → 217 Re [O2]	1.00000	0.10176	0.35688	5.85794	µg/L
O2	MS/MS	35	51	Cl	185 → 217 Re [O2]	0.99980	0.03558	87.85	1471	µg/L
O2	MS/MS	39	39	K	103 → 103 Rh [O2]	0.99992	0.01266	0.05862	0.56989	µg/L
H2	MS/MS	40	40	Ca	103 → 103 Rh [O2]	0.99997	0.00764	0.01570	0.14177	µg/L
O2	MS/MS	45	61	Sc	185 → 217 Re [O2]	0.99997	0.00007	0.00055	0.00018	µg/L
O2	MS/MS	47	63	Ti	103 → 103 Rh [O2]	0.99965	0.00000	0.00191	0.00204	µg/L
O2	MS/MS	51	67	V	185 → 217 Re [O2]	0.99970	0.00075	0.00097	0.00158	µg/L
O2	MS/MS	52	52	Cr	103 → 103 Rh [O2]	0.99965	0.00141	0.00525	0.04863	µg/L
O2	MS/MS	55	55	Mn	103 → 103 Rh [O2]	0.99998	0.00031	0.00221	0.00633	µg/L
H2	MS/MS	56	56	Fe	103 → 103 Rh [H2]	0.99964	0.00274	0.00242	0.04236	µg/L
O2	MS/MS	59	59	Co	103 → 103 Rh [O2]	0.99966	0.00011	0.00132	0.00284	µg/L
O2	MS/MS	60	60	Ni	103 → 103 Rh [O2]	0.99987	0.00008	0.00518	0.00885	µg/L
O2	MS/MS	63	63	Cu	103 → 103 Rh [O2]	0.99977	0.00078	0.00578	0.03317	µg/L

Tune Mode	Scan Type	Q1	Q2	Name	ISTD	R	b (blank)	DL	BEC	Units
H2	MS/MS	66	66	Zn	103 → 103 Rh [H2]	0.99996	0.00021	0.01752	0.02715	µg/L
H2	MS/MS	71	71	Ga	103 → 103 Rh [H2]	0.99986	0.00001	0.00031	0.00022	µg/L
O2	MS/MS	75	91	As	103 → 103 Rh [O2]	0.99999	0.00001	0.00168	0.00133	µg/L
H2	MS/MS	78	78	Se	103 → 103 Rh [H2]	1.00000	0.00002	0.00773	0.00819	µg/L
O2	MS/MS	79	79	Br	103 → 103 Rh [O2]	0.99971	0.00006	0.22654	0.24675	µg/L
O2	MS/MS	85	85	Rb	103 → 103 Rh [O2]	0.99964	0.00029	0.00236	0.00568	µg/L
H2	MS/MS	88	88	Sr	103 → 103 Rh [H2]	0.99980	0.00045	0.00144	0.00390	µg/L
O2	MS/MS	89	105	Y	185 → 217 Re [O2]	0.99999	0.00007	0.00011	0.00007	µg/L
O2	MS/MS	90	106	Zr	185 → 217 Re [O2]	0.99997	0.00003	0.00030	0.00011	µg/L
O2	MS/MS	93	125	Nb	103 → 103 Rh [O2]	0.99999	0.00001	0.00015	0.00010	µg/L
O2	MS/MS	95	127	Mo	185 → 217 Re [O2]	0.99996	0.00080	0.00716	0.00722	µg/L
O2	MS/MS	107	107	Ag	103 → 103 Rh [O2]	0.99932	0.00018	0.00214	0.00666	µg/L
O2	MS/MS	111	111	Cd	103 → 103 Rh [O2]	0.99923	0.00000	0.00050	0.00013	µg/L
H2	MS/MS	115	115	In	103 → 103 Rh [H2]	0.99999	0.00001	0.00006	0.00007	µg/L
O2	MS/MS	118	118	Sn	103 → 103 Rh [O2]	0.99997	0.00004	0.00114	0.00189	µg/L
O2	MS/MS	121	137	Sb	103 → 103 Rh [O2]	0.99998	0.00000	0.00029	0.00006	µg/L
O2	MS/MS	133	133	Cs	103 → 103 Rh [O2]	0.99990	0.00010	0.00043	0.00113	µg/L
O2	MS/MS	137	137	Ba	103 → 103 Rh [O2]	1.00000	0.00002	0.00024	0.00027	µg/L
O2	MS/MS	139	155	La	103 → 103 Rh [O2]	0.99970	0.00000	0.00006	0.00005	µg/L
O2	MS/MS	140	156	Ce	103 → 103 Rh [O2]	0.99998	0.00001	0.00013	0.00010	µg/L
O2	MS/MS	141	157	Pr	103 → 103 Rh [O2]	1.00000	0.00001	0.00005	0.00006	µg/L
O2	MS/MS	146	162	Nd	185 → 217 Re [O2]	0.99950	0.00002	0.00024	0.00009	µg/L
O2	MS/MS	147	163	Sm	185 → 217 Re [O2]	0.99999	0.00002	0.00017	0.00009	µg/L
O2	MS/MS	153	153	Eu	103 → 103 Rh [O2]	1.00000	0.00000	0.00028	0.00009	µg/L
O2	MS/MS	157	173	Gd	185 → 217 Re [O2]	0.99999	0.00001	0.00016	0.00004	µg/L

Tune Mode	Scan Type	Q1	Q2	Name	ISTD	R	b (blank)	DL	BEC	Units
O2	MS/MS	159	175	Tb	185 → 217 Re [O2]	0.99998	0.00007	0.00005	0.00005	µg/L
O2	MS/MS	163	179	Dy	185 → 217 Re [O2]	0.99997	0.00001	0.00013	0.00004	µg/L
O2	MS/MS	165	181	Ho	185 → 217 Re [O2]	0.99999	0.00008	0.00009	0.00005	µg/L
O2	MS/MS	166	182	Er	185 → 217 Re [O2]	0.99998	0.00003	0.00013	0.00006	µg/L
O2	MS/MS	169	185	Tm	103 → 103 Rh [O2]	0.99995	0.00001	0.00013	0.00007	µg/L
O2	MS/MS	172	172	Yb	185 → 217 Re [O2]	0.99998	0.00001	0.00017	0.00005	µg/L
O2	MS/MS	175	191	Lu	185 → 217 Re [O2]	0.99997	0.00008	0.00004	0.00006	µg/L
O2	MS/MS	178	194	Hf	185 → 217 Re [O2]	1.00000	0.00000	0.00000	0.00000	µg/L
O2	MS/MS	181	213	Ta	185 → 217 Re [O2]	0.99998	0.00008	0.00012	0.00008	µg/L
O2	MS/MS	182	214	W	185 → 217 Re [O2]	0.99997	0.00016	0.00073	0.00070	µg/L
H2	MS/MS	195	195	Pt	193 → 193 Ir [H2]	0.99992	0.00004	0.00140	0.00230	µg/L
O2	MS/MS	197	197	Au	193 → 193 Ir [O2]	0.99998	0.00265	0.01189	0.06838	µg/L
O2	MS/MS	202	202	Hg	193 → 193 Ir [O2]	1.00000	0.00058	0.01098	0.04467	µg/L
H2	MS/MS	205	205	Tl	193 → 193 Ir [H2]	0.99999	0.00007	0.00202	0.00123	µg/L
O2	MS/MS	208	208	Pb	193 → 193 Ir [O2]	0.99964	0.00282	0.00204	0.01475	µg/L
H2	MS/MS	209	209	Bi	193 → 193 Ir [H2]	0.98866	0.00001	0.00040	0.00035	µg/L
O2	MS/MS	232	248	Th	193 → 193 Ir [O2]	0.99997	0.00000	0.00007	0.00001	µg/L
H2	MS/MS	238	238	U	103 → 103 Rh [H2]	0.99864	0.00019	0.01675	0.00341	µg/L

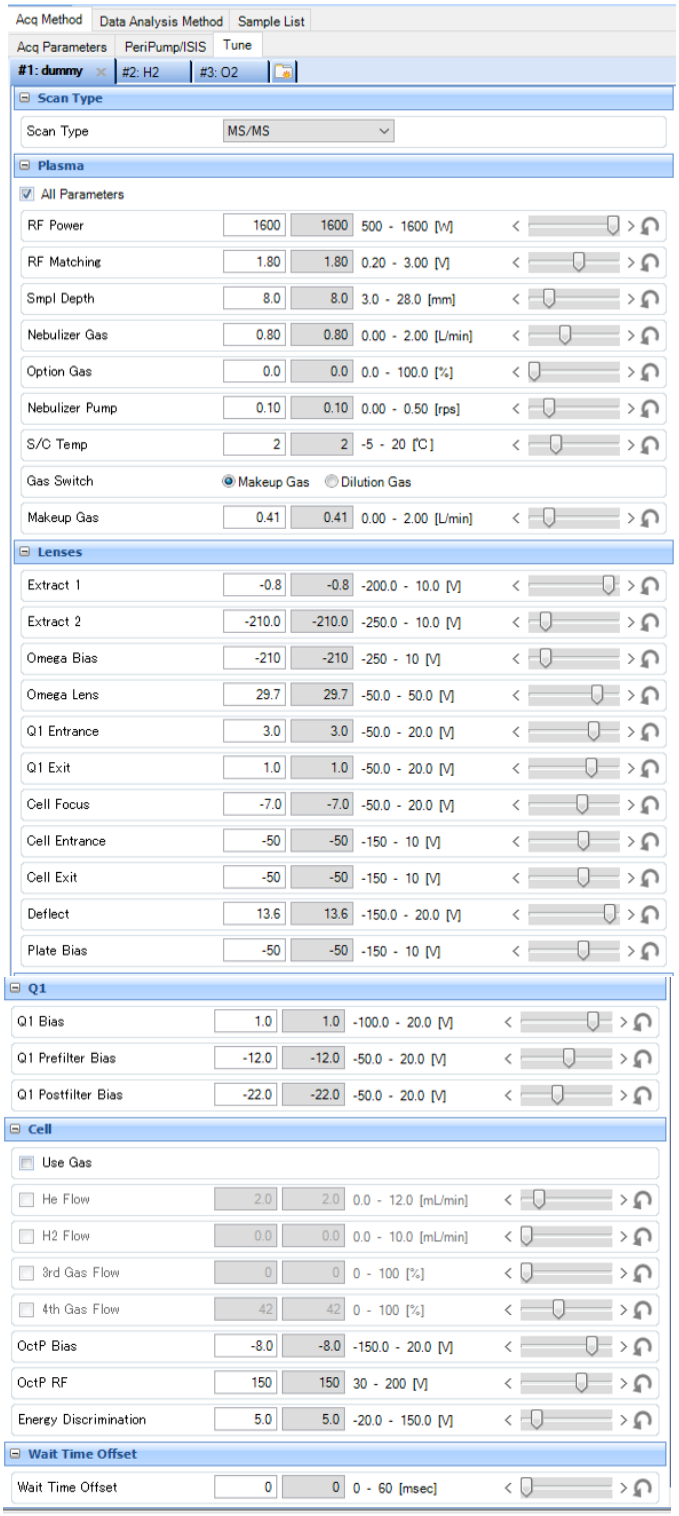

Figure D.1.: Tuning parameters for no gas mode for HP-ICP-MS analysis with Agilent 8800 ICP-QQQ instrument for 64 elements performed at NTNU.

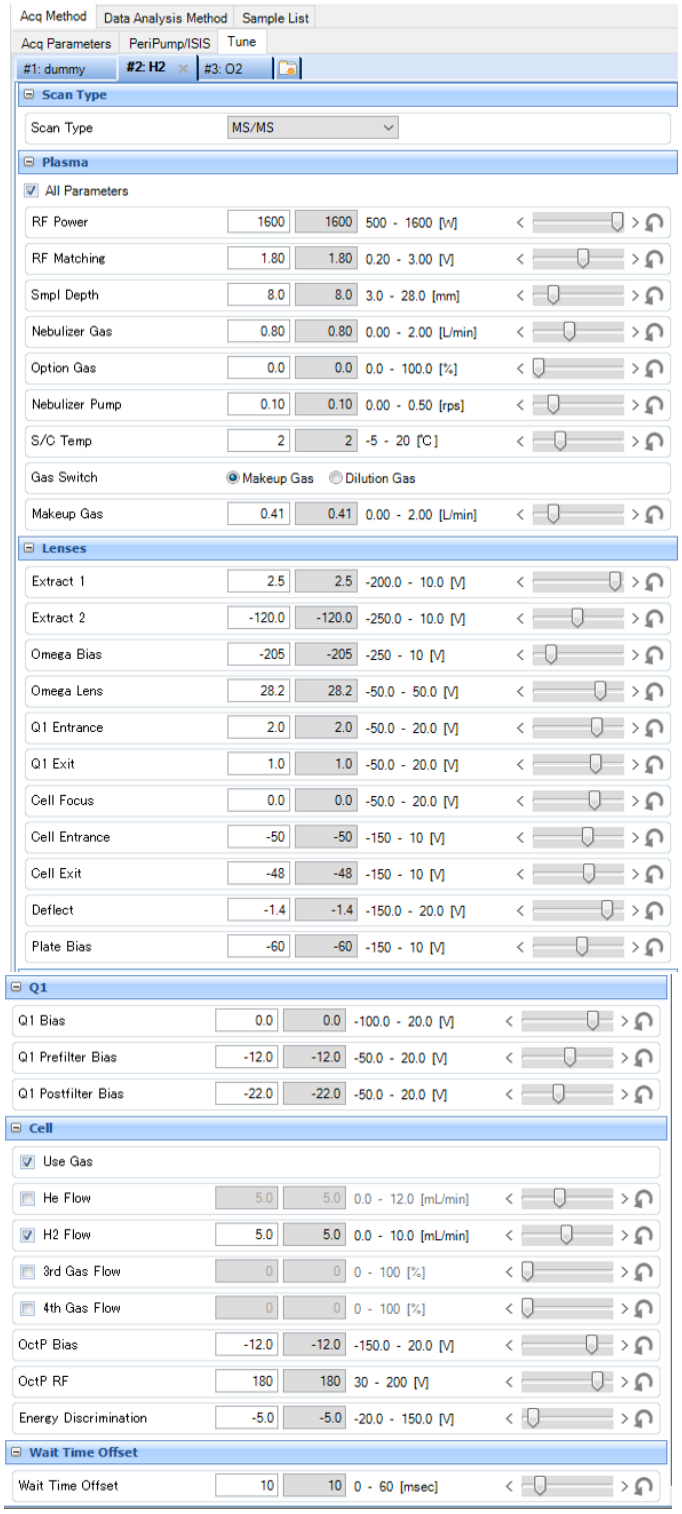

Figure D.2.: Tuning parameters for hydrogen gas mode for HP-ICP-MS analysis with Agilent 8800 ICP-QQQ instrument for 64 elements performed at NTNU.

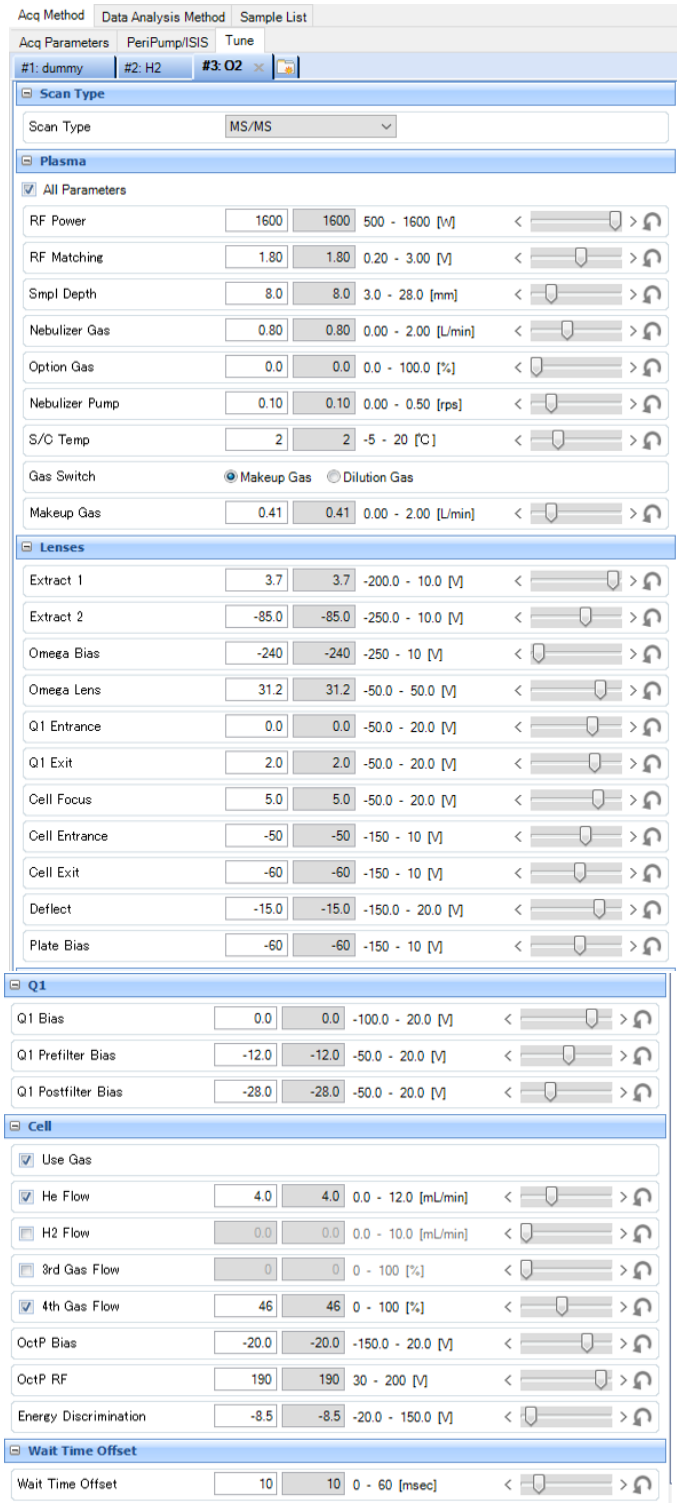

Figure D.3.: Tuning parameters for oxygen gas mode for HP-ICP-MS analysis with Agilent 8800 ICP-QQQ instrument for 64 elements performed at NTNU.

D.2. Determination of Total Carbon and Total Nitrogen content

Calibration for determination of Total Carbon and Total Nitrogen content of 6.3 mg, 11.1 mg, 20.0 mg, 40.6 mg, 80.5 mg, 122.0 mg and 160.3 mg of TOC standard made of dry glycine with carbon content of 32.00% and nitrogen content of 18.66% in the range of 2-52 mg C abs. and 1-30 mg N abs are given in Table D.2. Plotted standard curve for determination of Total Carbon and Total Nitrogen content is presented in D.4a and D.4b respectively. Linear regression line for Total Carbon is $y = 54754x + 15998$ with $R^2 = 0.9999$ and linear regression line for Total Nitrogen is $y = 300000x + 1910.1$ with $R^2 = 1.0000$.

Table D.2.: Calibration for Total Carbon and Total Nitrogen content analysis of TOC standard made of dry glycine with carbon content of 32.00% and nitrogen content of 18.66%.

		Total Carbon results			Total Nitrogen results		
Sample	**Weight [mg]**	**Peak area**	**Result mg C abs**	**Result [%]**	**Peak area**	**Result mg N abs**	**Result [%]**
Standard	6.3	390947.9200	2.191	34.783	18965.0900	1.191	18.897
Standard	11.1	641575.2150	3.656	32.938	31732.5200	2.082	18.754
Standard	20.0	1122926.2000	6.469	32.346	55323.0400	3.728	18.642
Standard	40.6	2189278.8300	12.701	31.284	110051.7900	7.549	18.593
Standard	80.5	4390863.3500	25.568	31.762	217134.2500	15.024	18.663
Standard	122.0	6686415.8200	38.984	31.954	327848.4700	22.752	18.649
Standard	160.3	8825537.8700	51.486	32.119	430591.7900	29.924	18.667

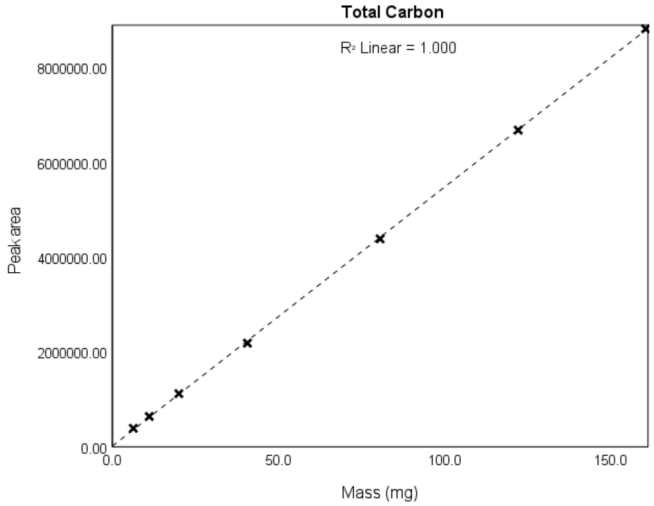

(a) Plotted standard curve for determination of Total Carbon content. Mass in mg plotted as a function of peak area of glycine. Linear regression line y = 54754x + 15998 with $R^2 = 0.9999$.

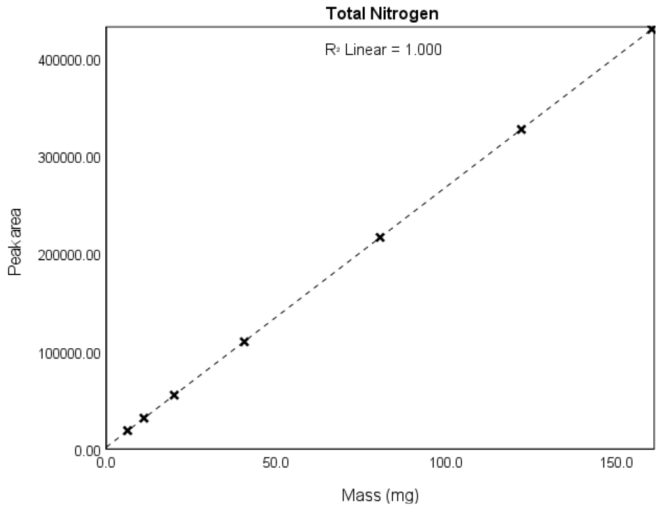

(b) Plotted standard curve for determination of Total Nitrogen content. Mass in mg plotted as a function of peak area of glycine. Linear regression line y = 300000x + 1910.1 with $R^2 = 1.0000$.

Figure D.4.: Plotted standard curves for determination of Total Carbon and Total Nitrogen content.

D.3. Determination of Total Organic, Inorganic and Residue Oxidizable Carbon content content

D.3.1. Program

Temperature program for determination of Total Organic Carbon (TOC400), Residue Oxidizable Carbon (ROC) and Total Inorganic Carbon (TIC900) is presented in Figure D.5.

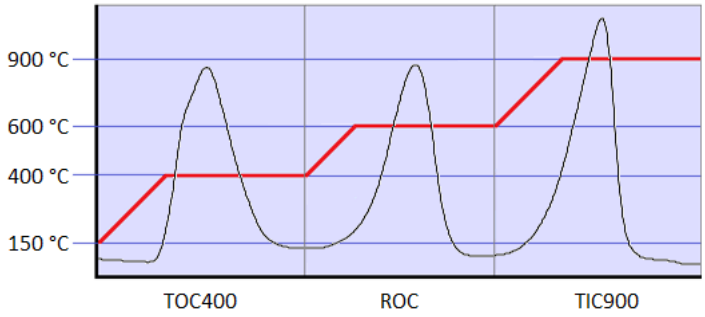

Figure D.5.: Temperature program for determination of Total Organic Carbon (TOC400), Residue Oxidizable Carbon (ROC) and Total Inorganic Carbon (TIC900).

D.3.2. Standard curve

Calibration for Total Organic Carbon (TOC), Total Inorganic Carbon (TIC) and Residue Oxidizable Carbon (ROC) of 10.5 mg, 25.5 mg, 50.6 mg, 78.7 mg, 100.3 mg, 124.8 mg and 150.6 mg of dry glycine with carbon content of ... are given in Table D.4.

Table D.4.: Calibration for Total Organic Carbon (TOC), Total Inorganic Carbon (TIC) and Residue Oxidizable Carbon (ROC) content analysis.

Sample	**Mass** [mg]	**TOC** [ppm]	**TIC** [ppm]	**ROC** [ppm]	**TOC** [%]	**TIC** [%]	**ROC** [%]
Standard	10.5	0.21	0.18	0.21	2.03	1.73	2.02
Standard	25.5	0.51	0.52	0.50	1.99	2.07	1.95
Standard	50.6	1.02	1.02	1.04	2.01	2.02	2.05
Standard	78.7	1.54	1.63	1.59	1.96	2.07	2.01
Standard	100.3	2.04	1.97	1.98	2.03	1.96	1.97
Standard	124.8	2.49	2.45	2.47	2.00	1.96	1.98
Standard	150.6	3.01	3.04	3.04	2.00	2.02	2.02

D.4. Determination of Total Organic Carbon with UV-spectromatry

Absorption at wavelength 2540 nm for 0.1, 0.5, 1.0, 2.0, 5.0 and 10.0 mg/L TOC Standard made of water with trace phosphoric acid (0.05% H_3PO_4) from KHP 1000 mg/L are given in D.5. Plotted standard curve is presented in Figure D.6 with the linear regression line y = 0.0165x + 0.0012 with $R^2 = 0.9989$.

Table D.5.: Absorption at wavelength 2540 nm with UV-spectromatry for TOC Standard made of water with trace phosphoric acid (0.05% H_3PO_4) from KHP 1000 mg/L. Plotted standard curve is presented in Figure D.6.

Sample	**Conc. [mg/L]**	**ABS**
Standard	0.100	0.003
Standard	0.500	0.006
Standard	1.000	0.020
Standard	2.000	0.036
Standard	5.000	0.083
Standard	10.000	0.166

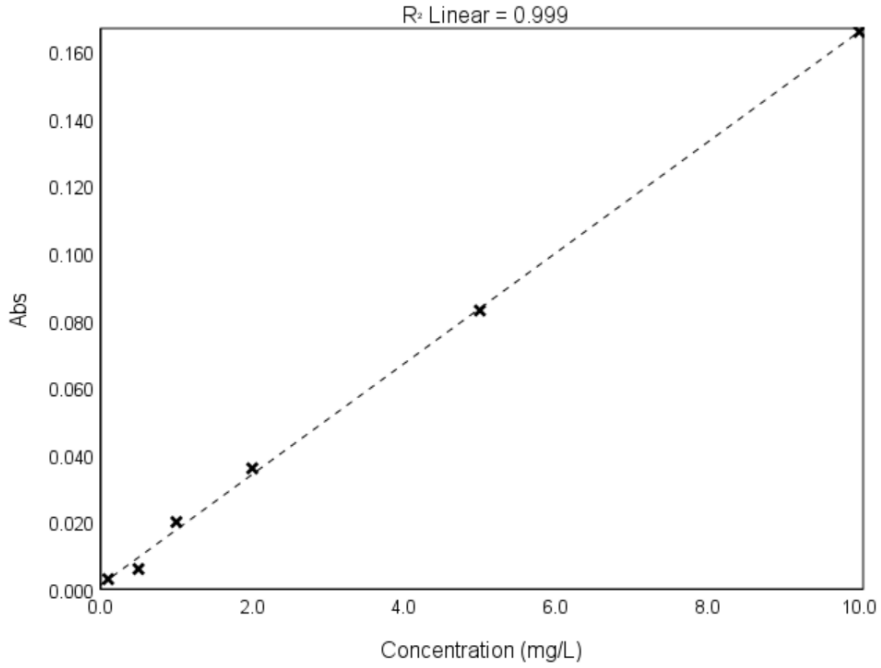

Figure D.6.: Plotted standard curve for determination of Total Organic Carbon content with UV-spectromatry at wavelength 2540 nm. Absorbance (Abs) plotted as a function of concentration (mg/L) of TOC Standard. Linear regression line y = 0.0165x + 0.0012 with $R^2 = 0.9989$.

D.5. Anion analysis with ion Chromatography

Calibration curves for 0.2, 1.0, 2.0, 5.0 and 10.0 mol/L of bromide, chloride, fluoride, nitrate, nitrite, phosphate and sulfate for ion chromatography analysis are presented in Figure D.7 - D.13.

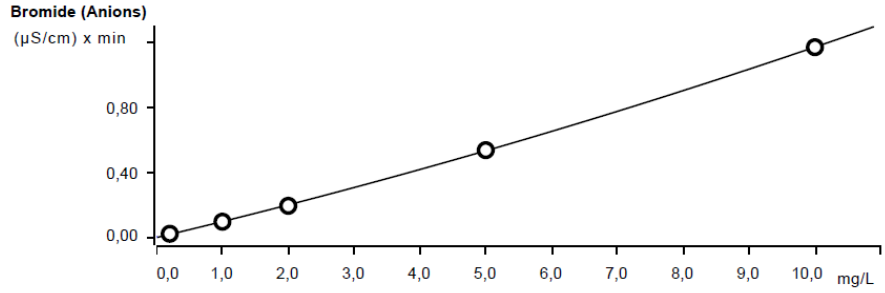

Function: . . . . . *A = - 6,61788E-3 + 4,83522E-3× Q + 5,23890E-6× Q²*

Relative standard deviation . . . . . *1,427836 %*

Correlation coefficient *0,999964*

Sample type	Index	Conc.	Volume	Dilution	Sample amount	Area	Ident	Date	Used
Standard 50	1	0,200	20,0	1,0	1,0	0,017	Std	2021-01-21 15:20:02 UTC+1	used
Standard 10	1	1,000	20,0	1,0	1,0	0,091	Std	2021-01-21 16:02:51 UTC+1	used
Standard 5	1	2,000	20,0	1,0	1,0	0,189	Std	2021-01-21 16:45:58 UTC+1	used
Standard 2	1	5,000	20,0	1,0	1,0	0,533	Std	2021-01-21 17:29:31 UTC+1	used
Standard 1	1	10,000	20,0	1,0	1,0	1,169	Std	2021-01-21 18:14:18 UTC+1	used

Figure D.7.: Standard curve of bromide for ion chromatography analysis.

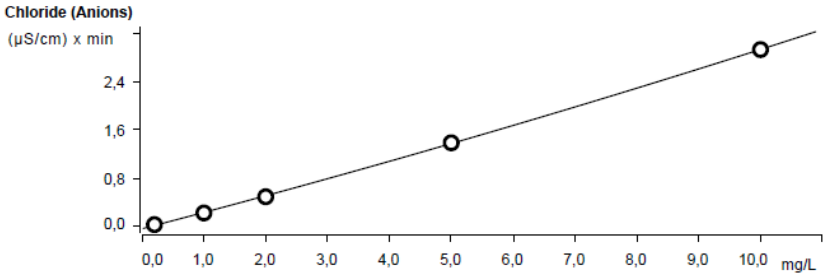

Function: . . . . . $A = -0{,}0295030 + 0{,}0133406 \times Q + 7{,}36946E\text{-}6 \times Q^2$
Relative standard deviation . . . . . 1,899222 %
Correlation coefficient 0,999934

Sample type	Index	Conc.	Volume	Dilution	Sample amount	Area	Ident	Date	Used
Standard 50	1	0,200	20,0	1,0	1,0	0,039	Std	2021-01-21 15:20:02 UTC+1	used
Standard 10	1	1,000	20,0	1,0	1,0	0,231	Std	2021-01-21 16:02:51 UTC+1	used
Standard 5	1	2,000	20,0	1,0	1,0	0,499	Std	2021-01-21 16:45:58 UTC+1	used
Standard 2	1	5,000	20,0	1,0	1,0	1,391	Std	2021-01-21 17:29:31 UTC+1	used
Standard 1	1	10,000	20,0	1,0	1,0	2,931	Std	2021-01-21 18:14:18 UTC+1	used

Figure D.8.: Standard curve of chloride for ion chromatography analysis.

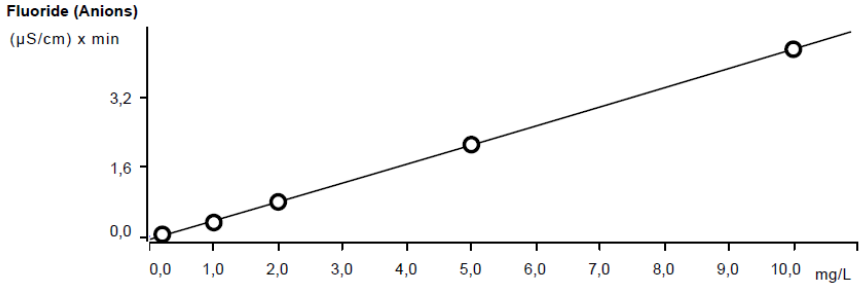

Function: . . . . . $A = -0{,}0671506 + 0{,}0214190 \times Q + 1{,}91273E\text{-}6 \times Q^2$
Relative standard deviation . . . . . 2,449037 %
Correlation coefficient 0,999887

Sample type	Index	Conc.	Volume	Dilution	Sample amount	Area	Ident	Date	Used
Standard 50	1	0,200	20,0	1,0	1,0	0,049	Std	2021-01-21 15:20:02 UTC+1	used
Standard 10	1	1,000	20,0	1,0	1,0	0,321	Std	2021-01-21 16:02:51 UTC+1	used
Standard 5	1	2,000	20,0	1,0	1,0	0,794	Std	2021-01-21 16:45:58 UTC+1	used
Standard 2	1	5,000	20,0	1,0	1,0	2,105	Std	2021-01-21 17:29:31 UTC+1	used
Standard 1	1	10,000	20,0	1,0	1,0	4,291	Std	2021-01-21 18:14:18 UTC+1	used

Figure D.9.: Standard curve of fluoride for ion chromatography analysis.

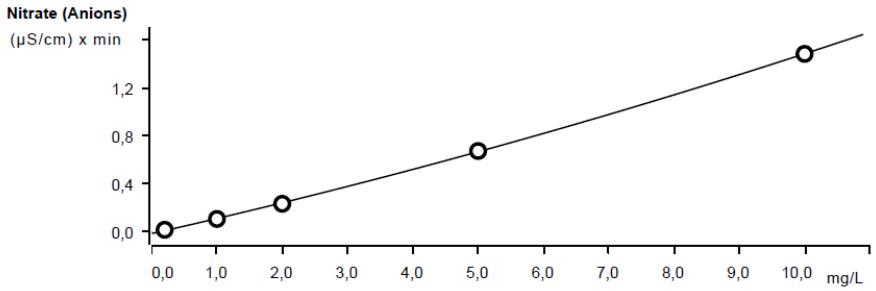

Function: . . . . . *A = - 0,0124306 + 6,12666E-3× Q + 6,70933E-6× Q²*
Relative standard deviation . . . . . *1,847329 %*
Correlation coefficient *0,999940*

Sample type	Index	Conc.	Volume	Dilution	Sample amount	Area	Ident	Date	Used
Standard 50	1	0,200	20,0	1,0	1,0	0,019	Std	2021-01-21 15:20:02 UTC+1	used
Standard 10	1	1,000	20,0	1,0	1,0	0,109	Std	2021-01-21 16:02:51 UTC+1	used
Standard 5	1	2,000	20,0	1,0	1,0	0,235	Std	2021-01-21 16:45:58 UTC+1	used
Standard 2	1	5,000	20,0	1,0	1,0	0,673	Std	2021-01-21 17:29:31 UTC+1	used
Standard 1	1	10,000	20,0	1,0	1,0	1,480	Std	2021-01-21 18:14:18 UTC+1	used

Figure D.10.: Standard curve of nitrate for ion chromatography analysis.

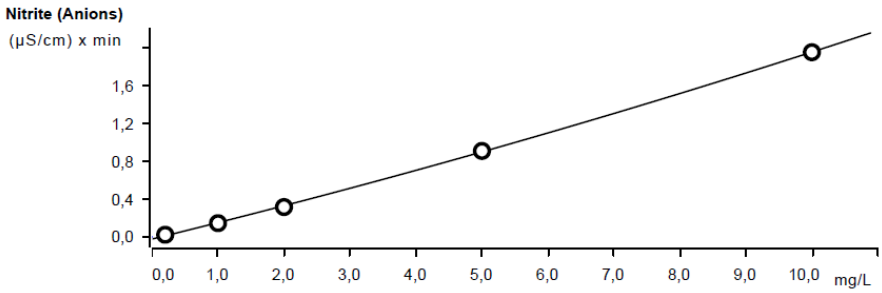

Function: . . . . . *A = - 0,0215100 + 8,49608E-3× Q + 6,69292E-6× Q²*
Relative standard deviation . . . . . *2,280439 %*
Correlation coefficient *0,999907*

Sample type	Index	Conc.	Volume	Dilution	Sample amount	Area	Ident	Date	Used
Standard 50	1	0,200	20,0	1,0	1,0	0,024	Std	2021-01-21 15:20:02 UTC+1	used
Standard 10	1	1,000	20,0	1,0	1,0	0,146	Std	2021-01-21 16:02:51 UTC+1	used
Standard 5	1	2,000	20,0	1,0	1,0	0,315	Std	2021-01-21 16:45:58 UTC+1	used
Standard 2	1	5,000	20,0	1,0	1,0	0,905	Std	2021-01-21 17:29:31 UTC+1	used
Standard 1	1	10,000	20,0	1,0	1,0	1,944	Std	2021-01-21 18:14:18 UTC+1	used

Figure D.11.: Standard curve of nitrite for ion chromatography analysis.

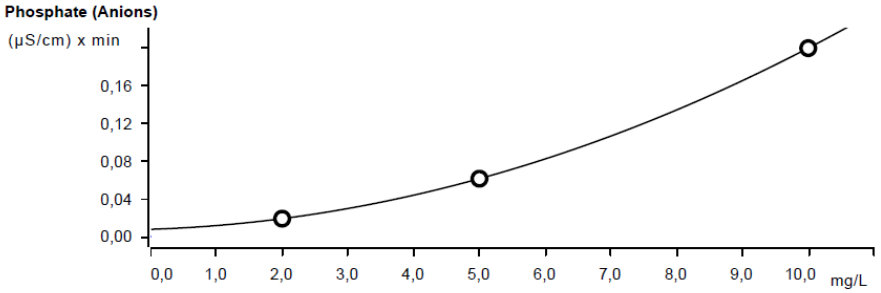

Function: . . . . . A = 7,79092E-3 + 1,12767E-4× Q + 4,20871E-6× Q²
Relative standard deviation . . . . . 0,000000 %
Correlation coefficient 1,000000

Sample type	Index	Conc.	Volume	Dilution	Sample amount	Area	Ident	Date	Used
Standard 50	1	0,200	20,0	1,0	1,0	n. d.	Std	2021-01-21 15:20:02 UTC+1	used
Standard 10	1	1,000	20,0	1,0	1,0	n. d.	Std	2021-01-21 16:02:51 UTC+1	used
Standard 5	1	2,000	20,0	1,0	1,0	0,019	Std	2021-01-21 16:45:58 UTC+1	used
Standard 2	1	5,000	20,0	1,0	1,0	0,061	Std	2021-01-21 17:29:31 UTC+1	used
Standard 1	1	10,000	20,0	1,0	1,0	0,199	Std	2021-01-21 18:14:18 UTC+1	used

Figure D.12.: Standard curve of phosphate for ion chromatography analysis.

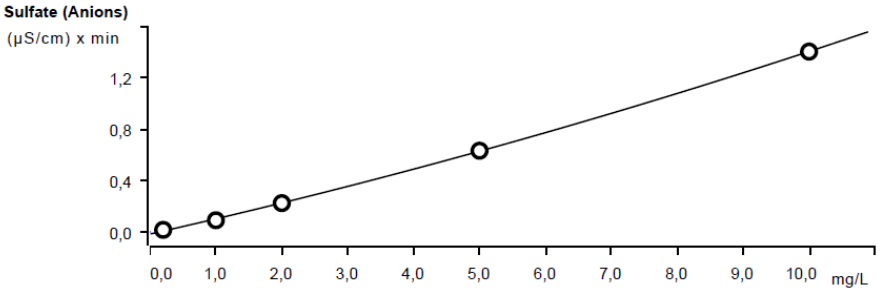

Function: . . . . . A = - 0,0140535 + 5,77570E-3× Q + 6,58758E-6× Q²
Relative standard deviation . . . . . 2,248044 %
Correlation coefficient 0,999913

Sample type	Index	Conc.	Volume	Dilution	Sample amount	Area	Ident	Date	Used
Standard 50	1	0,200	20,0	1,0	1,0	0,018	Std	2021-01-21 15:20:02 UTC+1	used
Standard 10	1	1,000	20,0	1,0	1,0	0,093	Std	2021-01-21 16:02:51 UTC+1	used
Standard 5	1	2,000	20,0	1,0	1,0	0,226	Std	2021-01-21 16:45:58 UTC+1	used
Standard 2	1	5,000	20,0	1,0	1,0	0,634	Std	2021-01-21 17:29:31 UTC+1	used
Standard 1	1	10,000	20,0	1,0	1,0	1,404	Std	2021-01-21 18:14:18 UTC+1	used

Figure D.13.: Standard curve of sulfate for ion chromatography analysis.

E. Results

E.1. Element analysis with ICP-MS

Concentrations (µg/g) of lead (Pb), cadmium (Cd), arsenic (As), chromium (Cr), zinc (Zn), iron (Fe), aluminum (Al) and calcium (Ca) for supraglacial material from Austre Brøggerbreen, overbank sediment from Bayelva and marine sediment from Kongsfjorden are presented in Table E.1.

Table E.1.: Concentrations (µg/g) of lead (Pb), cadmium (Cd), arsenic (As), chromium (Cr), zinc (Zn), iron (Fe), aluminum (Al) and calcium (Ca) for supraglacial material from Austre Brøggerbreen, overbank sediment from Bayelva and marine sediment from Kongsfjorden. The table continues on the next page.

Sample	Sample type	Pb	Cd	As	Cr	Zn	Fe	Al	Ca
1	Supraglacial material	39.5465	0.147	3.6767	79.3407	122.6078	52224.1106	55758.2461	3986.9454
2	Supraglacial material	39.3559	0.1367	4.8467	70.2367	115.2167	50723.4115	54631.8415	4085.4353
3	Supraglacial material	35.7207	0.0877	4.9316	68.7419	104.2599	48215.3219	51435.2629	3680.4914
4	Supraglacial material	34.5878	0.0984	4.2309	67.2744	98.3327	48276.1517	51629.7422	4035.1854
5	Supraglacial material	121.7278	0.1045	13.0009	68.9547	113.0597	43450.2062	48226.7179	3144.5003
6	Supraglacial material	115.3844	0.0906	12.6975	66.2998	108.7398	37189.4893	45961.1781	2765.5314
7	Supraglacial material	45.2013	0.0726	6.5361	58.3716	97.8901	42825.3336	40108.7012	3853.7648
8	Supraglacial material	40.3634	0.0529	4.9073	56.8598	103.5279	46222.0343	39122.5821	4620.4759
9	Supraglacial material	43.4956	0.1056	6.0629	63.3558	108.6427	50425.1675	45953.0803	4990.3464
10	Supraglacial material	37.3215	0.0917	5.8926	58.774	100.9612	48206.4285	40811.7501	5471.3369
11	Supraglacial material	70.7838	<LOQ	8.7804	59.4022	93.0528	40780.6517	41067.6858	3188.0130
12	Supraglacial material	77.4431	<LOQ	9.3633	60.4319	88.1225	39316.3532	40903.0704	2581.5067
13	Supraglacial material	40.2512	0.0669	5.3538	58.3095	108.2745	44657.5835	39988.781	5188.4273
14	Supraglacial material	40.5687	0.0805	4.728	57.5935	104.8548	44854.9979	39986.3219	5606.7625
31	Overbank sediment	12.6682	0.1187	3.353	29.6018	44.5258	21982.6745	21038.9414	21580.5480
32	Overbank sediment	11.4025	0.0971	3.6112	26.8239	46.1692	19754.8841	19047.5014	21721.6244
33	Overbank sediment	14.8563	0.1317	4.1254	39.279	51.2791	24270.2211	28595.5706	19767.7387
34	Overbank sediment	14.1171	0.178	4.5437	37.0802	49.9209	23636.35	28141.78	19212.8910
35	Overbank sediment	14.4204	0.1357	4.9028	38.3322	52.0172	24938.4098	27944.7645	19741.4450

Sample	Sample type	Pb	Cd	As	Cr	Zn	Fe	Al	Ca
36	Overbank sediment	13.8605	0.1093	4.6077	36.4263	50.1858	22669.5978	26066.941	18695.7321
37	Overbank sediment	5.4959	0.2763	3.8209	31.4327	32.4846	8823.2867	11888.4698	155457.0609
38	Overbank sediment	5.5949	0.3007	4.014	31.3891	39.9731	9147.7055	12201.8957	150049.6931
39	Overbank sediment	8.387	0.2228	4.6633	32.4274	40.2847	15239.3229	17418.8845	105683.6653
40	Overbank sediment	13.5387	0.1866	3.5604	35.496	53.9093	24158.2444	26451.5616	25143.3135
41	Overbank sediment	16.2257	0.1597	5.0924	40.209	53.1015	23793.2319	26012.1327	14392.4083
42	Overbank sediment	17.7826	0.1717	5.8932	45.2984	55.9866	1030.7785	1222.7641	20625.2689
93	Marine sediment	15.241	0.0883	11.4136	52.5654	66.2336	30269.0167	39339.3625	46273.6607
94	Marine sediment	14.0202	0.1169	5.297	44.8576	62.5275	24034.1581	32563.4815	48035.9560
95	Marine sediment	15.8842	0.1064	11.1316	56.3323	78.9314	30048.6372	40948.3702	49507.1873
96	Marine sediment	16.2425	0.1314	6.6079	53.3861	70.3554	28844.0398	39186.8629	47780.3169
97	Marine sediment	14.0726	0.0649	6.3206	43.6249	64.197	26383.5124	32160.4778	38140.2837
98	Marine sediment	13.3052	0.0571	7.2194	44.6932	64.7715	25086.5756	31406.4483	33135.7410
99	Marine sediment	14.1624	0.1118	3.2337	42.9095	66.8585	26148.9723	31992.0961	37714.2642
100	Marine sediment	13.2822	0.0827	4.5062	42.062	60.9179	23360.6212	29734.6995	38095.8739
101	Marine sediment	11.2803	0.0745	7.3088	37.1041	42.9269	20936.8368	26106.1238	45699.5518
102	Marine sediment	11.6142	0.0925	6.6632	37.4386	48.1708	21445.3849	27651.4254	46602.4819
103	Marine sediment	13.2444	0.106	4.7841	42.4422	54.234	23443.7725	29679.8714	49578.2894
104	Marine sediment	14.0282	0.1041	8.0166	46.5117	60.374	26494.8801	34020.6871	49365.7510

E.2. Determination of Total Carbon and Total Nitrogen content

Weight in grams, peak area and results for Total Carbon and Total Nitrogen content in mg C abs, mg N abs and percentage for supraglacial material samples are given in Table E.2.

Table E.2.: Weight in grams and results for Total Carbon and Total Nitrogen content for supraglacial material samples and blanks.

Sample	Weight [mg]	Total Carbon		Total Nitrogen	
		[ppm]	[%]	[ppm]	[%]
1	103.6	1.207	1.165	0.068	0.066
2	81.3	0.668	0.822	<LOQ	<LOQ
3	101.7	0.890	0.875	0.009	0.009
4	82.2	0.734	0.893	<LOQ	<LOQ
5	119.8	3.086	2.576	0.205	0.171
6	96.4	2.359	2.447	0.161	0.167
7	101.6	1.238	1.218	0.038	0.037
8	95.6	1.123	1.174	0.028	0.029
9	86.0	0.910	1.058	0.007	0.009
10	99.3	1.264	1.272	0.034	0.034
11	92.7	1.844	1.989	0.079	0.085
12	103.2	2.423	2.348	0.119	0.115
13	111.1	0.928	0.836	0.012	0.011
14	101.6	0.879	0.865	0.010	0.010
Blank	1.0	<LOQ	<LOQ	7.743	774.350
Blank	1.0	0.092	<LOQ	0.063	6.309
Blank	1.0	<LOQ	<LOQ	<LOQ	<LOQ
Blank	1.0	<LOQ	<LOQ	<LOQ	<LOQ
Blank	1.0	<LOQ	<LOQ	<LOQ	<LOQ
Blank	1.0	<LOQ	<LOQ	<LOQ	<LOQ

E.3. Determination of Total Organic, Inorganic and Residue Oxidizable Carbon content content

Mass (mg) of weighted out samples and results for Total Organic Carbon (TOC), Total Inorganic Carbon (TIC) and Residue Oxidizable Carbon (ROC) content in ppm and percentage for supraglacial material samples and blanks are given in Table E.4.

Table E.3.: Results for Total Organic Carbon (TOC), Total Inorganic Carbon (TIC) and Residue Oxidizable Carbon (ROC) content in ppm and percentage for supraglacial material samples and blanks.

Sample	**Mass [mg]**	**TOC [ppm]**	**TIC [ppm]**	**ROC [ppm]**	**TOC [%]**	**TIC [%]**	**ROC [%]**
1	101.6	0.84	0.15	0.08	0.91	0.18	0.06
2	101.5	0.65	0.11	0.08	0.82	0.16	0.05
3	114.0	0.82	0.14	0.7	1.78	0.43	0.06
4	104.0	0.83	0.16	0.06	1.58	0.37	0.06
5	100.6	2.05	0.54	0.07	1.41	0.22	0.05
6	102.3	1.80	0.59	0.07	1.03	0.19	0.06
7	102.2	1.53	0.29	0.06	1.27	0.23	0.06
8	109.8	1.40	0.26	0.07	1.49	0.28	0.06
9	104.5	1.08	0.19	0.06	1.76	0.57	0.07
10	102.2	1.44	0.22	0.06	2.04	0.54	0.07
11	106.0	1.67	0.39	0.07	0.80	0.15	0,06
12	104.3	1.86	0.45	0.07	0.72	0.12	0,06
13	105.8	0.87	0.17	0.06	0.64	0.11	0,08
14	100.0	0.91	0,18	0,06	0,83	0,15	0.08
Blank	<LOQ	0.02	<LOQ	0.01	1.72	<LOQ	1.13
Blank	<LOQ	<LOQ	<LOQ	<LOQ	<LOQ	<LOQ	<LOQ
Blank	<LOQ	<LOQ	<LOQ	<LOQ	<LOQ	<LOQ	<LOQ

E.4. Determination of Total Organic Carbon with UV-spectromatry

Absorption from UV-spectrometry at wavelength 2540 nm and calculated concentration in mg/L of glacier water samples are given in Table E.4. Standard curve is presented in Figure D.6.

Table E.4.: Absorption from UV-spectrometry at wavelength 2540 nm and calculated concentration of Total Organic carbon content in mg/L of glacier water samples. Standard curve is presented in D.6.

Sample	ABS	Conc. [mg/L]
1W	0.005	0.230
2W	0.010	0.533
7W	0.016	0.897
9W	0.005	0.230
10W	0.009	0.473
11W	0.088	5.261
13W	0.009	0.473
14W	0.012	0.655

E.5. Anion analysis with ion Chromatography

Results for analysis of chloride, nitrate and sulfate with ion chromatography in glacier water and river water samples are given in Tabel E.5. Chromatograms for each sample are presented in Figure E.1a - E.1i and Figure E.2a - E.2n. Two blanks were included in the analysis (Table E.5 and Figure E.3a - E.3b).

Table E.5.: Results for analysis of chloride, nitrate and sulfate with ion chromatography in glacier water samples, river water samples and blanks.

Sample	Chloride [mg/L]	Nitrate [mg/L]	Sulfate [mg/L]
1W	0.488	-	-
2W	0.470	-	-
3W	-	-	-
7W	0.518	-	0.080
9W	0.462	-	-
10W	0.490	-	-
11W	0.684	-	0.863
13W	0.577	-	-
14W	0.639	-	0.037
15	1.692	-	15.587
16	2.259	0.666	19.848
17	1.480	-	14.965
18	1.491	-	14.222
19	1.353	-	14.047
20	1.345	-	13.754
21	1.192	-	11.405
22	1.572	0.522	12.730
23	1.259	-	12.389
24	1.291	-	13.178
25	1.307	-	12.751
26	1.652	-	14.475
27	1.364	-	13.717
28	1.371	-	13.682
29	1.081	-	10.232
30	1.491	-	14.222
Blank	-	-	-
Blank	-	-	-

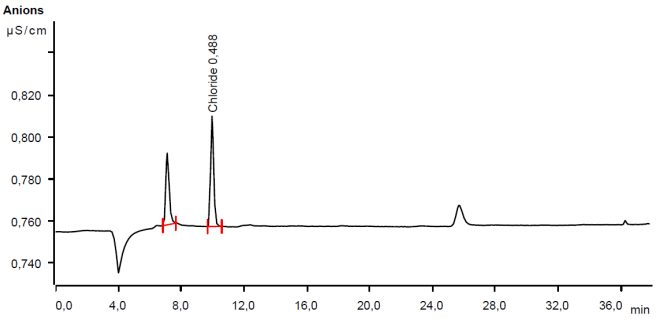

Peak number	Retention time	Area	Height	Concentration	Component name
	min	(µS/cm) x min	µS/cm	mg/L	
1	7,112	0,0085	0,034	invalid	
2	9,960	0,0116	0,053	0,488	Chloride

(a) Chromatogram for sample 1.

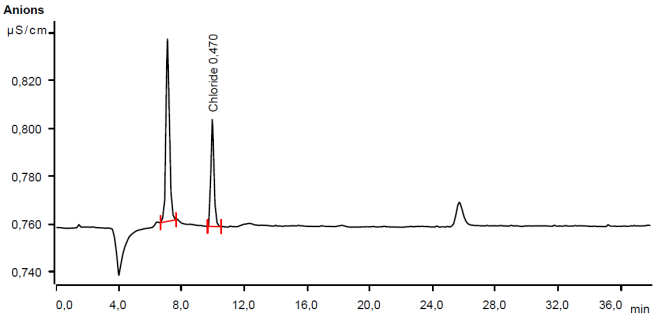

Peak number	Retention time	Area	Height	Concentration	Component name
	min	(µS/cm) x min	µS/cm	mg/L	
1	7,113	0,0193	0,076	invalid	
2	9,962	0,0100	0,045	0,470	Chloride

(b) Chromatogram for sample 2.

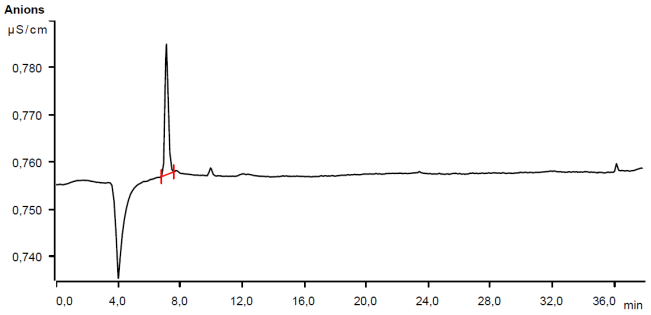

Peak number	Retention time	Area	Height	Concentration	Component name
	min	(µS/cm) x min	µS/cm	mg/L	
1	7,113	0,0068	0,028	invalid	

(c) Chromatogram for sample 3.

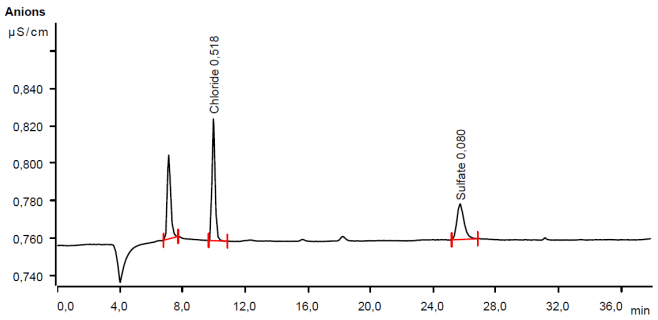

Peak number	Retention time	Area	Height	Concentration	Component name
	min	(µS/cm) x min	µS/cm	mg/L	
1	7,118	0,0111	0,045	invalid	
2	9,967	0,0144	0,065	0,518	Chloride
3	25,707	0,0099	0,019	0,080	Sulfate

(d) Chromatogram for sample 7.

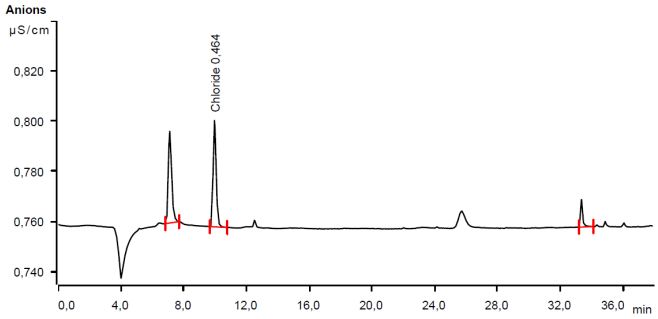

Peak number	Retention time	Area	Height	Concentration	Component name
	min	(µS/cm) x min	µS/cm	mg/L	
1	7,115	0,0091	0,037	invalid	
2	9,965	0,0094	0,042	0,464	Chloride
3	33,342	0,0016	0,011	invalid	

(e) Chromatogram for sample 9.

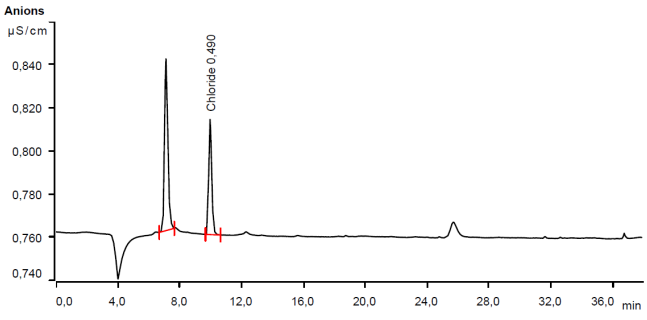

Peak number	Retention time	Area	Height	Concentration	Component name
	min	(µS/cm) x min	µS/cm	mg/L	
1	7,113	0,0197	0,080	invalid	
2	9,962	0,0118	0,053	0,490	Chloride

(f) Chromatogram for sample 10.

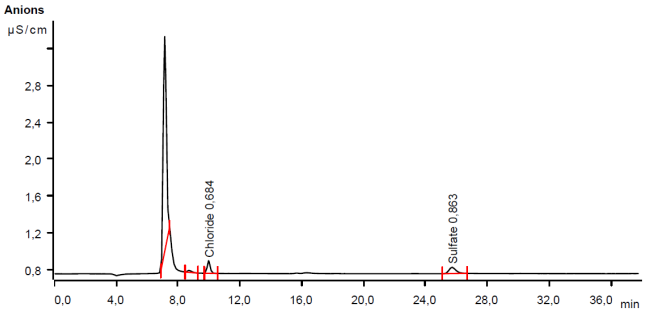

Peak number	Retention time	Area	Height	Concentration	Component name
	min	(µS/cm) x min	µS/cm	mg/L	
1	7,133	0,5407	2,328	invalid	
2	8,700	0,0067	0,021	invalid	
3	9,965	0,0297	0,137	0,684	Chloride
4	25,707	0,0352	0,068	0,863	Sulfate

(g) Chromatogram for sample 11.

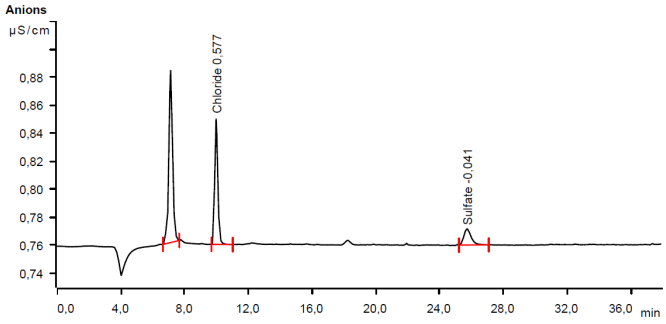

Peak number	Retention time	Area	Height	Concentration	Component name
	min	(µS/cm) x min	µS/cm	mg/L	
1	7,113	0,0328	0,123	invalid	
2	9,965	0,0198	0,090	0,577	Chloride
3	25,702	0,0061	0,012	-0,041	Sulfate

(h) Chromatogram for sample 13.

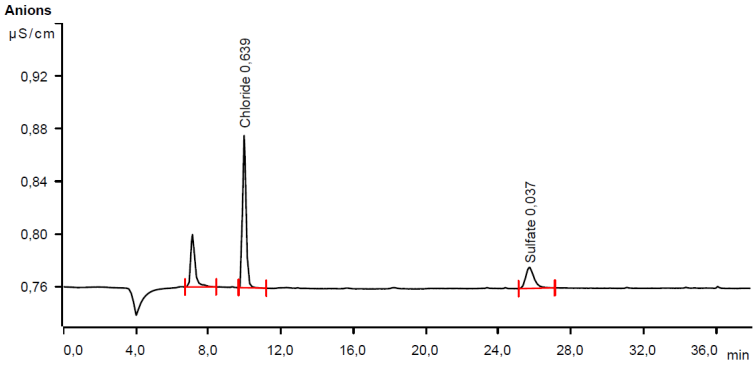

Peak number	Retention time	Area	Height	Concentration	Component name
	min	(µS/cm) x min	µS/cm	mg/L	
1	7,113	0,0110	0,040	invalid	
2	9,960	0,0255	0,116	0,639	Chloride
3	25,692	0,0086	0,016	0,037	Sulfate

(i) Chromatogram for sample 14.

Figure E.1.: Chromatograms for ion chromatography analysis for glacier water samples.

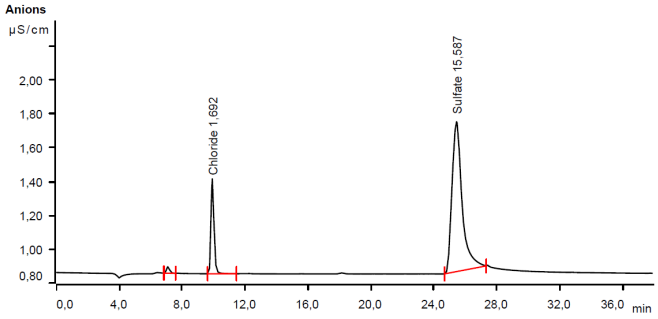

Peak number	Retention time	Area	Height	Concentration	Component name
	min	(µS/cm) x min	µS/cm	mg/L	
1	7,080	0,0092	0,038	invalid	
2	9,908	0,1219	0,560	1,692	Chloride
3	25,430	0,6573	0,885	15,587	Sulfate

(a) Chromatogram for sample 33.

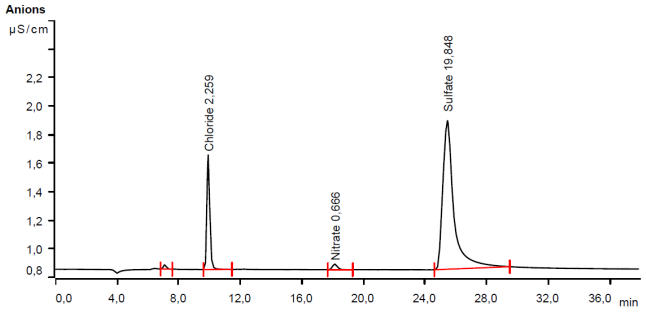

Peak number	Retention time	Area	Height	Concentration	Component name
	min	(µS/cm) x min	µS/cm	mg/L	
1	7,080	0,0071	0,030	invalid	
2	9,907	0,1731	0,802	2,259	Chloride
3	18,118	0,0149	0,039	0,666	Nitrate
4	25,440	0,8655	1,039	19,848	Sulfate

(b) Chromatogram for sample 34.

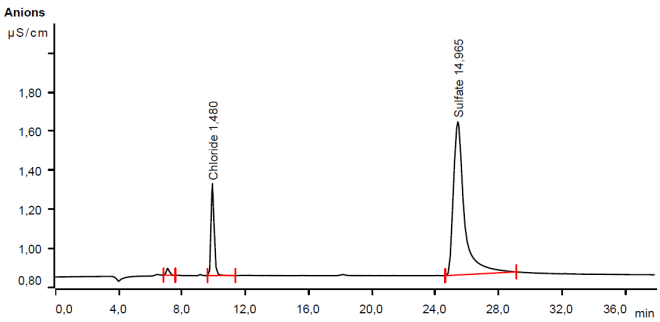

Peak number	Retention time	Area	Height	Concentration	Component name
	min	(µS/cm) x min	µS/cm	mg/L	
1	7,080	0,0086	0,035	invalid	
2	9,910	0,1028	0,471	1,480	Chloride
3	25,412	0,6278	0,783	14,965	Sulfate

(c) Chromatogram for sample 35.

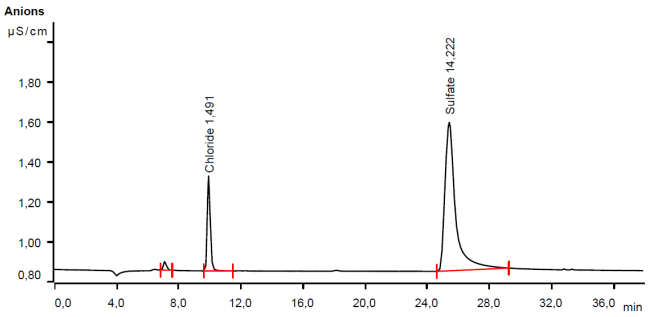

Peak number	Retention time	Area	Height	Concentration	Component name
	min	(µS/cm) x min	µS/cm	mg/L	
1	7,082	0,0105	0,043	invalid	
2	9,910	0,1038	0,475	1,491	Chloride
3	25,400	0,5928	0,743	14,222	Sulfate

(d) Chromatogram for sample 36.

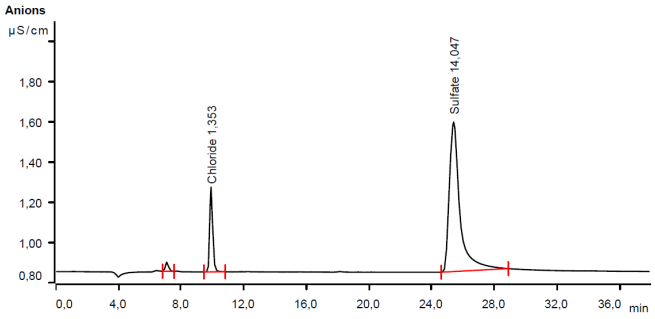

Peak number	Retention time	Area	Height	Concentration	Component name
	min	(µS/cm) x min	µS/cm	mg/L	
1	7,077	0,0110	0,045	invalid	
2	9,907	0,0914	0,421	1,353	Chloride
3	25,390	0,5846	0,743	14,047	Sulfate

(e) Chromatogram for sample 37.

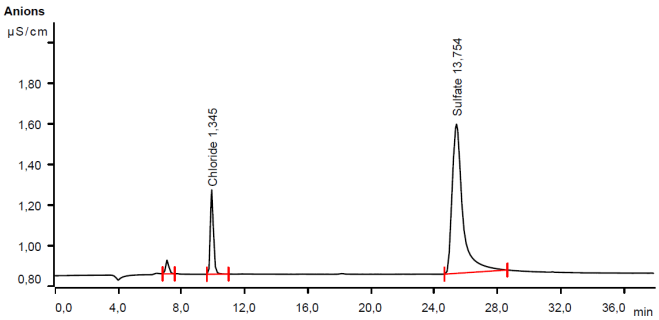

Peak number	Retention time	Area	Height	Concentration	Component name
	min	(µS/cm) x min	µS/cm	mg/L	
1	7,077	0,0164	0,067	invalid	
2	9,907	0,0907	0,416	1,345	Chloride
3	25,395	0,5709	0,735	13,754	Sulfate

(f) Chromatogram for sample 38.

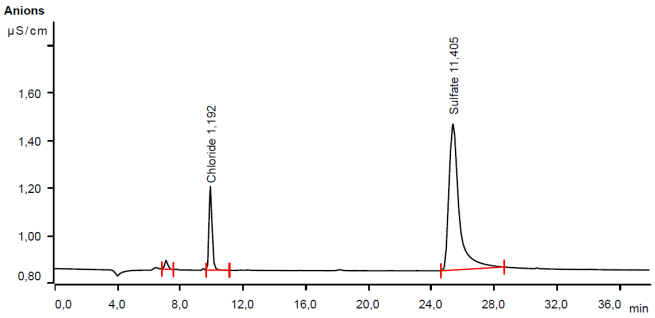

Peak number	Retention time	Area	Height	Concentration	Component name
	min	(µS/cm) x min	µS/cm	mg/L	
1	7,080	0,0089	0,037	invalid	
2	9,907	0,0770	0,352	1,192	Chloride
3	25,367	0,4632	0,614	11,405	Sulfate

(g) Chromatogram for sample 39.

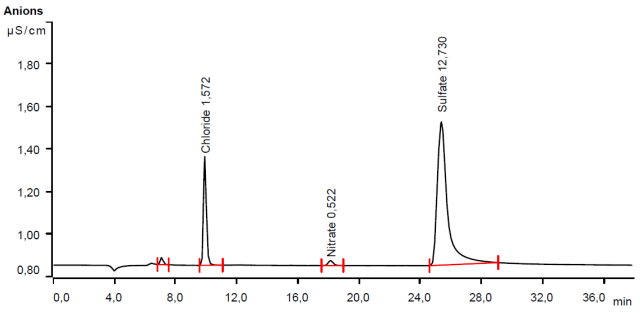

Peak number	Retention time	Area	Height	Concentration	Component name
	min	(µS/cm) x min	µS/cm	mg/L	
1	7,077	0,0080	0,033	invalid	
2	9,907	0,1111	0,512	1,572	Chloride
3	18,122	0,0090	0,024	0,522	Nitrate
4	25,373	0,5235	0,674	12,730	Sulfate

(h) Chromatogram for sample 40.

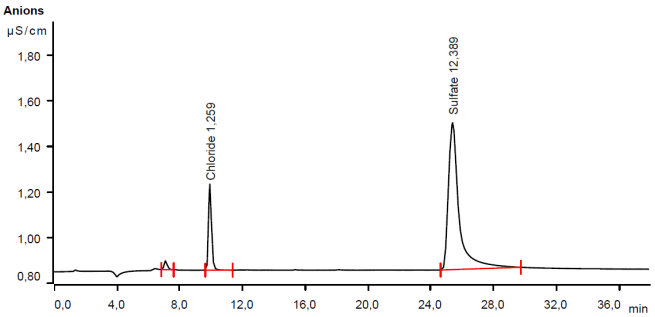

Peak number	Retention time	Area	Height	Concentration	Component name
	min	(µS/cm) x min	µS/cm	mg/L	
1	7,078	0,0095	0,039	invalid	
2	9,908	0,0830	0,378	1,259	Chloride
3	25,377	0,5079	0,645	12,389	Sulfate

(i) Chromatogram for sample 41.

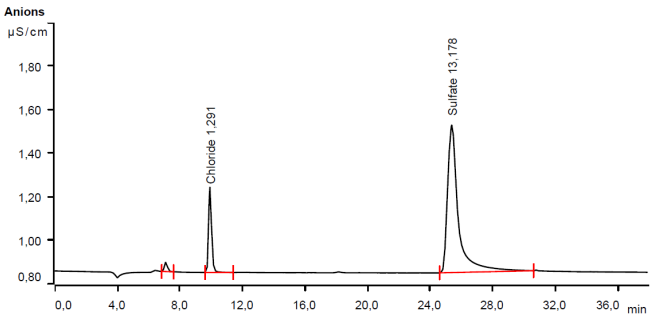

Peak number	Retention time	Area	Height	Concentration	Component name
	min	(µS/cm) x min	µS/cm	mg/L	
1	7,077	0,0102	0,042	invalid	
2	9,905	0,0859	0,392	1,291	Chloride
3	25,368	0,5442	0,677	13,178	Sulfate

(j) Chromatogram for sample 42.

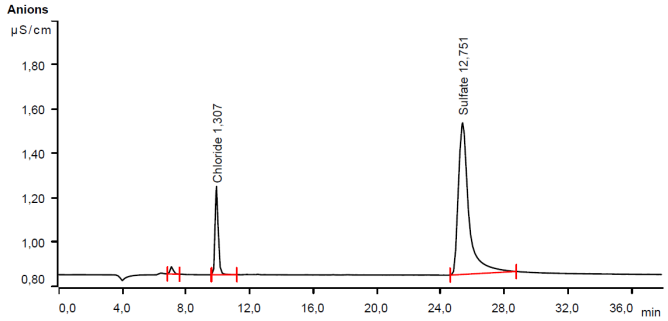

Peak number	Retention time	Area	Height	Concentration	Component name
	min	(µS/cm) x min	µS/cm	mg/L	
1	7,077	0,0079	0,033	invalid	
2	9,905	0,0873	0,399	1,307	Chloride
3	25,372	0,5245	0,684	12,751	Sulfate

(k) Chromatogram for sample 43.

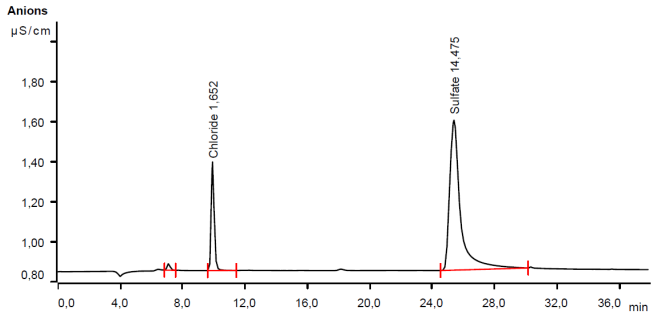

Peak number	Retention time	Area	Height	Concentration	Component name
	min	(µS/cm) x min	µS/cm	mg/L	
1	7,077	0,0077	0,032	invalid	
2	9,907	0,1183	0,543	1,652	Chloride
3	25,383	0,6047	0,749	14,475	Sulfate

(l) Chromatogram for sample 44.

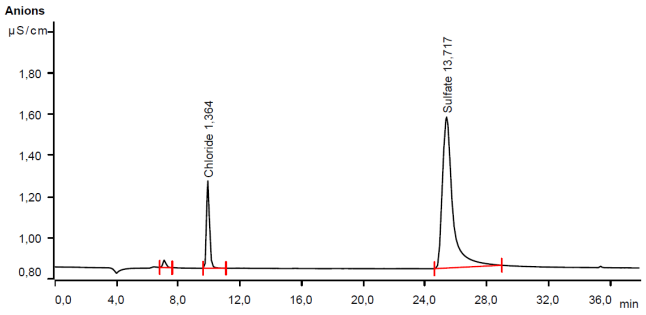

Peak number	Retention time	Area	Height	Concentration	Component name
	min	(µS/cm) x min	µS/cm	mg/L	
1	7,080	0,0087	0,036	invalid	
2	9,910	0,0925	0,424	1,364	Chloride
3	25,385	0,5692	0,733	13,717	Sulfate

(m) Chromatogram for sample 45.

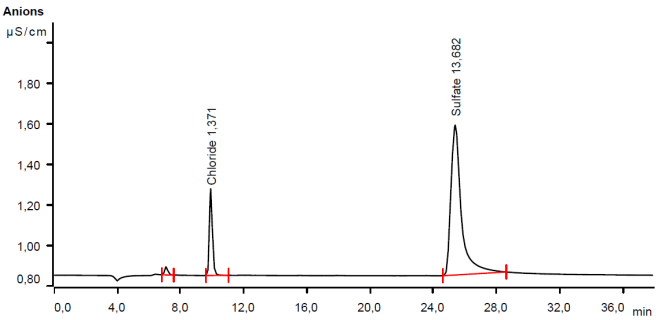

Peak number	Retention time	Area	Height	Concentration	Component name
	min	(µS/cm) x min	µS/cm	mg/L	
1	7,075	0,0097	0,040	invalid	
2	9,905	0,0931	0,428	1,371	Chloride
3	25,377	0,5676	0,739	13,682	Sulfate

(n) Chromatogram for sample 46.

Figure E.2.: Chromatograms for ion chromatography analysis for riverwater samples.

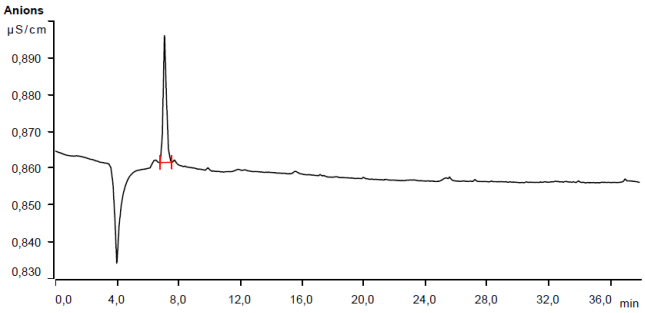

Peak number	Retention time	Area	Height	Concentration	Component name
	min	(µS/cm) x min	µS/cm	mg/L	
1	7,082	0,0085	0,034	invalid	

(a) Chromatogram for blank.

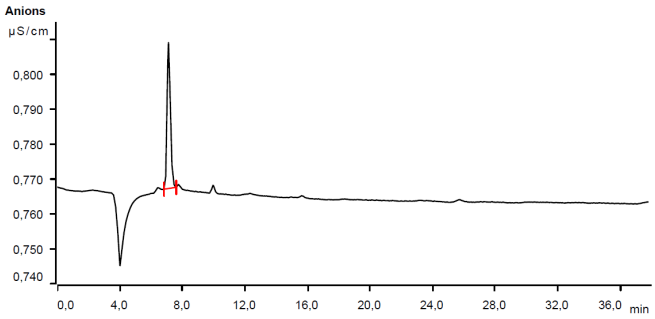

Peak number	Retention time	Area	Height	Concentration	Component name
	min	(µS/cm) x min	µS/cm	mg/L	
1	7,112	0,0102	0,042	invalid	

(b) Chromatogram for blank.

Figure E.3.: Chromatograms for ion chromatography analysis for blanks of Ultra Pure Type I water.

E.6. Determination of pH

Sample volume, volume added of 0.01 M potassium chloride (KCl) solution and results for pH measurement of supraglacial material (sample 1-14) are given in E.6. Samples from the same sample point are merged together and are marked with + sign between.

Table E.6.: Sample volume, volume added of 0.01 M potassium chloride (KCl) solution and results for pH measurement of supraglacial material samples. Samples from the same sample point was combined and are marked with + sign between.

Sample point	Sample	Sample volume [mL]	Volume 0.01 M KCl [mL]	pH
P1	1+2	1	9	6.13
P2	3+4	2	18	4.51
P3	5+6	2	18	4.50
P4	7+8	2	18	4.10
P5	9+10	1	9	4.57
P6	11+12	2	18	4.30
P7	13+14	2	18	4.25

F. Statistical data

F.1. Testing for normal distribution

The data sets were tested for normal distribution with a Shapiro-Wilk test. The significance level were set to 0.05, meaning that values below 0.05 rejects the null hypothesis of the data being normally distributed. p-values for the test for Total Carbon, Total Nitrogen, Total Organic Carbon, Total Inorganic Carbon and Residue Oxidazable Carbon content data in supraglacial material as well as for TOC content in supraglacial glacier water are presented in Table F.1. The results from the test for Pb, Cd, As, Cr, Zn, Fe and Al data in supraglacial material, overbank sediment and marine sediment are presented in Table F.2.

Table F.1.: p-values for a Shapiro-Wilk Normal Distribution test for Total Carbon (TC), Total Nitrogen (TN), Total Organic Carbon (TOC), Total Inorganic Carbon (TIC) and Residue Oxidazable Carbon (ROC) content, and pH data in supraglacial material, as well as for TOC content in supraglacial glacier water. The significance level were set to 0.05. p-values representing a non-normal distribution are marked in bold.

	p-vlaue
TC	**0.00385**
TN	**0.0169**
TOC	0.223
TIC	**0.0198**
ROC	**0.0111**
pH	**0.00670**
TOC (UV)	**0.000269**

Table F.2.: p-values for a Shapiro-Wilk Normal Distribution test for Pb, Cd, As, Cr, Zn and Fe data in supraglacial material, overbank sediment and marine sediment. p-values representing a non-normal distribution are marked in bold.

Element	Sample type	p-value
Pb	Supraglacial material	**0.000336**
	Overbank sediment	0.151
	Marine sediment	0.540
Cd	Supraglacial material	0.654
	Overbank sediment	0.242
	Marine sediment	0.957
As	Supraglacial material	**0.00817**
	Overbank sediment	0.725
	Marine sediment	0.334
Cr	Supraglacial material	0.0612
	Overbank sediment	0.985
	Marine sediment	0.299
Zn	Supraglacial material	1.00
	Overbank sediment	0.253
	Marine sediment	0.747
Fe	Supraglacial material	0.847
	Overbank sediment	**0.00958**
	Marine sediment	0.620
Al	Supraglacial material	**0.0275**
	Overbank sediment	0.0530
	Marine sediment	0.314
Ca	Supraglacial material	0.605
	Overbank sediment	**0.000178**
	Marine sediment	**0.0212**

F.2. Testing for statistical significance

Mean concentrations of lead (Pb), cadmium (Cd), arsenic (As), chromium (Cr), zinc (Zr), iron (Fe), aluminum (Al) and calcium (Ca) between supraglacial material from Austre Brøggerbreen, overbank sediment from Bayelva and marine sediment from Kongsfjorden was tested for statistical significance with a Kruskal-Wallis H test or a Student t-test depending on if the data set was normally distributed or not. p-values from the tests are presented in F.3. Green color denotes a significant difference between the means while the red denotes the opposite. * denotes that a Kruskal-Wallis H test was used.

Table F.3.: p-values from a Kruskal-Wallis H test or a Student t-test for mean concentrations of lead (Pb), cadmium (Cd), arsenic (As), chromium (Cr), zinc (Zr), iron (Fe), aluminum (Al) and calcium (Ca) in supraglacial material from Austre Brøggerbreen, overbank sediment from Bayelva and marine sediment from Kongsfjorden. Green color denotes a significant difference between the means while the red denotes the opposite. * denotes that a Kruskal-Wallis H test was used.

		Bayelva	**Kongsfjorden**
Pb	Austre	0.0000002071*	0.0000002071*
	Bayelva		0.115217
Cd	Austre	0.000351	0.495106
	Bayelva		0.000279
As	Austre	0.002502*	0.6308*
	Bayelva		0.001261
Cr	Austre	<0.00001	<0.00001
	Bayelva		0.000124
Zn	Austre	<0.00001	<0.00001
	Bayelva		0.00022
Fe	Austre	0.0000002071*	<0.00001
	Bayelva		0.008293*
Al	Austre	0.0000002071*	0.00001387*
	Bayelva		0.000113
Ca	Austre	0.0000002071*	0.0000002071*
	Bayelva		0.03872*

Maja O. L. Ryan

Particulate matter released from Austre Brøggerbreen

NTNU
Norwegian University of
Science and Technology